PATHOLOGIC FEATURES OF ECONOMICALLY IMPORTANT VIRAL DISEASES IN BROILERS

by

KATHRYN N. MCCULLOUGH

(Under the Direction of Holly S. Sellers)

ABSTRACT

Avian reoviruses (ARVs) and fowl adenoviruses (FAdVs) are ubiquitous, variably pathogenic viruses that are responsible for several economically costly diseases in commercial broilers due to high morbidity or mortality.

Pathogenic reoviruses are etiologic agents of viral arthritis and tenosynovitis in chickens and turkeys and have been associated with several additional clinical syndromes, including stunting/malabsorption syndrome and enteric disease, hepatitis, immunosuppression, myocarditis, and respiratory disease. As of yet, no genetic or antigenic factor has been found to be predictive of an avian reovirus's clinicopathologic manifestation of arthritic, enteric, or other disease. ARVs within genetic cluster (GC) 2 have been isolated from both arthritis and enteritis clinical cases. Here, the pathogenesis of a GC 2 isolate was examined via histopathology, *in situ* hybridization, and PCR, and the isolate was found to infect both epithelial cells within the intestine and synoviocytes within the tendon sheath.

Fowl adenoviurses are the etiologic agents of inclusion body hepatitis (IBH) and hepatitis-hydropericardium syndrome (HHS) in chickens, which both cause acute hepatic necrosis with high mortality rates. Rapid, cost-effective diagnosis of IBH can streamline further confirmatory

laboratory testing and facilitate timely communication in the interim to affected parties, especially in locations with delayed access to a diagnostic laboratory. Here, Romanowsky-stained impression smear cytopathology of the liver at the time of necropsy is demonstrated to successfully stain IBH intranuclear inclusion bodies, and IBH diagnosis via cytopathology maintains high agreement to the histopathologic diagnosis.

INDEX WORDS: Avian reovirus, tenosynovitis pathogenesis, fowl adenovirus, inclusion body hepatitis, cytopathology

# PATHOLOGIC FEATURES OF ECONOMICALLY IMPORTANT VIRAL DISEASES IN BROILERS

by

KATHRYN N. MCCULLOUGH

DVM, North Carolina State University, 2019

A Dissertation Submitted to the Graduate Faculty of The University of Georgia in Partial Fulfillment of the Requirements for the Degree

DOCTOR OF PHILOSOPHY

ATHENS, GEORGIA

2024

# PATHOLOGIC FEATURES OF ECONOMICALLY IMPORTANT VIRAL DISEASES IN BROILERS

by

KATHRYN N. MCCULLOUGH

| | |
|---|---|
| Major Professor: | Holly S. Sellers |
| Committee: | James Stanton |
| | Silvia Carnaccini |
| | Robert Porter |
| | Brian Jordan |

Electronic Version Approved:

Ron Walcott
Vice Provost for Graduate Education and Dean of the Graduate School
The University of Georgia
December 2024

ACKNOWLEDGEMENTS

First, I sincerely thank my family and friends for their constant support throughout my years of schooling. I am extremely fortunate to have such caring people invested in my wellbeing.

I thank my mentors throughout 4-H, undergraduate, veterinary, residency, and graduate stages. This culmination of my professional training would not have been possible without each of their contributions along the way.

I thank the laboratory staff and my fellow graduate and post-graduate peers for their generosity in sharing their time and knowledge and for their willing assistance for even the most mundane of tasks. It is the littlest things that have made the biggest impact.

I thank my major professor and my committee members, as this work is a direct reflection of their guidance, encouragement, and assistance.

Finally, I thank Boehringer Ingelheim Animal Health for sponsorship of this graduate student position and contributions to the development of poultry health professionals.

TABLE OF CONTENTS

Page

LIST OF TABLES

LIST OF FIGURES

# CHAPTER 1

# INTRODUCTION AND LITERATURE REVIEW:

# AVIAN REOVIRUSES IN CHICKENS

## INTRODUCTION

Avian reoviruses (ARVs) are ubiquitous, variably pathogenic to nonpathogenic, nonenveloped, double-stranded RNA viruses within the *Reoviridae* family and *Orthoreovirus* genus that infect poultry and other avian species. Pathogenic viruses are etiologic agents of viral arthritis and tenosynovitis in chickens and turkeys and contribute to several additional clinical syndromes, including stunting/malabsorption syndrome and enteric disease, hepatitis, immunosuppression, myocarditis, and respiratory disease. Reoviral arthritis and its resulting lameness can lead to significant economic losses in market-aged broilers and growing turkeys due to increased culling, carcass downgrading, and poor flock uniformity. Historically, commercially available live attenuated vaccine strains closely matched circulating serotypes within the United States, and vaccination of breeder chickens effectively protected progeny via maternally derived neutralizing antibodies. However, emerging antigenically variant viruses have now circumvented commercial vaccine protection, frequently necessitating the use of autogenous vaccines to achieve disease control.

# LITERATURE REVIEW

## *Public Health Significance*

No zoonoses of avian reoviruses have been documented.

## *History*

The first avian reovirus isolate in 1954 originated from chickens in Ontario with chronic respiratory disease (50). Another isolate in 1957 from chicken tenosynovitis cases in West Virginia (147) was later demonstrated to be the same agent (148), and both were classified as avian reoviruses (150,194). In the following years, additional serotypes of ARV were isolated from cases of tenosynovitis, malabsorption and enteritis, osteoporosis, hepatitis, and myocarditis in chickens and turkeys throughout the United States, Europe, and Japan (41,53,62,67,69,96,102,125), with consistent experimental reproduction of tenosynovitis and variable success in reproduction of other syndromes (65,88,97,146). Antigenic similarity was found amongst isolates mostly circulating in America and European countries and associated with tenosynovitis (204). The first commercially available live attenuated avian reovirus vaccine was developed in 1983 using the S1133 strain (66). Disease control in chickens was achieved worldwide for several decades via breeder vaccination by using live/live attenuated and inactivated commercial vaccines based on S1133, 1733, 2408, and 2177 strains (52,57,66,157,165,203), and disease in turkeys was prevented with autogenous vaccines. From the late 2000's to early 2010's, increasing numbers of tenosynovitis cases in chickens (123) and turkeys (138), as well as some cases of malabsorption in chickens (40) in the United States, Canada (149), Europe (68,190), and Israel (54) were associated with variant reoviruses that were antigenically distinct compared to common vaccine strains (122), and for which existing

commercial vaccines offered little protection. Increased use of autogenous vaccines by some poultry companies in the United States has assisted in disease control when field isolates represent geographically circulating viruses (165); however, widespread control is still lacking. The economic impact of avian reovirus culls and mortality in the United States is estimated at $90 million per year within the broiler industry and $33 million per year within the turkey industry, as of 2022 (51).

*Reoviral Taxonomy and Structure*

Taxonomy

The virus family *Reoviridae*, so named for the respiratory enteric orphan viruses initially isolated from humans, contains subfamilies *Spinareovirinae* and *Sedoreovirinae*, which are distinguished by the presence or absence, respectively, of 12 turrets located at capsid icosahedral vertices. *Spinareovirinae* contains the *Orthoreovirus* genus, which encompasses five species that infect birds, mammals, and reptiles (232). *Avian orthoreovirus* is distinguished from *mammalian, baboon, Nelson Bay,* and *reptilian orthoreovirus* species by a combination of host specificity, fusogenic potential within cell culture (142), and lack of hemagglutination ability (53). Because viruses within the *Avian orthoreovirus* species vary genetically and molecularly amongst host species, they have become further denoted by the host species affected and associated clinical syndrome, where applicable. Viruses of importance to commercial avian species include duck (DRV) and Muscovy duck (MDRV) reoviruses, turkey reoviruses (TRV), and avian (chicken) reoviruses (ARV) (63,151).

Structure

Avian reovirus (ARV) is a double stranded RNA (dsRNA) virus composed of ten linear genomic segments within a non-enveloped, turreted, double concentric icosahedral capsid with an 80–85 nm external diameter and a 50–60 nm internal diameter (14). The genomic segments are grouped according to electrophoretic mobility into large (L1, L2, L3), medium (M1, M2, M3), and small (S1, S2, S3, S4) sizes (14,191) and encode 18 proteins via a combination of primary translation and post-translational cleavage, resulting in 12 structural and 6 non-structural proteins (21,86,192). Viral proteins have both structural and non-structural functions that contribute to pathogenesis, which are reviewed in the following section.

Viral proteins and their functions

**Lambda A** (λA) is a 1293 residue structural protein that is a primary translational product of the 3958-nucleotide-long L1 segment (143,164,215). λA is the main protein that forms the inner viral capsid (14,129) and is highly conserved between ARV strains as well as to the mammalian reovirus (MRV) λ1 homologue (215). In the infected cell, λA is one of the earliest proteins recruited into viroplasms by μNS (see below) (13,187), where it is thought to serve as a scaffold for additional core assembly during early viral morphogenesis (14). Phylogenetic lineages from λA sequencing have not been shown to correlate with ARV serotypes or pathotypes (170).

**Lambda B** (λB) is a 1259 residue protein encoded by the 3830-nucleotide-long L2 segment (214). λB is a minor component of the inner viral capsid and is thought to be an RNA dependent RNA polymerase (RdRp) facilitated by cofactor μA (14,214), with putative function based on high conservancy between λB and the RdRp MRV homologue, λ3 (23,179,214). λB

interacts with σNS and σA in a strain-dependent manner, becomes associated with the viroplasm prior to σA, and may act to recruit σA to the viroplasm (13). In turkey reoviruses, phylogenetic analysis of λB sequencing did not predict arthritic versus enteric tropism (136).

**Lambda C** (λC) is a 1285 residue, 142.2 kDa structural protein that is a primary translational product of the 3907-nucletotide-long L3 segment (71,215). λC pentamers extend from the inner to outer capsid and form turrets along the virion surface (129,228). Within the N-terminal region of λC, a 42 kDa fragment contains a guanylyltransferase capable of autoguanylylation activity, which functions as a viral mRNA capping enzyme via GMP binding and transference between GDP and GTP acceptors (71,130). The C-terminal portion of λC may possess methylase activity, which is suggested by its high degree of homology with mammalian and grass carp reovirus counterparts (71). L3 and other genes encoding viral capsid proteins, S1 and M2, account for the majority of sequence variability between ARV isolates (46). In one study, differences in pathologic presentation were seen between two field isolates of the same genotype, as determined by a 99% shared identity based within the S1 gene, but that exhibited nucleotide divergence of 28% and 25% in the L3 and M2 genes, respectively (47). In other studies, phylogenetic lineages from λC sequencing have not been shown to correlate with serotype or pathotype in either chickens (170) or turkeys (137).

**Mu A** (μA) is a 732 amino acid residue structural protein that is a primary translational product of the 2283-nucleotide-long M1 genome segment (129,144,181,191). μA proteins are minor components of the viral core (14) with NTPase and RTPase activity (180). μA shares approximately 30% amino acid homology with, and may serve similar function as, MRV μ2 (144,181), which is an RNA-dependent RNA polymerase cofactor. Phylogenetic lineages of M1 sequencing do not correlate with ARV serotype or pathotype (181).

**Mu B** (μB) is the 676-residue structural protein that is a primary translational product of the 2158-nucletotide-long M2 genomic segment (144,181,191). μB undergoes post-translational cleavage into a large carboxy-terminal fragment μBC and a small N-myristoylated amino-terminal fragment, μBN (191). μB, μBC, and μBN are structural components of the outer capsid, and μB and μBC are capable of inducing neutralizing antibodies (4,58,129). μB cleavage to μBC and μBN occurs during viral entry and is dependent on a low pH that accompanies endosomal acidification (44). μBC is further cleaved twice to δ and δ' polypeptides during intralysosomal viral uncoating (44), which may alter the lysosomal membrane conformation and allow viral release into the cytoplasm (14,44). Following cell entry, μBC localizes to the cell surface with σB, where it likely participates in the induction of cell fusion (142). MRV μ1, which shares approximately 44% amino acid identity with μB (144), achieves membrane penetration by insertion of a hydrophobic conformer within the myristoyl group (24,105). However, the crystalline structure of ARV μB lacks the "hub and spokes" conformation and disulfide bridges present in MRV μ1 (144,228), which may indicate differences in function between these protein homologues. Within the cytoplasm, μB and μBC rapidly form a ternary hetero-oligomeric complex with σB, which is then recruited to viroplasms and incorporated into the outer capsid (187). In one study, increased post-attachment infective success of macrophages by a highly pathogenic ARV strain and its reassorted derivatives was associated with the M2 segment (145). In another study, differences in pathologic presentation were seen between two genotype I field isolates that exhibited 99% shared identity within the S1 gene but had a nucleotide divergence of 25% and 28% in the M2 and L3 genes, respectively (47). However, phylogenetic analysis of M2 in another study showed no correlation to serotype or pathotype (181).

**Mu NS** (μNS) is a 635-residue nonstructural protein that is a primary translational product of the 1996-nucletotide-long M3 genomic segment (187,188,191). μNS undergoes post-translational cleavage into the larger carboxy-terminal protein μNSC and the smaller amino-terminal protein, μNSN (21,154). μNS cleavage occurs in a regulated manner with approximately 30% efficiency along an exposed, flexible loop between residues 154 and 155, via host cell caspase 3-like proteases during apoptosis, such that all three isoforms are simultaneously present within ARV-infected cells (21,154). The production of infective ARV particles is not diminished when apoptosis and μNS cleavage is inhibited (154). Since μNS is the only ARV protein capable of independent inclusion formation in transfected cells, it is considered the minimal viral factor necessary for viroplasm nucleation (188). μNS and μNSC both localize within non-polyubiquitinated viroplasms (19,188) in a vimentin- and microtubule-independent manner (19,187); however, only μNS is able to attract λA and σNS to inclusions (154). μNS colocalizes with Caveolin-1 in lipid membranes (Wang 2020). μNS contains two α-helical coiled segments which facilitate formation of homo- or hetero-oligomers, allowing μNS to serve as a scaffold within the viroplasm (19,187,188). Oligomer establishment and orientation is determined by the carboxy-terminal domain (19), and λA and σNS likely bind in a non-competitive manner to the amino-terminal portion of μNS (14). μNS, λA, and σNS form strong, complex associations within viroplasms that resist purification (19,154); whereas μNSC is weakly associated and easily extracted (154). ARV μNS shares relatively low (~25%) amino acid identity with (144), and may somewhat differ in function from, its MRV counterpart, which has been shown to interact with viral RNA transcripts in addition to recruiting viral proteins to viroplasms (3,20).

**P10** is a 98-amino acid residue, 10.3 kDa, nonstructural, translational product of the first open reading frame of the tricistronic S1 genomic segment and is a fusion-associated small transmembrane (FAST) protein responsible for cell-cell fusion (17,174). The S1 sequence divergence of the p10-encoding gene is lower than that of the subsequent p17 and σC-encoding genes, with a predominance of synonymous substitutions over nonsynonymous substitutions, and a lack of correlation to serotype or clinical disease presentation (73,118). p10 migrates to cholesterol-rich lipid rafts within the cellular membrane, with localization governed by the extreme carboxy terminus in a sequence-independent manner, and transport via the endoplasmic reticulum, likely utilizing a signal recognition particle (SRP)-dependent targeting mechanism (17,98,174,199). p10 induced cell membrane fusion reactions depend on the following essential regions: the cytoplasmic tail and conserved, membrane-proximal polybasic and palmitoylated dicysteine motif within the carboxy terminal, 36-amino acid residue endodomain; the triglycine motif within the central, single pass transmembrane domain; and two functional motifs within the amino-terminal, 40-amino acid residue ectodomain (11,98,174,175). The 13 amino acid residue membrane-proximal ectodomain mediates p10 homomultimerization within cholesterol-rich lipid platforms and is connected to the fusion peptide by 2 residues (98,199). The p10 fusion peptide is a highly conserved, hydrophobic patch of 11 moderately apolar residues stablilized in a loop configuration by two flanking cystine residues joined by a disulfide bond, and substitutions within this motif result in loss of syncytiogenic activity (12,98,99). This cystine loop serves as a noose to expose hydrophobic residues, which drives pore formation, membrane partitioning, liposome lipid mixing, and cholesterol-dependent and tubulation-independent liposome membrane fusion (12,16,99). Within the p10 cytoplasmic tail, the membrane-distal 12 residues mediate pore formation, while the last 8 residues enhance pore expansion (11). p10

induces RhoA and Rac1 GTPase membrane translocation and signaling with downstream phosphorylation of JNK and myosin light chain and activation of AP-1 and NF-κB transcription factors; however, inhibition of these pathways prevents syncytiogenisis (120). Extensive p10-mediated syncytium formation increases plasma membrane permeability and initiates apoptosis (161). Increased syncytium formation between ARV strains does not influence viral replication *in vitro*, but has been associated with increased pathogenicity in chicken embryos (45). Targeting of the ectodomain causes p10 and E3 Ubiquitin Ligase Siah-1 to form a multicomponent complex utilizing a LAMP-1 scaffold that promotes rapid p10 degradation following synthesis and prior to membrane localization, which inhibits syncytia formation, apoptosis and ARV release (26,173,205).

**P17** is a 146-amino acid residue, 16.8 kDa nonstructural, translational product of the second open reading frame of the tricistronic S1 genomic segment and serves as a nucleocytoplasmic shuttling protein that interacts with numerous cellular components to modulate signaling pathways for cell cycling, gene transcription, autophagy, and DNA binding (17,30,34,35,39,78,119,226). The S1 sequence divergence of the p17-encoding gene is higher than that of the preceding p10-encoding gene, but less than that of the subsequent σC-encoding gene, with a predominance of synonymous substitutions over nonsynonymous substitutions, and a lack of correlation to serotype or clinical disease presentation (73,118). p17 distributes to both the cytoplasm and nucleus in a transcription-dependent manner, with nuclear entry via nuclear pore complexes reliant on signal- and energy-dependent mechanisms and nuclear exit occurring via a CRM1-independent pathway (39). Nuclear import relies on the nuclear localization signal from amino acid residues 119 to 127 of p17; and both nuclear import and export depend on the nuclear export signal and nucleocytoplasmic shuttling domain located from amino acid residues

19 to 40 of p17 that serve as a binding site to the cellular carrier protein hnRNP A1 and are facilitated by lamin A/C (34,39). p17 avoids ubiquitin-proteasome degradation by mediating phosphorylation of Cdc37 and facilitating Hsp90/Cdc37 chaperone complex formation, resulting in protection of p17. p17 suppresses Tpr via interaction and reduced transcription, which results in p53 and p21 nuclear accumulation and pathway activation, subsequent PTEN inhibition of ERK and the PI3K/AKT/mTORC1 pathway, PTEN- and p21-mediated downregulation of CDK4 and cyclin D1, and Rb activation which lead to cell cycle arrest and autophagosome formation (79,119). p17 promotes β-arrestin-PTEN translocation from the cytoplasm to the plasma membrane and protects PTEN from E3 ligase NEDD4-1 ubiquitin-mediated proteasome degradation (79). In addition to PTEN interaction, p17 drives autophagosome formation by positively regulating AMPK and PKR/eIF2α signaling pathways, resulting in increased levels of Beclin 1, a subunit in PI3K class III complexes, and LC3-II, a surface component of autophagosomes (30,106). p17 possesses a cyclin-binding motif and has been shown to broadly inhibit CDKs, cyclins, and CDK–cyclin complexes by downregulating CDK transcription, decreasing CDK activation, and sequestering CDKs and cyclins within the cytoplasm, which collectively promote viral replication (32). p17 mimics cyclin B1 to compete for CDK1 binding, interferes with CDK1/vimentin interactions, binds to the CDK2/cyclin A2 complex via its carboxy terminus, suppresses Plk1 via the ATM/Chk1/PP2A pathway, and disrupts mTORC2 assembly, which inhibits vimentin and Akt phosphorylation and promotes cell cycle arrest, translation shutoff, and autophagy (32,33,78,106). p17 activates the E3 ligase MDM2 to target ribosomal proteins for degradation, driving autophagy, and promotes ubiquitin-mediated proteosome degradation of CDC25, preventing CDK1 activation and halting mitotic progression through the G2/M phase (33,78). p17 further impedes cell cycle progression by binding and

downregulating the expression of the cellular mitotic checkpoint protein Bub3 (182). In human endothelial cells, p17 has been shown to upregulate tumor suppressor molecule DPP4, resulting in an antiangiogenic effect by inhibiting endothelial migration and new vessel formation (126).

**Sigma C** (σC) is a 326 amino acid residue, translational product of the third open reading frame of the tricistronic S1 genomic segment (17,164,168,191). The S1 sequence divergence of the σC-encoding gene is higher than that of the preceding p10- and p17-encoding genes as well as other S-class genes, with a predominance of nonsynonymous substitutions over synonymous substitutions (118). Structurally, homotrimers of σC form fibers that anchor in and project from the outer capsid and are responsible for viral cell attachment and induction of group- and type-specific neutralizing antibodies (59,60,129,131,166,167,177,201). Each monomer of σC consists of a stalk composed of two beta-spiral repeats and a conserved, hydrophilic, carboxy-terminal globular head that contains receptor binding domains composed of beta barrel secondary structures (22,166). A hydrophobic region of heptad repeats located amino-terminal to the stalk beta spirals is highly variable, sharing approximately 2% amino acid identity across 28 aligned sequences in one study, and serves a structural function to extend the receptor binding domain away from the capsid (22,116). The as of yet unidentified cell receptor for ARV σC is present on CEF cells at a density of approximately 2.2 x $10^5$ receptor units per CEF cell (60). σC colocalizes with Caveolin-1 in the cell membrane during endocytosis (199). Within cells, synthesized σC is detectable in viroplasms within 30 minutes, but is not incorporated into the subviral particle until the following 30 minutes of morphogenesis, during which outer capsid proteins coat the viral core (187). Accumulation of σC into viroplasms is enhanced by host Hsp90/Cdc37 complex chaperoning of p17 (80). Further, σC is stabilized and protected from ubiquitin-proteasome degradation by cellular TRiC chaperonins CCT2 and CCT5 (80).

Functionally, σC acts as an apoptin via a p53-dependent pathway as well as by inducing DNA damage signaling and by interaction with eukaryotic elongation factor 1 alpha 1 (EEF1A1); with deletion of the σC carboxyl-terminus preventative for apoptosis induction (111,113,172,230). Comparatively, Muscovy duck reovirus (MDRV) σC and p10.8 proteins drive cell cycle arrest and apoptosis via ubiquitin-proteasome degradation of CDK2 and CDK4, mediated by cellular CCT2 and CCT5 stabilization of Cdc20 (195). Additionally, novel duck reovirus (NDRV) σC has been shown to interact with TRAM1, a cellular regulator of ER stress, with viral replication promoted or inhibited, respectively, by silencing or overexpression of TRAM1 (208).

**Sigma A** (σA) is a 416-amino acid residue, primary translational product of the 1643 nucleotide-long S2 genomic segment with both major structural and functional roles (82,129,163,185,222). σA monomers form 150 homopolymeric nodules throughout the inner capsid that join and stabilize λA proteins, as well as minorly contact λC and outer capsid protein μB via three α-helix and β-sheet rich, positively-charged domains, which may contribute to core coating, shell rigidity, and RNA impermeability during morphogenesis (61,216,228). In transfected cells, σA forms cytoplasmic, nonubiquitinated, perinuclear aggresomes that are protected from ubiquitin- proteasome degradation by the molecular chaperone TRiC (80,193). In the infected cell, σA distributes to viroplasm via uncharacterized interaction with ARV p17 and host Hsp90/Cdc37 chaperone complex at a later phase of core assembly (77), and to the nucleolus via an energy independent, non-diffusional, nucleoporin-dependent pathway that does not utilize cytosolic factors (13,193). Post-translational cleavage of σA yields a small amino-terminus fragment, σAN, and a larger carboxy-terminus fragment, σAC, with σAC demonstrating both cytosolic and nuclear localization as well as progressive time and dose dependent accumulation rather than immediate degradation (86). σA self-assembles into two

hexamers that form a double helix around a centrally located, sequence-independent, 21 nucleotide minimum length of dsRNA that is tightly bound in a cooperative manner (61,128,189,222). Nucleolar entry and dsRNA binding capabilities of σA are closely related, and both are dependent on the presence of arginine residues Arg 155 and Arg 273 (61). Additionally, σA possesses nonspecific nucleotidyl phosphatase activity that allows hydrolysis of all four types of nucleoside triphosphates (NTPs) into their respective di- and monophosphates and free phosphate (223). These various abilities allow σA to modulate host cell functions in several ways. σA downregulates activation of interferon-inducible and dsRNA-dependent protein kinase (PKR), contributing to interferon resistance (55,128). σA upregulates transcription of several genes associated with innate immunity, including IFN-α, IFN-β, IL-6, IL-8, TLR3, TLR7, MDA5, MyD88, MAVS, TRIF, NF-κB, IFITM3, Mx1, and OASL, but downregulates IRF3/7 expression (75). The PXXP motif of σA activates the phosphatidylinositol3-kinase-dependent Akt signaling pathway, resulting in an anti-apoptotic response (114,210,211). The MDRV homologue of σA colocalizes with caveolin-1 during caveolin-dependent endocytosis and colocalizes with LC3-II, an autophagosome marker, supporting the role of the autophagosome in viral replication (107,108). σA enhances cellular energy available for viral replication by driving the TCA cycle, glycolysis, and ATP production via activation of the mTOC1/eIF4E/HIF-1α pathway (29) and by promoting fatty acid oxidation via upregulation of PSMB6 and suppression of Akt, SREBP1, ACC1, and ACC2 (72,78). In contrast, σA interaction with gallus NME/NM23 nucleoside diphosphate kinase 2 impairs viral replication (209). Mutation within the S2 gene has been associated with maintenance of persistent infection (74).

**Sigma B** (σB) is a 367 amino acid residue structural protein that is the primary translational product of the 1196-1204 nucletotide-long S3 genomic segment (129,143,185,229).

σB is a major outer capsid component with monomers forming approximately 600 knobby projections along the virion surface (129,228). The σB protein contains a leucine zipper pattern and basic amino acid motifs, with a secondary structure composed of 33% turn, 28% β-sheet, 20% α-helix, and 19% random coil, in which 63% of α-helices are distributed within the N-terminus (229). σB is involved in viral entry via interaction with caveolin-1 in lipid rafts and is capable of inducing group-specific neutralizing antibodies via two identified epitopes (115,197,200,218). Following cell entry, σB localizes to the cell surface with μBC, where it likely contributes to the induction of syncytium formation, as treatment with virus specific antisera or chymotrypsin inhibit this process (142). Membrane anchoring of σB may be due to the presence of a hydrophobic region between residues 246 and 268 (221). Within the cytoplasm, σB rapidly forms a ternary hetero-oligomeric complex with μB and μBC, with equal ratios of each component, which is then recruited to viroplasms and incorporated into the outer capsid (187). Transfection of cells with σB results in activation of several genes associated with progression of tenosynovitis and arthritis (152).

**Sigma NS** (σNS) is a 367-residue nonstructural protein that is the primary translational product of the 1185 nucletotide-long S4 genomic segment (31,163,191). σNS acts as an RNA chaperone to aid selection of genome segments for encapsidation by facilitating RNA–RNA interactions and annealing and accelerating RNA folding (18,219). Suppression of σNS expression secondarily reduces the expression of other viral proteins, including σA and σC, likely due to disruption of inner core assembly and secondary transcript availability (84). σNS locates to viroplasms within 6 hpi, due to μNS recruitment, where it incorporates into large ribonucleoprotein complexes (187–189). The secondary structure of σNS is predicted to be 33% α-helix predominantly within the carboxy-terminal, and 23% β-sheet distributed towards the

amino-terminal, both of which may influence binding affinities, and contains one YXXXM and two PXXP motifs, and 5 potential glycosylation sites (31,76,211). Free σNS forms homodimers and homotrimers, but assembles into stable, elongated hexamers with high affinity electrostatic bonds to interact with single-stranded nucleic acids that have a minimum of 10-20 nucleotides (18,189). The σNS hexamer can unwind helices of partially double-stranded RNA and can bind and anneal multiple complimentary single-stranded RNA molecules (18). Binding of shorter, less stable RNA stem-loops is more efficient than with longer, more stable RNA helices, and affinity to the formed dsRNA decreased following spontaneous annealing, allowing dissociation prior to encapsidation and exclusion from the virion (18). RNA binding occurs with little sequence specificity, but with slight preference of poly(A) over poly(U), and lack of poly(C) or poly(G) affinity (18,189,219,220). σNS-ssRNA binding occurs within oligomers, but not monomers, in a conformation-dependent manner involving five conserved basic residues distributed throughout the polypeptide (76,189). In contrast, a native conformation is not required for interaction between monoclonal antibodies and ssRNA binding site epitopes between residues 178–194 (70). Within this region, residues 180–188 are highly conserved amongst strains, and changes in amino acid sequences at this and various other σNS epitopes do not correlate with either serotype or pathotype of ARV (76); however, mutation within the S4 gene has been associated with maintenance of persistent infection (74). Following infection, σNS has been shown to interact with several host cell molecules and processes. σNS is stabilized by and protected from ubiquitin-proteasome degradation by the host cell molecular chaperone TRiC, which facilitates viral replication (80). σNS activates the host cell phosphatidylinositol 3-kinase (PI3K)-dependent Akt signaling pathway, which modulates several cell functions, including survival, proliferation, migration, differentiation, and apoptosis (210). Multiple σNS PXXP or YXXXM/YXXM motifs

or other motifs may be involved in host PI3K p85 subunit interaction and PI3K/Akt pathway activation (210,211). Comparatively, the MDRV σNS protein, which is encoded by the S3 genome segment and shares up to 90% amino acid identity with its ARV homologue, has been shown to increase intracellular levels of LC3-II and decrease levels of phosphorylated mTOR, which supports that this protein contributes to the induction of autophagy (103,206). Use of recombinant σNS in ELISAs may allow differentiation between vaccinated and naturally infected animals (213).

*Pathogenesis and Pathophysiology*

Transmission

Horizontal transmission is the primary mode of ARV spread, predominantly via contaminated fecal matter, and to a lesser extent via respiratory secretions (69,89,90,94,124). Entry of infectious material to the enteric system via ingestion, the respiratory system via inhalation, or to the plantar subcutaneous tissues via traumatic inoculation represent the primary routes of experimental infection and documented or proposed routes of natural infection (1,65,90,94,97,146,169). Chicks older than 1 week-of-age are more resistant to infection than younger birds (159).

Vertical transmission of ARV occurs transovarially (2,42,53) at a low rate of approximately 2% between 17–19 days post-infection of breeders (132). Congenitally infected chicks may then serve as nuclei for horizontal spread to hatch-mates.

Viral distribution within the host

ARVs have been detected throughout the gastrointestinal, respiratory, and female reproductive tracts, the cloacal bursa, liver, pancreas, spleen, kidneys, hock joint, flexor and

extensor tendons, heart, bone marrow, thymus, nervous system, and the blood (91,100,133,141,224). As ARVs may be detected within tissues without gross or microscopic lesions, or may not be isolated from tissues with extensive pathology, and viral replication sites may not necessarily be predicted solely by the presence or absence of tissue pathology (49,92,169).

Sites of ARV infection, replication, and tissue distribution are dependent on both the route of inoculation and the isolate properties. Trypsin-sensitive strains readily colonize the respiratory tract and synovial tissues when inoculated locally but may be partially inactivated when introduced orally (1,95). In contrast, trypsin-resistant strains are better able to survive in gastrointestinal conditions to establish primary enteric infections (2,95).

ARV sites of infection are described below, but in summary, following oral inoculation, ARV initially infects and replicates within enterocytes throughout the intestinal tract and cloacal bursal epithelial cells within 1 dpi and may persist for 21 dpi or longer. Pathogenic viruses may cause viremia between 1 to 10 dpi, with subsequent colonization of secondary target organs between 1 to 14 dpi and variable persistence within tissues. Parenteral inoculation follows a similar course, with initial isolation within 1 dpi from the respiratory tract following intranasal administration or from the hock following foot pad inoculation, and subsequent isolation at 2+ dpi from additional organs, including the gastrointestinal tract.

**Gastrointestinal tract.** The gastrointestinal tract is considered the predominant site of ARV infection following oral introduction, representing an important site of viral replication and a portal of entry to systemic spread. Additionally, high viral titers and viral persistence indicate the intestinal tract as an important source of viral shedding via contaminated feces. In chicks inoculated orally with the arthrotropic, trypsin-resistant R2 strain, ARV was detected initially

within the gastrointestinal tract between 6 and 24 hours post infection (hpi) via virus isolation (VI) (91,95,100), immunofluorescence (IF) (91), or immunohistochemistry (IHC) (91). IF and IHC localized viral antigen to the cytoplasm of epithelial cells and lamina propria of the duodenum, jejunum, and ileum, with the highest staining density within the duodenum and jejunum. Transmission electron microscopy (TEM) confirmed the presence of viral particles within cytoplasmic vesicles as well as interdigitated along the microvillous surface of some epithelial cells from 12–96 hpi (91). Viral titers within the intestinal tract peak between 2 and 10 hours post infection (dpi), and persist until 12 to 21 dpi, a timepoint which often represented the end of the study (91,95,100). Generally, ARV was detected within the upper gastrointestinal tract prior to, or simultaneously to, detection within the lower tract, and viral persistence was greater within the lower tract. Specifically, ARV was isolated from the proventriculus until 7 dpi, the duodenum until 12 dpi, the ileum until 18 dpi, and the cecal tonsils and rectum until 21 dpi (100). In adult hens, intestinal colonization follows a similar timeline, with combined respiratory and enteric inoculation of the FDO-1 strain resulting in positive fluorescent antibody tests and virus isolation for ARV throughout all levels of the gastrointestinal tract at early timepoints (4 dpi) and persistence within the intestines and cloaca at later timepoints (14–15 dpi) (133).

In chicks inoculated via footpad or intranasally with the trypsin-sensitive TR1 strain, ARV was isolated from the jejunum from 2–12 dpi, and from the jejunum and ileum at 6–7 dpi, respectively (95). The delay in enteric replication following parenteral inoculation was interpreted as secondary colonization following viremia, a route by which the virus was protected from trypsin degradation via bypass of the intestinal lumen.

**Cloacal bursa.** The cloacal bursa is considered a primary site of ARV infection and replication, and a portal to systemic spread following oral introduction. In orally inoculated

chicks, ARV was isolated from the cloacal bursa from 1 dpi until 12 dpi, with peak viral titers at 2–3 dpi that surpassed paired gastrointestinal peak viral titers (91,95). Virion-containing vesicles within bursal epithelial cells were observed via TEM from 12–96 hpi (91). Intracytoplasmic viral antigen was detected within epithelial cells, macrophages, lymphoid follicles, and/or subserosal and stromal connective tissues via immunofluorescence from 1–2 dpi until 4–5 dpi (91,141) or via immunohistochemistry from 1–3 dpi until 5 dpi (91,183). In intranasally inoculated chicks, ARV was isolated from the cloacal bursa from 1–5 dpi, with a viral titer peak at 2 dpi (95).

**Liver.** The liver may represent primary and secondary sites of ARV replication, with viral presence occurring 6–24 hpi and persisting up to 13 dpi across various strains and routes of inoculation. In chicks inoculated orally with the R2 strain, ARV was isolated from the liver within 6–24 hpi, with peak viral titers at 2–3 dpi, with persistence through 7 dpi (91,95,100). Footpad inoculation with TR1 or UM 1-203 strains resulted in ARV isolations from the liver from 2–12 dpi (95), and 2–6 dpi, respectively, with viral titer peaks at 4 dpi (125). Intranasal inoculation of the TR1 strain resulted in ARV isolation from the liver from 1–12 dpi, with viral titer peak at 2 dpi (95). ARV antigen has been demonstrated via IF and IHC from 1–3 dpi until 6–13 dpi within viable hepatocytes or with initial viral staining within the cytoplasm of Kupffer cells, followed by presence within degenerating hepatocytes, and finally within histiocytic infiltrate (91,141,183). *In situ* hybridization demonstrated presence of the R2 strain within the liver following subcutaneous inoculation of chicks (117). Ultrastructurally, viral particles form paracrystalline arrays within the cytoplasm of hepatocytes and polykaryocytes (125).

In studies with oral inoculation, ARV presence in hepatocytes within 6 hpi likely represents a primary phase of replication rather than one following intestinal replication and subsequent systemic distribution (91). Macro-molecular transport, by bursal follicle-associated

epithelial (FAE) cells or gut-associated lymphoid tissue (GALT) M cells (15,83), may facilitate early extra-intestinal viral transport to the blood or lymph (91); however, this method of distribution has not been documented.

**Kidney.** The kidney may represent primary and secondary sites of ARV replication. In chicks inoculated orally with the R2 strain, ARV was isolated from the kidney from 1–9 dpi in one study (91) and at 5–7 dpi in one study (100). Immunofluorescence demonstrated ARV in the kidney from 4–6 dpi following oral or footpad inoculation with the 176 strain (141).

**Blood.** Viremia may occur from 1–14 dpi, allowing systemic ARV distribution from the initial site of inoculation. In chicks inoculated orally with the R2 strain, ARV was isolated from the erythrocyte fraction at 24 hours pi, with erythrocyte and plasma fraction viral titer peaks at 30 hours pi, and persistence for 5 days. In contrast, isolation of ARV within the mononuclear fraction occurred at 7 and 10 dpi (100). In a similar study, the R2 strain was isolated from serum from 2 dpi until 5 dpi (91). In chicks inoculated intra-tracheally with the 1733 strain, ARV was isolated from the plasma at 1 week post inoculation (wpi) and from leukocytes at 1- and 2- wpi (155).

ARV proliferates within cultured bone marrow and peripheral blood macrophages but not heterophils, thrombocytes, or thymus-derived lymphocytes (135,145). In chickens, viral isolation from the cellular fractions suggests cell-associated viral circulation, and immunofluorescent double staining indicates ARV infection of mononuclear phagocytes (27,100). Viral particles have been ultrastructurally visualized within phagosomes of histiocytes infiltrating CAM pocks of infected embryos and within macrophages in vasculature adjacent to lesions (10). Replication within mononuclear cells may impede neutralization from circulating antibodies and facilitate dissemination to secondary sites of infection, such as the spleen (27,100).

**Heart.** In chicks inoculated orally with the R2 strain, ARV was isolated from the heart at 10 dpi in one study (100), and from 12–72 hours pi until 12 dpi in other studies (91,95). Similarly, intranasal inoculation of the TR1 strain resulted in ARV isolation from the heart from 2–12 dpi, with viral titer peak at 4 dpi (95). *In situ* hybridization demonstrated presence of the R2 strain within the heart following subcutaneous inoculation of chicks (117). Immunofluorescence demonstrated ARV in the heart from 4–8 dpi following oral or footpad inoculation with the 176 strain (141).

**Spleen.** In chicks inoculated orally with the R2 strain, ARV was isolated from the spleen at 5 dpi (100). Immunofluorescence demonstrated ARV in the spleen from 2–8 dpi following oral or footpad inoculation with the 176 strain (141). Immunohistochemistry targeting σNS demonstrated ARV replication within splenic periellipsoid lymphoid sheaths at 1.5 and 2.5 dpi following footpad inoculation with ARV strain 2408 (27).

**Bone marrow.** In chicks inoculated orally with the arthrotropic R2 strain, ARV was isolated from the bone marrow at 4, 5, and 10 dpi (100).

**Thymus.** In chicks inoculated intra-tracheally with the 1733 strain, ARV was isolated from the thymus at 1 and 2 weeks pi (155).

**Pancreas.** In chicks inoculated orally with the R2 strain, ARV was isolated from the pancreas from 12–24 hpi until 8–12 dpi (91,95). *In situ* hybridization demonstrated presence of the R2 strain within the pancreas following subcutaneous inoculation of chicks (117).

**Respiratory tract.** In chicks inoculated intranasally with the TR1 strain, ARV was isolated from the trachea and lung from 1 dpi until 10 dpi, with viral titer peak at 2 dpi (95). In hens inoculated via respiratory and enteric routes with the FDO-1 strain, ARV was isolated from

the nasal turbinates, larynx, trachea, lung, and airsacs at 4 dpi, but were negative at 14–15 dpi (133). Viral antigen was detected via FA within the nasal turbinate connective tissue, tracheal mucosa and submucosa, lung alveolar cells, and the air sacs (133).

**Reproductive tract.** In hens inoculated via respiratory and enteric routes with the FDO-1 strain, ARV was isolated from the ovary, infundibulum, magnum, isthmus, uterus, and vagina at 4 dpi, and persisted within the isthmus, uterus, and vagina at 14–15 dpi. Viral antigen was detected via FA within the ovarian connective tissue and oviductal connective and glandular tissue (133).

**Central and peripheral nervous system.** In chicks inoculated orally or intramuscularly with the ERS-2 strain, ARV was detected via IHC within choroid plexus epithelial cells and underlying connective tissue from 4–5 dpi until 7 dpi and within a thoracic spinal cord ganglion neuron at 7 dpi (224). Viral antigen was also detected in areas of inflammation within connective tissue surrounding the spinal cord and sciatic nerve (224).

**Joints and tendons.** The hock joint, gastrocnemius tendon, and digital flexor tendons are important sites for primary or secondary ARV replication following footpad or enteric infection, respectively, as well as sites for long-term viral persistence. Despite likely underlying arthritogenic potential of most ARVs (90,159), expressed arthrotropism is highly variable *in vivo* (58,90,155). ARV isolation titers within the hock are similar between chicks with homologous maternal antibodies and chicks without maternal antibodies, despite a reduction in gross and microscopic lesions (93). In 1-day-old chicks inoculated orally with the R2 strain, ARV was isolated from the hock and tendons at 14 and 21 dpi in one study (100), and from 2 dpi until 12 dpi in another study (91). Intranasal or footpad inoculation with the TR1 strain similarly resulted in ARV isolation from 2–12 dpi with viral titer peak at 8 dpi (95). Footpad inoculation of various

genotypes resulted in peak viral titers in the tendons at 3 dpi and reduced titers from 7–45 dpi (7). In chicks inoculated intratracheally with intermediately (2035) and highly (1733) pathogenic strains, ARV was isolated up to 7 wpi and 22 wpi, respectively, from gastrocnemius tendons (155). Viral antigen was detected via FA within the hock synovial stroma and peritendinous tissues at 4 dpi and 6 dpi following chick inoculation with the 176 strain via oral or footpad routes, respectively (141). *In situ* hybridization demonstrated presence of the R2 strain within the tendon synovial membrane following subcutaneous inoculation of chicks (117). In hens inoculated via respiratory and enteric routes with the FDO-1 strain, virus isolation and fluorescent antibody tests were positive for ARV within flexor and extensor tendons at 4 dpi and 14–15 dpi, but were negative at 30 dpi (133).

**Chorioallantoic membrane (CAM).** The CAM represents an important tissue for ARV isolation as well as a model for infection in hatched birds. On light microscopy, viral inclusions are visible within the cytoplasm of infected mesenchymal cells. On electron microscopy, viral particles are associated with fibrillar material and ribosome-lined structures within these cells (194).

ARV-induced Cellular pathology

ARV entry and replication involves numerous interdependent interactions between viral and host molecules that have been described in varying degrees.

ARV virions attach to host cell surface receptors via outer-capsid protein σC (59,60), and enter the cell via caveolin-1-mediated and dynamin-2-dependent endocytosis (81,125). Although the host cell surface receptor for ARV is unidentified, β-adrenergic receptors are the suspected binding site for MDRV, which enters cells similarly to ARV via caveolae-mediated endocytosis

and may utilize similar receptors (108). Cholesterol-rich lipid rafts are not only necessary for ARV entry in the form of caveolae, but have been found to be essential components for ARV replication (199,200). ARV transport to the early endosome is regulated by cellular GTPase Rab5, facilitated by microtubules, and mediated via p38 MAPK and Src signaling pathways (81). Acidification of the endosome is required for productive infection (81), which presumably coincides with viral uncoating and subsequent release into the cytoplasm (44). *In vitro*, cell-associated ARV growth has a lag phase of 6–15 hours, followed by a logarithmic phase that lasts 8–21 hours (150,160).

Viral uncoating is a necessary step to initiate numerous downstream signals within the cell (104,121), and ARV infection modulates cellular signal transduction proteins to upregulate those involved in apoptosis, DNA synthesis and energy production and downregulate those involved in RNA processing and the ubiquitin-proteasome pathway (25). Several key processes have been identified *in vitro* that result in successful viral propagation, including induction of autophagy, induction of apoptosis, formation of syncytia, and resistance to interferon (139).

**Growth arrest, Autophagy, and Anti-Apoptotic signals.**

Cell survival and an anti-apoptotic state occurs during early stages of ARV S1133 infection in Vero cells, from 0.5 to 2 hpi (114), and autophagosome formation occurs in early to middle stages in Vero and CEF cells infected with various ARVs, between 3 to 48 hpi (30,134). Cell survival signaling via PI3K/Akt/NF-κB and STAT3 pathways occurs independent of cellular protein synthesis or virus replication (114). The PI3K pathway is activated by ARV σA via a PXXP motif and by σNS via an unknown PXXP or YXXXM/YXXM motif (114,210,211). ARV activation of class I PI3K/Akt/mTOR pathways and activation of the Beclin-1 promoter,

with formation of RhoA, ROCK1, and Beclin-1 complexes leads to induction of autophagy (134,230).

ARV downregulates host protein synthesis by modulating the phosphorylation of cellular translation initiation and elongation factors, including decreased phosphorylation of eIF4G, eIF4E, 4E-BP1, and p70S6K, and increased phosphorylation of eEF2 (87). p17 suppresses cellular cycling and growth and promotes autophagosome formation via interaction with p53, p21, and numerous other cell signaling pathways as described in a previous section (30,32,33,78,79,106,119,182). σNS may also contribute to the induction of autophagy, as MDRV σNS, which shares up to 90% amino acid identity with ARV σNS, causes LC3-II to increase and mTOR phosphorylation to decrease in DF-1 cells (103,206).

The autophagosome likely serves as a membranous platform for viral replication, as ARV replication has been shown to be dependent on lipid rafts, which are found within phospholipid membranes (114,199). While endoplasmic reticulum membranes have been shown to play a role in mammalian orthoreovirus viroplasm formation (38,186), the role of the ER is less defined for avian reoviruses. However, colocalization of autophagosome marker LC3-II and viral σA and σNS in MDRV infected DF-1 cells indicates viral replication within the autophagosome (108). ARV and MDRV infection each induce autophagosome formation, and viral yields are higher when autophagy is enhanced (108,134). ARV yields are lower when autophagosome and lysosome fusion are inhibited (30), and MDRV inhibits autophagolysosome degradation (108).

**Pro Apoptotic signals**

Apoptosis following ARV infection is a significant cause of tissue damage (109). Apoptosis induction occurs in middle to late stages of ARV infection and is both temporarily

inhibited by, and dependent upon the prior autophagic state, as induction of autophagy delays apoptosis, but the inhibition of autophagy inhibits apoptosis (30,43,112,134). The switch from ARV induced autophagy to apoptosis is regulated by RhoA/ROCK1 signaling (112) and occurs in mid to late stages of infection (104,172). ARV-induced apoptosis in cell culture varies in kinetics between CEF, DF1, and Vero cells and utilizes a variety of cell signaling pathways following viral uncoating which can occur independent of, or in conjunction with, viral gene expression (104,110,113,114).

The mitochondrial pathway of apoptosis can be triggered *in vitro* by ARV activation of p53-dependent signaling via σC or by Src, Ras, p38, JNK/SAPK, MAPK, and PKCδ signaling pathways, leading to increased BAX and BAD expression, cytochrome C release, and caspase activation (37,110,112,113,172). ARV S1133 induced JNK phosphorylation also promotes BiP/GRP78-mediated Bim translocation to the endoplasmic reticulum, increasing ER stress, and triggering caspase 3 activation (112). Similarly, in MDRV, the Bip/IRE1/XBP1 pathway and ER stress are triggered by the p10.8 protein. ARV upregulates unfolded protein response proteins PERK, IRE1, and ATF6, followed by caspase-3 expression and apoptosis when cellular compensatory capacity to manage ER stress is overwhelmed (225).

ARV σC can also induce apoptosis *in vitro* and *in vivo* by upregulating oxidative-stress-mediated DNA damage signaling, as well as *in vitro* by interaction with eukaryotic elongation factor 1 alpha 1 (EEF1A1), presumably by triggering stress signaling (111,172,230). ARV p10 contributes to apoptosis in cell culture by increasing plasma membrane permeability, an effect that is curtailed, alongside syncytia formation and viral release, by rapid E3 Ubiquitin Ligase Siah-1 and LAMP-1-directed p10 degradation (26,161,205). ARV-induced apoptosis and viral replication are reliant on the cellular ubiquitin-proteasome system, as proteosome inhibition

leads to decreased p53 phosphorylation and caspase 3 activation, decreased viral RNA transcription, reduced σA, σC, and σNS expression, and decreased viral titer (28).

### Syncytogenesis

Syncytia formation propensity between isolates *in vitro* has been associated with increased pathogenicity *in ovo*; however, differing rates of syncytiogenesis do not affect viral replication levels (45). ARVs have been shown to induce syncytium formation as early as 1 dpi in cell culture, including CEK, CEL, CEF, Vero (8,69,100,101,111,153), and between 2-5 dpi in infected tissues (109,125). In S1133-infected Vero and DF-1 cells, syncytium formation and viral production require Rac1 activation (81,120). Rac-1-directed syncytiogenesis may occur via p10-mediated RhoA GTPase activation or via ARV-induced, Ras-dependent p38 MAPK and Src signaling – pathways that concurrently mediate caveolin-1 phosphorylation and dynamin-2 expression during viral entry and early infection (81,85). Cellular ubiquitylation and proteosomal degradation of p10 inhibits syncytia formation, apoptosis and ARV release (26,173,205).

## Early innate immune response to ARV

### Interferon and ARV interferon resistance

Interferons (IFNs) are cytokines released from virus-infected cells that upregulate antiviral gene transcription levels (56). Type I IFNs, which include IFNα and IFNβ, are highly expressed in some viral infections (127,178), are induced by contact with double stranded RNA (162), and have the strongest antiviral activity of the three types of IFNs (56). The type II IFN IFN-γ induces antiviral activity, is a major macrophage-activating factor, and drives the Th1 immune response via T helper type 1 cells (56,178). ARV has demonstrated higher resistance to

IFN antiviral effects during replication *in vitro* than other virus types, including Semliki Forest virus, vesicular stomatitis virus, and vaccinia virus (55,128).

In CEK cells, several ARVs were unsuccessful at inducing IFN, in contrast to successful IFN induction by other viral genera (48). In plaque reduction assays utilizing CEK cells incubated with embryo-origin IFN, ARVs exhibited increased IFN resistance compared to other virus genera similarly evaluated (48).

In CEF cells, several ARVs induced low levels of IFN production; however, pretreatment of CEF cells with IFN prior to ARV infection allowed enhanced subsequent IFN production (48,196). Further, ARV S1133, but not two other viral genera studied, induced expression of IFNα and IFNβ in CEF cells, with IFN expression occurring via a caspase-independent mechanism and unrelated to apoptosis, but coinciding with ARV uncoating, and subsequently inducing dsRNA-dependent protein kinase (PKR) expression (121). In one study utilizing rcIFN-primed CEF cells, the induced antiviral state successful at inhibiting other virus genera was unable to impair ARV S1133 replication, and σA was purported to contribute to this interferon resistant state via binding PKR (128). In another study using IFNα- primed CEF cells, ARV S1133 infection induced expression levels of IFITM3 higher than levels in non-primed or negative control cell cultures, and higher IFITM3 expression correlated with inhibition of ARV replication (196). In CEF cells transfected with ARV σA, transcription of several genes associated with innate immunity were modulated, with downregulated IRF3/7 mRNA, and upregulated IFN-α, IFN-β, TRIF, and TLR3 expression peaks between 3–6 hpi; IL-6, MDA5, IFITM3, Mx1, and OASL peaks between 9–12 hpi; and IL-8, NF-κB, TLR7, MyD88, MAVS peaks between 24–36 hpi (75). In 6-day-old and 4-week-old chickens inoculated with various ARV isolates via various routes, older chickens expressed IFN earlier, at 12 hpi in the serum and

24 hpi in the lungs, and at higher viral titers than the younger chicks; whereas the younger chicks displayed a greater viral distribution and persistence within tissues (49).

In joints, rising and falling viral copy number was mirrored between 1 and 7 dpi by markedly increased expression of IFN- β and mildly increased IFN-α and as well as upregulation of interferon-stimulated genes IFIT5, MX, OAS, VIPERIN, ISG12, IFI6, IFITM3, PKR, and CD47 (198). In the spleen, cloacal bursa, and thymus, ARV S1133 replication was accompanied by marked upregulation of interferon-stimulated genes IFIT5, MX, OAS, VIPERIN, ISG12, and IFI6, with follow-up IFIT5 overexpression in DF-1 cells exerting an inhibitory effect on ARV replication (197). In ARV S1133 footpad-inoculated chicks, thymic and bursal, but not splenic, IFN-α and IFN-β were upregulated, with significantly higher levels of IFN-α than IFN-β in the cloacal bursa (197).

In DF-1 cells infected with an isolate from clinical tenosynovitis, ARV GX/2010/1 modulated 168 differentially expressed genes within the transcriptome, representing both an overall induction of a prolonged antiviral response as well as an interference in cell growth and death pathways (139). In DF-1 cells, cellular microRNA gga-miR-29a-3p exerts an antiviral effect by inhibiting caspase-3, thereby reducing ARV replication and virally-induced apoptosis (231).

**Additional Cytokine Responses to ARV infection**

Pro-inflammatory cytokines: TNF-α, IL-1β, and IL-6.

TNF-α was historically regarded as absent in chickens; however, recent characterization of this cytokine (156) may allow future investigation into its role in ARV pathogenesis. IL-1β and IL-6 increase expression in various cell types following ARV infection. In DF-1 and Vero

cells, ARV S1133 infection induced Akt and NF-κB signaling that resulted in upregulation of proinflammatory cytokines IL-1β and IL-6, but not IL-8, from 2 to 36 hpi, with peak cytokine expression between 8-16 hpi. Predominantly IL-1β, with minor contribution from IL-6, within media from these cell cultures promoted chemotaxis in cAMP-treated U937 monocytes from 4 to 36 hours post exposure, with a peak at 8 hours post exposure (114). In CEF cells, IL-1β and IL-6 expression and subsequent chemotactic effects were lower than that of DF1 and Vero cell cultures (114). In one study using LMH cells, IL-1β mRNA expression did not differ between ARV-CU98 exposed and non-exposed cells at 6 and 8 hpi, but IL-1β mRNA expression decreased from this baseline at 8 and 10 hours in virus-exposed cells, correlating with the decreased metabolic levels and increased cell death also observed in that treatment group (64). In chicken macrophages, ARV S1133 induced IL-1β mRNA expression in a biphasic manner that likely relied on differing pathways, with viral disassembly initiating rapid, transient expression at 30 minutes with peak at 2 hours and decrease by 6 hours pi; and viral RNA synthesis driving stable IL-1β mRNA expression at and beyond 6 hpi (207). Chicken macrophages exposed to ARV-CU98, a PEMS-associated virus, expressed high levels of IL-1β mRNA levels at 2 hpi that declined until 10 hpi (64). In ARV GX/2010/1 orally-infected chicks, IL-1β expression in various tissues correlated with the induction of autophagy during early stages of infection, with peaks of both at 72 hpi, and IL-1β expression decreased with autophagosome inhibition (140). In ARV S1133 or ARV 2408 footpad-inoculated chicks, both groups exhibited increased IL-1β expression in the spleens at 1.5 dpi, and increased IL-6 expression 1.5 dpi and 2.5 dpi (171).

Th1 cytokines: IL-18 and IFN-γ.

Interleukin-18 (IL-18), produced by many hematopoietic and non-hematopoietic cell types, enhances NK and CD8 T cell cytotoxic activity and induces the secretion of IFN-γ from

target cells (178,217). IFN-γ is a type II IFN that has weaker antiviral activity than the type I IFNs, but is a major macrophage-activating factor and drives the Th1 (cell-mediated) immune response via CD4+ T helper type 1 cells (56,178). In CEF cells, ARV S1133 induced both a monophasic mildly increased transcription of IL-18, with peak expression at 6 hpi and negative correlation to viral titer, as well as a biphasic, markedly increased transcription of IL-17 and IFN-γ, with expression peaks at both 6 and 48 hpi, and positive correlation to viral titer (227).

In ARV S1133 or ARV 2408 footpad-inoculated chicks, both groups exhibited increased IL-18 expression in the spleens at 1.5, and increased IFN-γ expression at 1.5 dpi and 2.5 dpi (171). In footpad-inoculated chicks, ARV S1133 triggered the RIG-I-like receptor MDA5 signaling pathway in peripheral blood lymphocytes and upregulation of IFN and IFN-stimulated genes, with peak IFN-γ, IL-6, IL-17, and IL-18 at 1 dpi; IFN-α, IFN-β, IL-12, IFITM1, IFITM2, IFITM5, Mx1, OASL, MDA5, MAVS, TRAF3, TRAF6, IRF7, IKKε, TBK1, and NF-κB at 3 dpi; IL-8 at 5 dpi; and IL-1β and TNF-α at 7 dpi (212).

Anti-inflammatory and Th2 cytokines: IL-10, IL-3, IL-4, IL-13, and GM-CSF.

In ARV S1133 or ARV 2408 footpad-inoculated chicks, slightly increased IL-10 expression in the spleens was seen in both groups at 1.5 and 2.5 dpi (171). IL-10 is an anti-inflammatory cytokine secreted predominantly by monocytes that downregulates nitric oxide production, MHC class II expression, and the transcription of the proinflammatory cytokines IL-1β and TNF-α, and enhances B cell survival, proliferation, and antibody production (158). The STAT3 signaling pathway mediates IL-10-related cytokine signaling (56). STAT3 signaling has been shown to be involved in delayed apoptosis during early ARV infection (114), and in human macrophages, constitutive STAT3 expression replicates IL-10 cytokine-suppressive activity (202).

The specific changes of the anti-inflammatory and Th2 cytokines IL-3, IL-4, IL-13, and GM-CSF have not been well characterized in relation to ARV infection. IL-3, IL-4, IL-13, and granulocyte-macrophage colony-stimulating factor (GM-CSF) belong to a cluster of cytokines responsible for the Th2 inflammatory response and generation of humoral immunity. In mammals, activated T lymphocytes are the predominant source of these cytokines; however, in chickens, these cytokines are also expressed at similar levels in non-lymphoid tissues. In one study in chickens, in addition to expression in lymphoid organs, all 4 cytokines were expressed in the lung; IL-3, IL-4 and IL-13 were expressed in kidney and brain; IL-3 and IL-13 were expressed in liver; IL-3 and GM-CSF were expressed in the heart; and IL-3 was expressed in the muscle (5).

Tissue Pathology

**Synovial tissues.** Various ARVs are capable of inciting an inflammatory response in synovial tissues following footpad inoculation in chicks. At 1 dpi, paratendinea and tendon sheaths contained edema and mild infiltrate of heterophils and mononuclear cells (184). At 1.5 dpi, mononuclear phagocytes contained viral antigen at a concentration of over 200 times greater than other cell types in the footpad (27). At 2.5 dpi, mononuclear phagocytes present within the footpad displayed evidence of ARV replication (27). At 3 dpi, the tendon lymphocytic population present consisted of predominantly γδ−(αβ+)CD3+ and CD8+ T lymphocytes (7). At 6–8 dpi, lymphocytic infiltration developed lymphoid follicles within the synovial stroma, and synovial membranes became hyperplastic (141). At 8 dpi, the severity of lymphocytic inflammation in the tendon varied from mild to severe between three compared σC genotype I isolates (47). From 7 to 13 dpi, fibroplasia and infiltration by macrophages, lymphocytes, plasma cells, and heterophils thickened the paratendineum and external peritendineum and mildly

extended to the synovial membranes, synoviocytes were hypertrophic and hyperplastic, and fibrin, inflammatory cells, and sloughed synovial cells were present in the synovial space (184). At 9 dpi, the tendon lymphocytic population contained γδ+ CD3+ and CD4+ T lymphocytes in addition to the previously identified γδ−(αβ+) CD3+ and CD8+ T lymphocytes (7). At 20 dpi, fibrous synechia joined the paratendineum and external peritendineum, and fewer inflammatory cells were present (184). At 45 dpi, γδ+ CD3+ T lymphocytes predominate, with fewer γδ−CD3+ T lymphocytes (7).

In chicks infected via subcutaneous (SC), intra-abdominal (IA), or oral routes with a tenosynovitis-causing field agent, mononuclear infiltrate and fibrosis was present in the tendon sheaths at 5 wpi for SC and IA groups and at 7.5 wpi for the oral group (65). In intranasally inoculated chicks, ARV S1133 induced apoptosis within the tendon at 5 dpi (109). Intratracheal inoculation with ARV 1733 at various ages, between 1 day of age to 4 weeks of age, resulted in acute heterophilic and histiocytic tenosynovitis at 2 wpi both in chicks inoculated at 1 day of age and in those inoculated at 3 weeks of age, with more severe lesions seen in chicks inoculated at 1 day of age (155). However, in the same study, chronic lymphoplasmacytic tenosynovitis with synovial hyperplasia and fibrosis was present with equal severity of lesions irrespective of age in groups inoculated at 1 day, 2 weeks, and 4 weeks of age (155).

In bursectomized or thymectomized chickens, gross and microscopic ARV lesions in tendon sheaths following bursectomy were similar to those of intact birds; whereas thymectomy resulted in milder ARV lesions (101). In another study, tissue apoptosis, IFN-γ producing CD8+ T lymphocyte levels, and clinical signs were reduced when antigen-presenting cells were depleted and when T-cell proliferation and cytokine production was inhibited experimentally, which suggests that lesion severity is associated with the trafficking of IFN-γ producing CD8+ T

cells to the site of infection (7). Further, disease severity varied by ARV isolate, with higher morbidity seen with isolates that elicit increased levels of IFN-γ producing CD8+ T lymphocytes in tendons (7).

**Heart.** In ARV GX/2010/1 orally infected chicks, cardiomyocytes contained increased numbers of autophagosomes on TEM at 48 hpi (140). In ARV 176 orally inoculated chicks, lymphocytes diffusely infiltrated the epicardium and adjacent myocardium at 6–8 dpi (141). In ARV S1133 intranasally inoculated chicks, the heart contained apoptotic cells, and lymphocytes with few heterophils and macrophages multifocally infiltrated the epicardium and myocardium at 5 dpi (109). In footpad inoculated chicks, the severity of lymphocytic inflammation in the heart varied from mild to moderate at 8 dpi and from mild to severe at 28 dpi between three compared σC genotype I isolates (47). At 20 dpi in ARV CO8 footpad inoculated chicks, the epicardium contained edema and mild infiltrates of heterophils, macrophages, lymphocytes, and plasma cells (184).

**Liver.** In intranasally inoculated chicks, ARV S1133 induced syncytium formation and apoptosis in the liver at 5 dpi (109). Cervical subcutaneous ARV 176 or ARV 81-5 inoculation in chicks induced scattered heterophilic and mononuclear infiltrate in the liver at 2 dpi and multifocal to coalescing hepatic necrosis with heterophilic and mononuclear infiltrate from 3–5 dpi (184). In ARV 176-orally inoculated chicks, the liver contained scattered necrotic foci at 2–4 dpi and widespread hepatocellular vacuolation at 6–8 dpi (141). Intratracheal inoculation with ARV 1733 resulted in hepatocellular swelling, sinusoidal dilation, and capsular fibrosis at 1–2 wpi in chicks inoculated at 1 day and 1 week of age, but not in chicks inoculated from 2 to 4 weeks of age (155). In UM 1-203 footpad-inoculated chicks, hepatic changes consisted of increasingly severe hepatocellular vacuolar degeneration and necrosis with formation of syncytia

from 2–5 dpi, which transitioned to some hepatocellular regeneration with macrophage influx and an absence of syncytia at 6 dpi (125).

**Spleen.** At 2.5 dpi following footpad inoculation, ARV 2408-infected mononuclear phagocytes were present within the spleen, predominantly within the periellipsoid lymphoid sheath, suggesting viral transport from a primary site of infection to the spleen via infected monocytes (27). In ARV S1133 footpad inoculated chicks, splenic changes included edema and lymphocyte degeneration and necrosis(197). Cervical subcutaneous ARV 176 or ARV 81-5 inoculation in chicks induced hyperplasia of splenic periarteriolar sheath stromal cells with intervening fibrin and rare necrosis as well as multifocal hyperplastic lymphoid aggregates from 2–4 dpi (184). In ARV 176-orally inoculated chicks, the spleen contained numerous foci of necrosis with eosinophilic material at 406 dpi (141). Intratracheal inoculation with ARV 1733 resulted in periarteriolar lymphocytic depletion and splenic edema with proteinaceous coagulation at 1 and 2 wpi in chicks inoculated at 1 day and 1 week of age, but not in chicks inoculated from 2 to 4 weeks of age (155).

**Thymus.** In ARV S1133 footpad inoculated chicks, the thymus displayed reduced numbers of cortical lymphocytes (atrophy) (197). In footpad inoculated chicks comparing three σC genotype I isolates, all isolates caused moderate lymphoid depletion in the thymus at 8 dpi and mild lymphoid depletion at 28 dpi (47). Cervical subcutaneous ARV 176 or ARV 81-5 inoculation in chicks resulted in mixed heterophil, macrophage, lymphocyte, and plasma cell infiltration of the thymic adventitia at 1 dpi, which invaded the thymic parenchyma at 3–4 dpi (184). Intratracheal inoculation with ARV 1733 resulted in thymic cortical and medullary lymphocytic depletion at 1 and 2 wpi in chicks inoculated at 1 day of age, but not in chicks inoculated from 1 to 4 weeks of age (155).

**Cloacal Bursa.** In ARV GX/2010/1 orally-infected chicks, the cloacal bursa contained increased numbers of autophagosomes on TEM at 48 hpi (140). In intranasally inoculated chicks, ARV S1133 induced apoptosis in the cloacal bursa at 5 dpi (109). Intratracheal inoculation with ARV 1733 resulted in lymphocytic depletion and cortical thinning with heterophilic infiltrate in bursal follicles at 1 and 2 wpi in chicks inoculated at 1 day of age, but not in chicks inoculated from 1 to 4 weeks of age (155). In ARV S1133 footpad inoculated chicks, bursal changes included follicular edema, lymphocyte degeneration and necrosis, and heterophilic infiltration and interstitial edema, fibrosis, and inflammatory cell infiltration (197). In footpad-inoculated chicks, an ARV isolated from wild birds caused hemorrhage, lymphocyte depletion, and heterophilic inflammation within the cortex and within the bursa at 5 dpi (36). In footpad inoculated chicks comparing three σC genotype I isolates, all isolates caused mild to marked lymphoid depletion in the cloacal bursa at 8 dpi and 28 dpi (47). Cervical subcutaneous ARV 176 or ARV 81-5 inoculation in chicks induced cortical depletion of bursal follicles and increased interstitial fibrous connective tissue(184). In ARV 176 orally inoculated chicks, the interstitium contained hypertrophic connective tissues and heterophilic and lymphocytic infiltrates, and bursal follicles contained decreased, unevenly distributed lymphocytes at 2 dpi (141).

In bursectomized chickens, gross and microscopic ARV lesions in tendon sheaths were similar to those of intact birds; however, the antibody response was delayed, and ARV could be recovered for a longer time period in bursectomized birds than intact birds, indicating a protective role of the B-cell system (101).

**Bone Marrow.** In ARV 176 oral or footpad-inoculated chicks, the bone marrow contained necrotic bone marrow cells from 4–8 dpi (141).

**Cecal Tonsils.** In ARV WVU 1675 footpad-inoculated chickens, the cecal tonsil tunica propria contained lymphoid hyperplasia at 4 dpi, with lymphoid necrosis and mild heterophilic infiltration from 4 to 25 dpi (97).

**Gastrointestinal tract.** In ARV GX/2010/1 orally-infected chicks, the cecal tonsil contained increased numbers of autophagosomes on TEM at 48 hpi (140). In orally-inoculated chicks with varying ARVs in genetic clusters 1, 4, and 5, with either malabsorptive or arthritic field presentations, all groups displayed intestinal epithelial vacuolar degeneration and sloughing along the tips of villi by 7 dpi (176). In intranasally inoculated chicks, ARV S1133 induced apoptosis in the intestines at 5 dpi (109). In chicks intramuscularly inoculated with a malabsorption syndrome (MAS) isolate of ARV, at 24 dpi, proventricular glands were dilated, and duodenal villi were atrophied, with cystic dilation of the crypts and heterophilic infiltration of the lamina propria (6). In chicks inoculated via oral or footpad routes with arthrotropic turkey reoviruses, mild lymphoplasmacytic duodenitis and jejunitis with villous blunting was present at 28 dpi (9). In an RSS field case of 10 to 21-day old broilers with ARV isolation, the duodenum and jejunum displayed villous atrophy and dilated crypts(40). In ARV WVU 1675 footpad-inoculated chickens, the proventricular tunica propria contained lymphoid hyperplasia at 4 dpi, with lymphoid necrosis from 4 to 25 dpi (97).

**Pancreas.** In footpad-inoculated chicks, an ARV isolated from wild birds caused dilated acini, hemorrhage, and inflammation within the pancreas at 5 dpi (36). In an RSS field case of 36-day old broilers with ARV isolation, the pancreas displayed atrophy, vacuolar degeneration, and necrosis of acinar cells (40).

**Kidney.** In intranasally inoculated chicks, ARV S1133 induced apoptosis in the kidney at 5 dpi (109). In ARV 176 orally inoculated chicks, the kidney contained random foci of

heterophils and lymphocytes at 6 dpi (141). In chicks intramuscularly inoculated with a malabsorption syndrome (MAS) isolate of ARV, at 24 dpi, the renal tubular epithelium of some birds displayed multifocal desquamation and hemorrhage (6).

**Brain.** In ARV WVU 1675 footpad-inoculated chickens, the meninges contained perivascular lymphoid accumulations 7 dpi (97).

**Embryos.** In CAM-, CAS, or yolk sac-inoculated embryos, various ARVs induced chorioallantoic membrane pocks histologically composed of mesodermal edema, mesodermal and ectodermal histiocytic and lymphoid infiltration, ectodermal necrosis, and ectodermal and fibroblastic proliferation containing large basophilic, granular intracytoplasmic inclusions ultrastructurally composed of viral cores (10,69). Additional embryonic lesions include multifocal hemorrhage, proventricular epithelial hyperplasia, cardiac necrosis, and hepatic necrosis, giant cell formation, and fibroblastic proliferation (8,69).

# INTRODUCTION AND LITERATURE REVIEW: FOWL ADENOVIRAL HEPATITIS IN CHICKENS

## INTRODUCTION

Fowl adenoviruses (FAdVs) are the etiologic agents of inclusion body hepatitis (IBH) and hepatitis-hydropericardium syndrome (HHS) in chickens. IBH is distributed globally throughout poultry-producing countries, and HHS occurrence varies by country throughout Asia, Europe, and the Americas, with rare, non-commercial incidence in the United States (26,37). These diseases predominantly affect broilers up to 5 weeks of age, and high economic cost can result from flock mortality reaching 30% for IBH and 90% for HHS, with additional losses due to decreased body weights and immunosuppression (8,34). Presumptive diagnosis of acute IBH and HHS can be made based on gross pathology, but confirmatory diagnosis relies on histopathology, virus isolation, or molecular detection (16). Treatment is not available for IBH and HHS. Prevention strategies rely on vaccination of parent stock with commercial vaccines where available, and autogenous vaccine where permitted (16,37).

## LITERATURE REVIEW

### *Taxonomy*

*Adenoviridae* contains six genera, of which *Aviadenovirus, Barthadenovirus* (formerly *Atadenovirus*), and *Siadenovirus* contain species infecting birds (7). *Aviadenovirus* contains five species (A–E), wherein the fowl adenoviruses account for twelve serotypes (1–8a,8b – 11) based

on serum cross-neutralization (16,20). Fowl adenovirus A (FAdV-A) contains serotype FAdV-1; FAdV-B contains serotype FAdV-5; FAdV-C contains FAdV-4 and FAdV-10; FAdV-D contains FAdV-2, FAdV-3, FAdV-9, and FAdV-11; and FAdV-E contains FAdV-6, FAdV -7, FAdV -8a, and FAdV -8b (16). Typically, IBH follows infection with an FAdV-D or FAdV-E serotype, and HHS most often involves FAdV-C4 infection; however there is overlap in disease presentations across these serotypes, and mixed infections are common (11,24,27–29).

*Structure, infection, and replication*

*Aviadenoviruses* consist of a linear, non-segmented dsDNA genome within a non-enveloped, 90 nm icosahedral capsid (7). The capsid is formed by hexon and penton proteins, and single or paired fibers protrude from the penton bases (21,33). The hexon and fiber proteins represent the primary target of neutralizing antibodies and are major determinants of antigenicity, while the penton is a lesser antigenic target (40,45). The fibers are responsible for cell receptor interaction and attachment, with FAdV-2, FAdV-7, FAdV-8a, FAdV-8b, and FAdV-11 displaying single fibers, and FAdV-4 displaying paired fibers (21,33,40). The chicken homologue of the coxsackievirus and adenovirus receptor (CAR) has been demonstrated as a receptor for FAdV-4, but avian-specific receptors for the remaining IBH serotypes have been less characterized (33,41). Adenoviral protein functions during infection and replication are predominantly characterized in mastadenoviruses. These are briefly summarized, acknowledging that these interactions may not fully represent those of aviadenovirus. Entry via clathrin-coated endosome is followed by endosome acidification and protein VI-mediated lytic release into the cytoplasm (46). Viral hexon interaction with cytoplasmic dynein initiates transport along microtubules, and nuclear entry is facilitated by nuclear-pore complex proteins (9,43). The leucine-zipper region of minor capsid protein IX is responsible for inclusion body formation, and

virion core proteins V and VII, μ, terminal protein (TP), DNA-binding-protein (DBP), and adenovirus protease (ADP) responsible for unwinding the viral genome, initiating replication, and repackaging the genome (2,44). The adenovirus death protein (ADP) induces host cell lysis with viral release following cell membrane rupture (17).

*Transmission*

Horizontal and vertical transmission contribute to the spread of FAdVs. Horizontal transmission is predominantly the fecal-oral route, with lesser contribution by respiratory secretions (15). The highest fecal viral load occurs between 4–7 dpi, and shedding can continue for up to 6 weeks (15). Further, adenoviral persistence in the environment and personnel movement of contaminated materials between flocks can contribute to viral spread (3,4,35). Vertical transmission to progeny may occur between 1–5 wpi for naïve flocks, but transmission is unlikely in flocks with established antibody titers (18,36,42). Young chickens are most susceptible to FAdV infection, with age-related resistance seen at 10-days-of-age (13–15). However, increased susceptibility to and severity of adenoviral disease is seen during coinfection with immunosuppressive agents, such as chicken anemia virus, avian orthoreovirus, or infectious bursal disease virus among others (42,48,49).

*Clinical signs and pathology*

Adenoviral hepatitis is most commonly seen in meat-type birds between 3-5 weeks of age, but can be seen less commonly and with less severity in breeding and laying flocks (6,12,39). IBH and HHS display similar clinical signs with low morbidity, with sick birds exhibiting nonspecific signs of decreased feed intake, ruffled feathers, and crouched posture

(28,37). IBH and HHS differ in mortality rate, as IBH mortality generally ranges from 10-30% of an affected flock, but HHS mortality generally exceeds 50% (28,39).

The predominant IBH lesion is a grossly swollen, friable, pale liver containing multifocal necrosis and hemorrhage (37). In severe IBH cases, the pancreas and kidneys may also be swollen and hemorrhagic (19,47). HHS is characterized by the presence of pericardial effusion and cardiac necrosis in addition to the hepatic, pancreatic, and renal changes encompassed by IBH (5,10,30). Ascites, pulmonary edema, splenic necrosis, thymic and bursal atrophy, and muscular hemorrhage may also be seen with HHS (10,22,30).

Microscopically, the diagnostic feature of IBH and HHS is the presence of intranuclear inclusion bodies (INIBs) within hepatocytes, which are present between 4–9 dpi (1,25). In HHS or severe cases of IBH, INIBs may also be observed within pancreatic acinar cells, renal tubular epithelium and glomeruli, splenic lymphocytes, and proventricular glandular epithelium (22,25,30). HHS is characterized by myocardial necrosis, especially within the papillary muscles, and may also display arterial intimal vacuolation (10,30,31). Necrotic to degenerative lesions in other organs include pancreatic necrosis; glomerulonephritis and renal tubular necrosis; and thymic, bursal, and splenic lymphoid depletion (26,30,38,47).

*Diagnosis*

Because the lesions of IBH and HHS may overlap with features of other disease states in chickens, gross tentative diagnosis of these diseases should be confirmed by additional laboratory tests (50). As mentioned previously, histopathologic confirmation of adenoviral hepatitis is dependent on the presence of intranuclear inclusion bodies within hepatocytes. However, inclusion bodies may not be present for observation in later stages of disease (1,25).

Virus isolation is readily achieved in chicken embryos or various cell cultures, including primary chicken liver or kidney cells or hepatoma cell lines, among others (20,32). Electron microscopy may be utilized to confirm the presence of adenoviral particles (16). Historically, serotypes were established and isolates were differentiated via restriction enzyme analysis and serologic methods of cross neutralization and indirect enzyme-linked immunosorbent assay (ELISA) for group-specific antigen (20). Currently, molecular techniques are more often used, with quantitative PCR representing a readily accessible means of diagnosis in many laboratories, and genome sequencing offering further options for viral characterization (16). Immunocytochemistry and *in situ* hybridization have been employed as means of adenoviral detection in research settings, but these methods are not widely used for diagnostic purposes (Hess 2000, el-shall). ELISA may also be used to monitor flock antibody titers, whether from natural exposure or to monitor vaccination efforts (23).

REFERENCES: AVIAN REOVIRUS IN CHICKENS


1. al Afaleq, A. I., and R. C. Jones. Localisation of avian reovirus in the hock joints of chicks after entry through broken skin. Res Vet Sci 48: 381–382. 1990.

2. Al-Muffarej, S. I., C. E. Savage, and R. C. Jones. Egg transmission of avian reoviruses in chickens: Comparison of a trypsin-sensitive and a trypsin-resistant strain. Avian Pathol 25: 469–480. 1996.

3. Antczak, J. B., and W. K. Joklik. Reovirus genome segment assortment into progeny genomes studied by the use of monoclonal antibodies directed against reovirus proteins. Virology 187 : 760–776. 1992.

4. Astawa, N. M. Neutralization of avian reovirus 1091 in chick kidney and vero cell cultures by monoclonal antibodies against μB/μBC and σC proteins. Media Kedokteran Hewan 22: 68–73. 2006.

5. Avery, S., L. Rothwell, W. D. J. Degen, V. E. J. C. Schijns, J. Young, J. Kaufman, and P. Kaiser. Characterization of the First Nonmammalian T2 Cytokine Gene Cluster: The Cluster Contains Functional Single-Copy Genes for IL-3, IL-4, IL-13, and GM-CSF, a Gene for IL-5 That Appears to Be a Pseudogene, and a Gene Encoding Another Cytokinelike Transcript, KK34. Journal of Interferon and Cytokine Research 24: 600–610. 2004.

6. Awandkar, S. P., S. D. Moregaonkar, S. J. Manwar, B. P. Kamdi, and M. B. Kulkarni. Comparative investigations of infectious runting and stunting syndrome in vaccinated breeder chicks by inactivated reovirus and chicks from non-vaccinated breeders. Iran J Vet Res 18: 6–12. 2017.

7. Ayalew, L. E., K. A. Ahmed, S. Popowich, B.-C. Lockerbie, A. Gupta, S. K. Tikoo, D. Ojkic, and S. Gomis. Virulence of Emerging Arthrotropic Avian Reoviruses Correlates With Their Ability to Activate and Traffic Interferon-γ Producing Cytotoxic CD8+ T Cells Into Gastrocnemius Tendon. Front Microbiol 13: 1–14. 2022.

8. Bagust, T. J., and H. A. Westbury. Isolation of reoviruses associated with diseases of chickens in Victoria. Aust Vet J 51: 406–407. 1975.

9. Bampi Rafael Azambuja. Pathogenicity of variant field isolates of avian reovirus and molecular characterization of Brazilian variants from commercial broilers (Publication No. 9949332941002959)[Master's thesis, University of Georgia]. 2016.

10. Baroni, A., P. Bertoncin, P. N. D'aprile, and B. Felluga. Ultrastructural histopathology of chick embryo chorioallantoic membrane infected with an avian reovirus. Avian Pathol 9: 341–354. 1980.

11. Barry, C., and R. Duncan. Multifaceted Sequence-Dependent and -Independent Roles for Reovirus FAST Protein Cytoplasmic Tails in Fusion Pore Formation and Syncytiogenesis. J Virol 83: 12185–12195. 2009.

12. Barry, C., T. Key, R. Haddad, and R. Duncan. Features of a spatially constrained cystine loop in the p10 FAST protein ectodomain define a new class of viral fusion peptides. J Biol Chem 285: 16424–16433. 2010.

13. Benavente, J., and J. Martínez-Costas. Early steps in avian reovirus morphogenesis. Curr Top Microbiol Immunol 309: 67–85. 2006.

14. Benavente, J., and J. Martínez-Costas. Avian reovirus: Structure and biology. Virus Res 123: 105–119. 2007.

15. Bockman, D. E., and M. D. Cooper. Pinocytosis by epithelium associated with lymphoid follicles in the bursa of fabricius, appendix, and Peyer's patches. An electron microscopic study. Am J Anat136: 455–477. 1973.

16. Bodelón, G., L. Labrada, J. Marťnez-Costas, and J. Benavente. Modification of late membrane permeability in avian reovirus-infected cells. Viroporin activity of the S1-encoded nonstructural p10 protein. J Biol Chem 277: 17789–17796. 2002.

17. Bodelón, G., L. Labrada, J. Martønez-Costas, and J. Benavente. The avian reovirus genome segment S1 is a functionally tricistronic gene that expresses One structural and two nonstructural proteins in infected cells. Virology 290: 181–191. 2001.

18. Borodavka, A., J. Ault, P. G. Stockley, and R. Tuma. Evidence that avian reovirus σnS is an RNA chaperone: Implications for genome segment assortment. Nucleic Acids Res 43: 7044–7057. 2015.

19. Brandariz-Nuñez, A., R. Menaya-Vargas, J. Benavente, and J. Martinez-Costas. Avian Reovirus μNS Protein Forms Homo-Oligomeric Inclusions in a Microtubule-Independent Fashion, Which Involves Specific Regions of Its C-Terminal Domain. J Virol 84: 4289–4301. 2010.

20. Broering, T. J., J. S. L. Parker, P. L. Joyce, J. Kim, and M. L. Nibert. Mammalian Reovirus Nonstructural Protein μNS Forms Large Inclusions and Colocalizes with Reovirus Microtubule-Associated Protein μ2 in Transfected Cells. J Virol 76: 8285–8297. 2002.

21. Busch, L. K., J. Rodríguez-Grille, J. I. Casal, J. Martínez-Costas, and J. Benavente. Avian and mammalian reoviruses use different molecular mechanisms to synthesize their μNS isoforms. J Gen Virol 92: 2566–2574. 2011.

22. Calvo, P. G., G. C. Fox, X. L. Hermo Parrado, A. L. Llamas-Saiz, C. Costas, J. Martínez-Costas, J. Benavente, and M. J. Van Raaij. Structure of the carboxy-terminal receptor-binding domain of avian reovirus fibre sigmaC. J Mol Biol 354: 137–149. 2005.

23. Cashdollar, L. W. Characterization and structural localization of the reovirus λ3 protein. Res Virol 145: 277–285. 1994.

24. Chandran, K., D. L. Farsetta, and M. L. Nibert. Strategy for Nonenveloped Virus Entry: a Hydrophobic Conformer of the Reovirus Membrane Penetration Protein μ1 Mediates Membrane Disruption. J Virol 76: 9920–9933. 2002.

25. Chen, W.-T., Y.-L. Wu, T. Chen, C.-S. Cheng, H.-L. Chan, H.-C. Chou, Y.-W. Chen, and H.-S. Yin. Proteomics Analysis of the DF-1 Chicken Fibroblasts Infected with Avian Reovirus Strain S1133. PLoS One 9: e92154. 2014.

26. Chen, X., Z. He, M. Fu, Y. Wang, H. Wu, X. Li, H. Cao, and S. J. Zheng. The E3 Ubiquitin Ligase Siah-1 Suppresses Avian Reovirus Infection by Targeting p10 for Degradation. J Virol 92. 2018.

27. Chen, Y. S., P. C. Shen, B. S. Su, T. C. Liu, C. C. Lin, and L. H. Lee. Avian reovirus replication in mononuclear phagocytes in chicken footpad and spleen after footpad inoculation. Can J Vet Res 79: 87–94. 2015.

28. Chen, Y. T., C. H. Lin, W. T. Ji, S. K. Li, and H. J. Liu. Proteasome inhibition reduces avian reovirus replication and apoptosis induction in cultured cells. J Virol Methods 151: 95–100. 2008.

29. Chi, P. I., W. R. Huang, H. C. Chiu, J. Y. Li, B. L. Nielsen, and H. J. Liu. Avian reovirus σA-modulated suppression of lactate dehydrogenase and upregulation of glutaminolysis and the mTOC1/eIF4E/HIF-1α pathway to enhance glycolysis and the TCA cycle for virus replication. Cell Microbiol 20. 2018.

30. Chi, P. I., W. R. Huang, I. H. Lai, C. Y. Cheng, and H. J. Liu. The p17 Nonstructural Protein of Avian Reovirus Triggers Autophagy Enhancing Virus Replication via Activation of Phosphatase and Tensin Deleted on Chromosome 10 ( PTEN ) and AMP-activated Protein Kinase ( AMPK ), as well as dsRNA-dependent Protein Kinase. J Biol Chem 288: 3571–3584. 2013.

31. Chiu, C. J., and L. H. Lee. Cloning and nucleotide sequencing of the S4 genome segment of avian reovirus S1133. Arch Virol 142: 2515–2520. 1997.

32. Chiu, H. C., W. R. Huang, T. L. Liao, P. I. Chi, B. L. Nielsen, J. H. Liu, and H. J. Liu. Mechanistic insights into avian reovirus p17-modulated suppression of cell cycle CDK-cyclin complexes and enhancement of p53 and cyclin H interaction. J Biol Chem 293: 12542–12562. 2018.

33. Chiu, H.-C., W.-R. Huang, T.-L. Liao, H.-Y. Wu, M. Munir, W.-L. Shih, and H.-J. Liu. Suppression of Vimentin Phosphorylation by the Avian Reovirus p17 through Inhibition of CDK1 and Plk1 Impacting the G2/M Phase of the Cell Cycle. PLoS One 11: e0162356. 2016.

34. Chiu, H.-C., W. Huang, Y.-Y. Wang, J. Li, T.-L. Liao, B. L. Nielsen, and H.-J. Liu. Heterogeneous Nuclear Ribonucleoprotein A1 and Lamin A/C Modulate Nucleocytoplasmic Shuttling of Avian Reovirus p17. J Virol 93: 851–870. 2019.

35. Chiu, H.-C., S. Richart, F.-Y. Lin, W.-L. Hsu, and H.-J. Liu. The Interplay of Reovirus with Autophagy. Biomed Res Int 2014: 1–8. 2014.

36. Choi, Y. R., S. W. Kim, K. Shang, J. Y. Park, J. F. Zhang, H. K. Jang, B. Wei, S. Y. Cha, and M. Kang. Avian Reoviruses From Wild Birds Exhibit Pathogenicity to Specific Pathogen Free Chickens by Footpad Route. Front Vet Sci 9: 1–10. 2022.

37. Chulu, J. L. C., L. H. Lee, Y. C. Lee, S. H. Liao, F. L. Lin, W. L. Shih, and H. J. Liu. Apoptosis induction by avian reovirus through p53 and mitochondria-mediated pathway. Biochem Biophys Res Commun 356: 529–535. 2007.

38. Coffey, C. M., A. Sheh, I. S. Kim, K. Chandran, M. L. Nibert, and J. S. L. Parker. Reovirus Outer Capsid Protein μ1 Induces Apoptosis and Associates with Lipid Droplets, Endoplasmic Reticulum, and Mitochondria. J Virol 80: 8422–8438. 2006.

39. Costas, C., J. Martínez-Costas, G. Bodelón, and J. Benavente. The Second Open Reading Frame of the Avian Reovirus S1 Gene Encodes a Transcription-Dependent and CRM1-Independent Nucleocytoplasmic Shuttling Protein. J Virol 79: 2141–2150. 2005.

40. Davis, J. F., A. Kulkarni, and O. Fletcher. Reovirus infections in young broiler chickens. Avian Dis 57: 321–325. 2013.

41. Deshmukh, D. R., and B. S. Pomeroy. Avian reoviruses. I. Isolation and serological characterization. Avian Dis 13: 239–243. 1969.

42. Deshmukh, D. R., and B. S. Pomeroy. Avian reoviruses. III. Infectivity and egg transmission. Avian Dis 13: 427–439. 1969.

43. Duan, S., J. Cheng, C. Li, L. Yu, X. Zhang, K. Jiang, Y. Wang, J. Xu, and Y. Wu. Autophagy inhibitors reduce avian-reovirus-mediated apoptosis in cultured cells and in chicken embryos. Arch Virol 160: 1679–1685. 2015.

44. Duncan, R. The Low pH-Dependent Entry of Avian Reovirus Is Accompanied by Two Specific Cleavages of the Major Outer Capsid Protein μ2C. Virology 219: 179–189. 1996.

45. Duncan, R., and K. Sullivan. Characterization of Two Avian Reoviruses That Exhibit Strain-Specific Quantitative Differences in Their Syncytium-Inducing and Pathogenic Capabilities. Virology 250: 263–272. 1998.

46. Egaña-Labrin, S., R. Hauck, A. Figueroa, S. Stoute, H. L. Shivaprasad, M. Crispo, C. Corsiglia, H. Zhou, C. Kern, B. Crossley, and R. A. Gallardo. Genotypic Characterization of Emerging Avian Reovirus Genetic Variants in California. Sci Rep 9: 9351. 2019.

47. Egaña-Labrin, S., C. Jerry, H. J. Roh, A. P. da Silva, C. Corsiglia, B. Crossley, D. Rejmanek, and R. A. Gallardo. Avian Reoviruses of the Same Genotype Induce Different Pathology in Chickens. Avian Dis 65: 530–540. 2021.

48. Ellis, M. N., C. S. Eidson, J. Brown, and S. H. Kleven. Studies on interferon induction and interferon sensitivity of avian reoviruses. Avian Dis 27: 927–936. 1983.

49. Ellis, M. N., C. S. Eidson, O. J. Fletcher, and S. H. Kleven. Viral tissue tropisms and interferon production in white leghorn chickens infected with two avian reovirus strains. Avian Dis 27: 644–651. 1983.

50. Fahey, J. E., and J. F. Crawley. Studies On Chronic Respiratory Disease Of Chickens II. Isolation of A Virus. Can J Comp Med Vet Sci 18: 13–21. 1954.

51. French, D. Incidence and Economic Impact of Reovirus in the Poultry Industries in the United States. Avian Dis 66: 432–434. 2022.

52. Giambrone, J. J., and R. P. Clay. Evaluation of broiler breeder pullet vaccination programs for preventing clinical reovirus infections in the progeny. Poult Sci 65: 457–461. 1986.

53. Glass, S. E., S. A. Naqi, C. F. Hall, and K. M. Kerr. Isolation and characterization of a virus associated with arthritis of chickens. Avian Dis 17: 415–424. 1973.

54. Goldenberg, D., M. Pasmanik-Chor, M. Pirak, N. Kass, A. Lublin, A. Yeheskel, D. Heller, and J. Pitcovski. Genetic and antigenic characterization of sigma C protein from avian reovirus. Avian Pathol 39: 189–199. 2010.

55. González-López, C., J. Martínez-Costas, M. Esteban, and J. Benavente. Evidence that avian reovirus σA protein is an inhibitor of the double-stranded RNA-dependent protein kinase. J Gen Virol 84: 1629–1639. 2003.

56. Goossens, K. E., A. C. Ward, J. W. Lowenthal, and A. G. D. Bean. Chicken interferons, their receptors and interferon-stimulated genes. Dev Comp Immunol 41: 370–376. 2013.

57. Gouvea, V., D. D. Huang, T. Ramos, and T. J. Schnitzer. In vitro characterization of an avian reovirus vaccine strain. Virology 126: 240–247. 1983.

58. Gouvea, V., and T. J. Schnitzer. Pathogenicity of avian reoviruses: Examination of six isolates and a vaccine strain. Infect Immun 38: 731–738. 1982.

59. Grande, A., C. Costas, and J. Benavente. Subunit composition and conformational stability of the oligomeric form of the avian reovirus cell-attachment protein σC. J Gen Virol 83: 131–139. 2002.

60. Grande, A., E. Rodriguez, C. Costas, E. Everitt, and J. Benavente. Oligomerization and cell-binding properties of the avian reovirus cell-attachment protein σC. Virology 274: 367–377. 2000.

61. Guardado-Calvo, P., L. Vazquez-Iglesias, J. Martinez-Costas, A. L. Llamas-Saiz, G. Schoehn, G. C. Fox, X. L. Hermo-Parrado, J. Benavente, and M. J. van Raaij. Crystal Structure of the Avian Reovirus Inner Capsid Protein σA. J Virol 82: 11208–11216. 2008.

62. Gur Lavie, A., and J. Weisman. Infectious synovitis in Turkeys: Isolation of tenosynovitis virus-like agent. Avian Pathol 9: 1–4. 1980.

63. Heffels-Redmann, U., H. Müller, and E. F. Kaleta. Structural and Biological Characteristics of Reoviruses Isolated From Muscovy Ducks (Cairina Moschata). Avian Pathol 21: 481–491. 1992.

64. Heggen-Peay, C. L., M. A. Cheema, R. A. Ali, K. A. Schat, and M. A. Qureshi. Interactions of poult enteritis and mortality syndrome-associated reovirus with various cell types in vitro. Poult Sci 81: 1661–1667. 2002.

65. van der Heide, L., J. Geissler, and E. S. Bryant. Infectious tenosynovitis: serologic and histopathologic response after experimental infection with a Connecticut isolate. Avian Dis 18: 289–296. 1974.

66. van der Heide, L., M. Kalbac, and M. Brustolon. Development of an attenuated apathogenic reovirus vaccine against viral arthritis/tenosynovitis. Avian Dis 27: 698–706. 1983.

67. van der Heide, L., D. Lutticken, and M. Horzinek. Isolation of Avian Reovirus as a Possible Etiologic Agent of Osteoporosis (“Brittle Bone Disease”; “Femoral Head Necrosis”) in Broiler Chickens. Avian Dis 25: 847. 1981.

68. De Herdt, P., G. Paul, R. Koopman, and S. Van De Zande. Field experiences with ERS type reovirus infections in diseased broilers reared under Western European field circumstances. Vlaams Diergeneeskd Tijdschr 77: 171–175. 2008.

69. Hieronymus, D. R., P. Villegas, and S. H. Kleven. Identification and serological differentiation of several reovirus strains isolated from chickens with suspected malabsorption syndrome. Avian Dis 27: 246–254. 1983.

70. Hou, H. S., Y. P. Su, H. K. Shieh, and L. H. Lee. Monoclonal antibodies against different epitopes of nonstructural protein σNS of avian reovirus S1133. Virology 282: 168–175. 2001.

71. Hsiao, J., J. Martínez-Costas, J. Benavente, and V. N. Vakharia. Cloning, expression, and characterization of avian reovirus guanylyltransferase. Virology 296: 288–299. 2002.

72. Hsu, C.-Y., Y.-H. Chen, W.-R. Huang, J.-W. Huang, I.-C. Chen, Y.-K. Chang, C.-Y. Wang, C.-D. Chang, T.-L. Liao, B. L. Nielsen, and H.-J. Liu. Oncolytic avian reovirus σA-modulated fatty acid metabolism through the PSMB6/Akt/SREBP1/acetyl-CoA carboxylase pathway to increase energy production for virus replication. Vet Microbiol 273: 109545. 2022.

73. Hsu, H. W., H. Y. Su, P. H. Huang, L. H. Lee, and H. J. Liu. Sequence and phylogenetic analysis of P10- and P17-encoding genes of avian reovirus. Avian Dis 49: 36–42. 2005.

74. Huang, D. D., M. A. Nugent, J. K. Rosenberger, and T. J. Schnitzer. Association of avian reovirus M and S genes with viral behavior in vivo. I. Viral persistence. Avian Dis 31: 438–445. 1987.

75. Huang, L., Z. Xie, L. Xie, S. Wang, J. Huang, Q. Fan, S. Luo, Y. Zhang, T. Zeng, M. Zhang, X. Deng, and Z. Xie. Regulation of avian reovirus σA gene on expression of innate immune genes in chicken embryo fibroblasts. Chinese Veterinary Science 49: 611–618. 2019.

76. Huang, P. H., Y. J. Li, Y. P. Su, L. H. Lee, and H. J. Liu. Epitope mapping and functional analysis of sigma A and sigma NS proteins of avian reovirus. Virology 332: 584–595. 2005.

77. Huang, W., J.-Y. Li, Y.-Y. Wu, T.-L. Liao, B. L. Nielsen, and H.-J. Liu. p17-Modulated Hsp90/Cdc37 Complex Governs Oncolytic Avian Reovirus Replication by Chaperoning p17, Which Promotes Viral Protein Synthesis and Accumulation of Viral Proteins σC and σA in Viral Factories. J Virol 96: e0007422. 2022.

78. Huang, W.-R., P.-I. Chi, H.-C. Chiu, J.-L. Hsu, B. L. Nielsen, T.-L. Liao, and H.-J. Liu. Avian reovirus p17 and σA act cooperatively to downregulate Akt by suppressing mTORC2 and CDK2/cyclin A2 and upregulating proteasome PSMB6. Sci Rep 7: 5226. 2017.

79. Huang, W.-R., H.-C. Chiu, T.-L. Liao, K.-P. Chuang, W.-L. Shih, and H.-J. Liu. Avian Reovirus Protein p17 Functions as a Nucleoporin Tpr Suppressor Leading to Activation of p53, p21 and PTEN and Inactivation of PI3K/AKT/mTOR and ERK Signaling Pathways. PLoS One 10: e0133699. 2015.

80. Huang, W.-R., J.-Y. Li, T.-L. Liao, C.-M. Yeh, C.-Y. Wang, H.-W. Wen, N.-J. Hu, Y.-Y. Wu, C.-Y. Hsu, Y.-K. Chang, C.-D. Chang, B. L. Nielsen, and H.-J. Liu. Molecular chaperone TRiC governs avian reovirus replication by protecting outer-capsid protein σC and inner core protein σA and non-structural protein σNS from ubiquitin- proteasome degradation. Vet Microbiol 264: 109277. 2022.

81. Huang, W. R., Y. C. Wang, P. I. Chi, L. Wang, C. Y. Wang, C. H. Lin, and H. J. Liu. Cell entry of avian reovirus follows a caveolin-1-mediated and dynamin-2-dependent endocytic pathway that requires activation of p38 Mitogen-activated Protein Kinase (MAPK) and Src signaling pathways as well as microtubules and small GTPase Rab5 protein. J Biol Chem 286: 30780–30794. 2011.

82. Hung Jen Liu, and Pi Hsin Huang. Sequence and phylogenetic analysis of the σA-encoding gene of avian reovirus. J Virol Methods 98: 99–107. 2001.

83. Jeurissen, S. H. M., F. Wagenaar, and E. M. Janse. Further characterization of M cells in gut-associated lymphoid tissues of the chicken. Poult Sci 78: 965–972. 1999.

84. Ji, W. T., J. L. C. Chulu, F. L. Lin, S. K. Li, L. H. Lee, and H. J. Liu. Suppression of protein expression of three avian reovirus S-class genome segments by RNA interference. Vet Microbiol 129: 252–261. 2008.

85. Ji, W. T., L. H. Lee, F. L. Lin, L. Wang, and H. J. Liu. AMP-activated protein kinase facilitates avian reovirus to induce mitogen-activated protein kinase (MAPK) p38 and MAPK kinase 3/6 signalling that is beneficial for virus replication. J Gen Virol 90: 3002–3009. 2009.

86. Ji, W. T., F. L. Lin, Y. C. Wang, W. L. Shih, L. H. Lee, and H. J. Liu. Intracellular cleavage of σA protein of avian reovirus. Virus Res 149: 71–77. 2010.

87. Ji, W. T., L. Wang, R. C. Lin, W. R. Huang, and H. J. Liu. Avian reovirus influences phosphorylation of several factors involved in host protein translation including eukaryotic translation elongation factor 2 (eEF2) in Vero cells. Biochem Biophys Res Commun 384: 301–305. 2009.

88. Johnson, D. C. Diagnosis, pathology, and etiology of tenosynovitis in broilers and broiler breeders. Avian Dis 16: 1067–1072. 1972.

89. Jones, R. C. Characteristics of reovirus isolated from ruptured gastrocnemius tendons of chickens. Veterinary Record 96: 153. 1975.

90. Jones, R. C., and J. R. M. Guneratne. The pathogenicity of some avian reoviruses with particular reference to tenosynovitis. Avian Pathol 13: 173–189. 1984.

91. Jones, R. C., M. R. Islam, and D. F. Kelly. Early pathogenesis of experimental reovirus infection in chickens. Avian Pathol 18: 239–253. 1989.

92. Jones, R. C., and F. S. B. Kibenge. Reovirus-induced tenosynovitis in chickens: The effect of breed. Avian Pathol 13: 511–528. 1984.

93. Jones, R. C., and B. N. Nwajei. Reovirus-induced tenosynovitis: persistence of homologous challenge virus in broiler chicks after vaccination of parents. Res Vet Sci 39: 39–41. 1985.

94. Jones, R. C., and O. Onunkwo. Studies on experimental tenosynovitis in light hybrid chickens. Avian Pathol 7: 171–181. 1978.

95. Jones, R. C., C. E. Savage, A. Al-Afaleq, and M. R. Islam. Early pathogenesis in chicks of infection with a trypsin-sensitive avian reovirus. Avian Pathol 23: 683–692. 1994.

96. Kawamura, H., and H. Tsubahara. Common antigenicity of avian reoviruses. Natl Inst Anim Health Q (Tokyo) 6: 187–193. 1966.

97. Kerr, K. M., and N. O. Olson. Pathology of chickens experimentally inoculated or contact-infected with an arthritis-producing virus. Avian Dis 13: 729–745. 1969.

98. Key, T., and R. Duncan. A Compact, Multifunctional Fusion Module Directs Cholesterol-Dependent Homomultimerization and Syncytiogenic Efficiency of Reovirus p10 FAST Proteins. PLoS Pathog 10: e1004023. 2014.

99. Key, T., M. Sarker, R. de Antueno, J. K. Rainey, and R. Duncan. The p10 FAST protein fusion peptide functions as a cystine noose to induce cholesterol-dependent liposome fusion without liposome tubulation. Biochimica et Biophysica Acta (BBA) - Biomembranes 1848: 408–416. 2015.

100. Kibenge, F. S. B., G. E. Gwaze, R. C. Jones, A. F. Chapman, and C. E. Savage. Experimental reovirus infection in chickens: Observations on early viraemia and virus distribution in bone marrow, liver and enteric tissues. Avian Pathol 14: 87–98. 1985.

101. Kibenge, F. S. B., R. C. Jones, and C. E. Savage. Effects of experimental immunosuppression on reovirus-induced tenosynovitis in light-hybrid chickens. Avian Pathol 16: 73–92. 1987.

102. Krasselt, M., and E. J. Voute. Synovitis bij slachtkuikenouderdieren [Synovitis in broiler parent chickens]. Tijdschrift voor diergeneeskunde [Netherlands journal of veterinary science] 94: 601–607. 1969.

103. Kuntz-Simon, G., G. Le Gall-Reculé, C. de Boisséson, and V. Jestin. Muscovy duck reovirus σC protein is atypically encoded by the smallest genome segment. J Gen Virol 83: 1189–1200. 2002.

104. Labrada, L., G. Bodelón, J. Viñuela, and J. Benavente. Avian Reoviruses Cause Apoptosis in Cultured Cells: Viral Uncoating, but Not Viral Gene Expression, Is Required for Apoptosis Induction. J Virol 76: 7932–7941. 2002.

105. Liemann, S., K. Chandran, T. S. Baker, M. L. Nibert, and S. C. Harrison. Structure of the Reovirus Membrane-Penetration Protein, μ1, in a Complex with Its Protector Protein, σ3. Cell 108: 283–295. 2002.

106. Li, J.-Y., W.-R. Huang, T.-L. Liao, B. L. Nielsen, and H.-J. Liu. Oncolytic Avian Reovirus p17-Modulated Inhibition of mTORC1 by Enhancement of Endogenous mTORC1 Inhibitors Binding to mTORC1 To Disrupt Its Assembly and Accumulation on Lysosomes. J Virol 96: e00836-22. 2022.

107. Li, M., P. Yan, Z. Liu, D. Cai, Y. Luo, X. Wu, Q. Wang, Y. Huang, and Y. Wu. Muscovy duck reovirus enters susceptible cells via a caveolae-mediated endocytosis-like pathway. Virus Res 276: 197806. 2020.

108. Li, M., P. Yan, X. Shen, Z. Liu, Q. Wang, Y. Huang, and Y. Wu. Muscovy duck reovirus promotes virus replication by inhibiting autophagy-lysosomal degradation pathway. Vet Microbiol 253: 108945. 2021.

109. Lin, H. Y., S. T. Chuang, Y. T. Chen, W. L. Shih, C. D. Chang, and H. J. Liu. Avian reovirus-induced apoptosis related to tissue injury. Avian Pathol 36: 155–159. 2007.

110. Lin, P. Y., J. W. Lee, M. H. Liao, H. Y. Hsu, S. J. Chiu, H. J. Liu, and W. L. Shih. Modulation of p53 by mitogen-activated protein kinase pathways and protein kinase C δ during avian reovirus S1133-induced apoptosis. Virology 385: 323–334. 2009.

111. Lin, P.-Y., H.-J. Liu, C.-D. Chang, C.-I. Chang, J.-L. Hsu, M.-H. Liao, J.-W. Lee, and W.-L. Shih. Avian reovirus S1133-induced DNA damage signaling and subsequent apoptosis in cultured cells and in chickens. Arch Virol 156: 1917–1929. 2011.

112. Lin, P. Y., H. J. Liu, C. D. Chang, Y. C. Chen, C. I. Chang, and W. L. Shih. Avian reovirus S1133-induced apoptosis is associated with Bip/GRP78-mediated Bim translocation to the endoplasmic reticulum. Apoptosis 20: 481–490. 2015.

113. Lin, P.-Y., H.-J. Liu, M.-J. Lai, F.-L. Yu, H.-Y. Hsu, J.-W. Lee, and W.-L. Shih. Avian Reovirus activates a novel proapoptotic signal by linking Src to p53. Apoptosis 11: 2179–2193. 2006.

114. Lin, P. Y., H. J. Liu, M. H. Liao, C. D. Chang, C. I. Chang, H. L. Cheng, J. W. Lee, and W. L. Shih. Activation of PI 3-kinase/Akt/NF-κB and Stat3 signaling by avian reovirus S1133 in the early stages of infection results in an inflammatory response and delayed apoptosis. Virology 400: 104–114. 2010.

115. Lin, Y. H., L. H. Lee, W. L. Shih, Y. C. Hu, and H. J. Liu. Baculovirus surface display of σC and σB proteins of avian reovirus and immunogenicity of the displayed proteins in a mouse model. Vaccine 26: 6361–6367. 2008.

116. Liu, H. J., and J. J. Giambrone. Amplification, cloning and sequencing of the σC-encoded gene of avian reovirus. J Virol Methods 63: 203–208. 1997.

117. Liu, H. J., and J. J. Giambrone. In situ detection of reovirus in formalin-fixed, paraffin-embedded chicken tissues using a digoxigenin-labeled cDNA probe. Avian Dis 41: 447–451. 1997.

118. Liu, H. J., L. H. Lee, H. W. Hsu, L. C. Kuo, and M. H. Liao. Molecular evolution of avian reovirus: Evidence for genetic diversity and reassortment of the S-class genome segments and multiple cocirculating lineages. Virology 314: 336–349. 2003.

119. Liu, H. J., P. Y. Lin, J. W. Lee, H. Y. Hsu, and W. L. Shih. Retardation of cell growth by avian reovirus p17 through the activation of p53 pathway. Biochem Biophys Res Commun 336: 709–715. 2005.

120. Liu, H. J., P. Y. Lin, L. R. Wang, H. Y. Hsu, M. H. Liao, and W. L. Shih. Activation of small GTPases RhoA and Rac1 is required for Avian Reovirus p10-induced syncytium formation. Mol Cells 26: 396–403. 2008.

121. Lostalé-Seijo, I., J. Martínez-Costas, and J. Benavente. Interferon induction by avian reovirus. Virology 487: 104–111. 2016.

122. Lublin, A., D. Goldenberg, E. Rosenbluth, E. D. Heller, and J. Pitcovski. Wide-range protection against avian reovirus conferred by vaccination with representatives of four defined genotypes. Vaccine 29: 8683–8688. 2011.

123. Lu, H., Y. Tang, P. A. Dunn, E. A. Wallner-Pendleton, L. Lin, and E. A. Knoll. Isolation and molecular characterization of newly emerging avian reovirus variants and novel strains in Pennsylvania, USA, 2011-2014. Sci Rep 5: 1–11. 2015.

124. Macdonald, J. W., C. J. Randall, M. D. Dagless, and D. A. McMartin. Observations on viral tenosynovitis (viral arthritis) in scotland. Avian Pathol 7: 471–482. 1978.

125. Mandelli, G., T. Rampin, and M. Finazzi. Experimental reovirus hepatitis in newborn chicks. Vet Pathol 15: 531–543. 1978.

126. Manocha, E., A. Bugatti, M. Belleri, A. Zani, S. Marsico, F. Caccuri, M. Presta, and A. Caruso. Avian reovirus p17 suppresses angiogenesis by promoting dpp4 secretion. Cells 10: 1–19. 2021.

127. Marcus, P. I., J. M. Rojek, and M. J. Sekellick. Interferon Induction and/or Production and Its Suppression by Influenza A Viruses. J Virol 79: 2880–2890. 2005.

128. Martínez-Costas, J., C. González-López, V. N. Vakharia, and J. Benavente. Possible Involvement of the Double-Stranded RNA-Binding Core Protein σA in the Resistance of Avian Reovirus to Interferon. J Virol 74: 1124–1131. 2000.

129. Martínez-Costas, J., A. Grande, R. Varela, C. García-Martínez, and J. Benavente. Protein architecture of avian reovirus S1133 and identification of the cell attachment protein. J Virol 71: 59–64. 1997.

130. Martinez-Costas, J., R. Varela, and J. Benavente. Endogenous enzymatic activities of the avian reovirus S1133: Identification of the viral capping enzyme. Virology 206: 1017–1026. 1995.

131. Meanger, J., R. Wickramasinghe, C. E. Enriquez, M. D. Robertson, and G. E. Wilcox. Type-specific antigenicity of avian reoviruses. Avian Pathol 24: 121–134. 1995.

132. Menendez, N. A., B. W. Calnek, and B. S. Cowen. Experimental egg transmission of avian reovirus. Avian Dis 19: 104–111. 1975.

133. Menendez, N. A., B. W. Calnek, and B. S. Cowen. Localization of avian reovirus (FDO isolant) in tissues of mature chickens. Avian Dis 19: 112–117. 1975.

134. Meng, S., K. Jiang, X. Zhang, M. Zhang, Z. Zhou, M. Hu, R. Yang, C. Sun, and Y. Wu. Avian reovirus triggers autophagy in primary chicken fibroblast cells and Vero cells to promote virus production. Arch Virol 157: 661–668. 2012.

135. Mills, J. N., and G. E. Wilcox. Replication of four antigenic types of avian reovirus in subpopulations of chicken leukocytes. Avian Pathol 22: 353–361. 1993.

136. Mor, S. K., D. Marthaler, H. Verma, T. A. Sharafeldin, N. Jindal, R. E. Porter, and S. M. Goyal. Phylogenetic analysis, genomic diversity and classification of M class gene segments of turkey reoviruses. Vet Microbiol 176: 70–82. 2015.

137. Mor, S. K., T. A. Sharafeldin, R. E. Porter, and S. M. Goyal. Molecular characterization of L class genome segments of a newly isolated turkey arthritis reovirus. Infect Genet Evol 27: 193–201. 2014.

138. Mor, S. K., T. A. Sharafeldin, R. E. Porter, A. Ziegler, D. P. Patnayak, and S. M. Goyal. Isolation and characterization of a Turkey arthritis reovirus. Avian Dis 57: 97–103. 2013.

139. Niu, X., Y. Wang, M. Li, X. Zhang, and Y. Wu. Transcriptome analysis of avian reovirus-mediated changes in gene expression of normal chicken fibroblast DF-1 cells. BMC Genomics 18: 911. 2017.

140. Niu, X., C. Zhang, Y. Wang, M. Guo, B. Ruan, X. Wang, T. Wu, X. Zhang, and Y. Wu. Autophagy induced by avian reovirus enhances viral replication in chickens at the early stage of infection. BMC Vet Res 15: 173. 2019.

141. Ni, Y., and M. C. Kemp. A comparative study of avian reovirus pathogenicity: Virus spread and replication and induction of lesions. Avian Dis 39: 554–566. 1995.

142. Ni, Y., and R. F. Ramig. Characterization of Avian Reovirus-Induced Cell Fusion: The Role of Viral Structural Proteins. Virology 194: 705–714. 1993.

143. Ni, Y., R. F. Ramig, and M. C. Kemp. Identification of proteins encoded by avian reoviruses and evidence for post-translational modification. Virology 193: 466–469. 1993.

144. Noad, L., J. Shou, K. M. Coombs, and R. Duncan. Sequences of avian reovirus M1, M2 and M3 genes and predicted structure/function of the encoded μ proteins. Virus Res 116: 45–57. 2006.

145. O'Hara, D., M. Patrick, D. Cepica, K. M. Coombs, and R. Duncan. Avian Reovirus Major μ-Class Outer Capsid Protein Influences Efficiency of Productive Macrophage Infection in a Virus Strain-Specific Manner. J Virol 75: 5027–5035. 2001.

146. Olson, N. O., and M. A. Khan. The effect of intranasal exposure of chickens to the Fahey-Crawley virus on the development of synovial lesions. Avian Dis 16: 1073–1078. 1972.

147. Olson, N. O., D. C. Shelton, and D. A. Munro. Infectious synovitis control by medication; effect of strain differences and pleuropneumonia-like organisms. Am J Vet Res 18: 735–739. 1957.

148. Olson, N. O., and R. Weiss. Similarity between arthritis virus and Fahey-Crawley virus. Avian Dis 16: 535–540. 1972.

149. Palomino-Tapia, V., D. Mitevski, T. Inglis, F. van der Meer, and M. F. Abdul-Careem. Molecular characterization of emerging avian reovirus variants isolated from viral arthritis cases in Western Canada 2012–2017 based on partial sigma (σ)C gene. Virology 522: 138–146. 2018.

150. Petek, M., B. Felluga, G. Borghi, and A. Baroni. The Crawley agent: An avian reovirus. Arch Gesamte Virusforsch 21: 413–424. 1967.

151. Pitcovski, J., and S. M. Goyal. Avian Reovirus Infections. In: Diseases of Poultry, Fourteenth. vol. 1. D. F. Swayne, ed. Wiley. pp. 382–400. 2020.

152. Praharaj, M. R., A. P. Sahoo, T. K. S. Chauhan, R. K. Gandham, S. Saxena, R. K. Agarwal, K. Dhama, B. Mishra, A. K. Marriappan, A. K. Tiwari, P. P. Goswami, B. P. Mishra, and D. Kumar. In vitro study on role of σB protein in avian reovirus pathogenesis. Oncotarget 9: 19569–19583. 2018.

153. Rau, W. E., L. van der Heide, M. Kalbac, and T. Girshick. Onset of Progeny Immunity against Viral Arthritis / Tenosynovitis after Experimental Vaccination of Parent Breeder Chickens and Cross-Immunity against Six Reovirus Isolates. Avian Dis 24: 648–657. 1980.

154. Rodríguez-Grille, J., L. K. Busch, J. Martínez-Costas, and J. Benavente. Avian reovirus-triggered apoptosis enhances both virus spread and the processing of the viral nonstructural muNS protein. Virology 462–463: 49–59. 2014.

155. Roessler, D. E., and J. K. Rosenberger. In vitro and in vivo characterization of avian reoviruses. III. Host factors affecting virulence and persistence. Avian Dis 33: 555–565. 1989.

156. Rohde, F., B. Schusser, T. Hron, H. Farkašová, J. Plachý, S. Härtle, J. Hejnar, D. Elleder, and B. Kaspers. Characterization of Chicken Tumor Necrosis Factor-α, a Long Missed Cytokine in Birds. Front Immunol 9: 605. 2018.

157. Rosenberger, J. K., F. J. Sterner, S. Botts, K. P. Lee, and A. Margolin. In vitro and in vivo characterization of avian reoviruses. I. Pathogenicity and antigenic relatedness of several avian reovirus isolates. Avian Dis 33: 535–544. 1989.

158. Rothwell, L., J. R. Young, R. Zoorob, C. A. Whittaker, P. Hesketh, A. Archer, A. L. Smith, and P. Kaiser. Cloning and Characterization of Chicken IL-10 and Its Role in the Immune Response to Eimeria maxima. The Journal of Immunology 173: 2675–2682. 2004.

159. Sahu, S. P. Comparison of the characteristics of avian reoviruses isolated from the digestive and respiratory tract, with viruses isolated from the synovia. Am J Vet Res 36: 847. 1975.

160. Sahu, S. P., N. O. Olson, and R. W. Townsend. Characterization of Avian Reoviruses Isolated from the Synovia and Breast Blister. Avian Dis 23: 896–903. 1979.

161. Salsman, J., D. Top, J. Boutilier, and R. Duncan. Extensive Syncytium Formation Mediated by the Reovirus FAST Proteins Triggers Apoptosis-Induced Membrane Instability. J Virol 79: 8090–8100. 2005.

162. Samuel, C. E. Antiviral actions of interferons. Clin Microbiol Rev 14: 778–809. 2001.

163. Schnitzer, T. J. Protein coding assignment of the S genes of the avian reovirus S1133. Virology 141: 167–170. 1985.

164. Schnitzer, T. J., T. Ramos, and V. Gouvea. Avian Reovirus Polypeptides: Analysis of Intracellular Virus-Specified Products, Virions, Top Component, and Cores. J Virol 43: 1006–1014. 1982.

165. Sellers, H. S. Current limitations in control of viral arthritis and tenosynovitis caused by avian reoviruses in commercial poultry. Vet Microbiol 206: 152–156. 2017.

166. Shapouri, M. R. S., M. Arella, and A. Silim. Evidence for the multimeric nature and cell binding ability of avian reovirus σ3 protein. J Gen Virol 77: 1203–1210. 1996.

167. Shapouri, M. R. S., D. Frenette, R. Larochelle, M. Arella, and A. Silim. Characterization of monoclonal antibodies against avian reovirus strain S1133. Avian Pathol 25: 57–67. 1996.

168. Shapouri, M. R. S., M. Kane, M. Letarte, J. Bergeron, M. Arella, and A. Silim. Cloning, sequencing and expression of the S1 gene of avian reovirus. J Gen Virol 76: 1515–1520. 1995.

169. Sharafeldin, T. A., S. K. Mor, A. Z. Bekele, H. Verma, S. M. Goyal, and R. E. Porter. The role of avian reoviruses in turkey tenosynovitis/arthritis. Avian Pathol 43: 371–378. 2014.

170. Shen, P. C., Y. F. Chiou, H. J. Liu, C. H. Song, Y. P. Su, and L. H. Lee. Genetic variation of the λA and λC protein encoding genes of avian reoviruses. Res Vet Sci 83: 394–402. 2007.

171. Shen, P.-C., J.-L. Yang, B.-S. Su, and L.-H. Lee. Cytokine mRNA Expression in Chicken Experimentally Infected with Different Avian Reovirus Strains. Taiwan Veterinary Journal 40: 29–36. 2014.

172. Shih, W. L., H. W. Hsu, M. H. Liao, L. H. Lee, and H. J. Liu. Avian reovirus σC protein induces apoptosis in cultured cells. Virology 321: 65–74. 2004.

173. Shmulevitz, M., J. Corcoran, J. Salsman, and R. Duncan. Cell-Cell Fusion Induced by the Avian Reovirus Membrane Fusion Protein Is Regulated by Protein Degradation. J Virol 78: 5996–6004. 2004.

174. Shmulevitz, M., and R. Duncan. A new class of fusion-associated small transmembrane (FAST) proteins encoded by the non-enveloped fusogenic reoviruses. EMBO Journal 19: 902–912. 2000.

175. Shmulevitz, M., J. Salsman, and R. Duncan. Palmitoylation, Membrane-Proximal Basic Residues, and Transmembrane Glycine Residues in the Reovirus p10 Protein Are Essential for Syncytium Formation. J Virol 77: 9769–9779. 2003.

176. Songserm, T., D. van Roozelaar, A. Kant, J. Pol, A. Pijpers, and A. Ter Huurne. Enteropathogenicity of Dutch and German avian reoviruses in SPF white leghorn chickens and broilers. Vet Res 34: 285–295. 2003.

177. Spandidos, D. A., and A. F. Graham. Physical and chemical characterization of an Avian Reovirus. J Virol 19: 968–976. 1976.

178. Staeheli, P., F. Puehler, K. Schneider, T. W. Göbel, and B. Kaspers. Cytokines of Birds: Conserved Functions—A Largely Different Look. J Interferon Cytokine Res21: 993–1010. 2001.

179. Starnes, M. C., and W. K. Joklik. Reovirus protein λ3 is a poly(c)-dependent poly(g) polymerase. Virology 193: 356–366. 1993.

180. Su, Y. P., J. H. Shien, H. J. Liu, H. S. Yin, and L. H. Lee. Avian reovirus core protein μA expressed Escherichia coli possesses both NTPase and RTPase activities. J Gen Virol 88: 1797–1805. 2007.

181. Su, Y. P., B. S. Su, J. H. Shien, H. J. Liu, and L. H. Lee. The sequence and phylogenetic analysis of avian reovirus genome segments M1, M2, and M3 encoding the minor core protein μa, the major outer capsid protein μB, and the nonstructural protein μNS. J Virol Methods 133: 146–157. 2006.

182. Tang, J., M. Fu, X. Chen, Y. Zhao, L. Gao, H. Cao, X. Li, S. J. Zheng, and Y. Wang. Arrest of Cell Cycle by Avian Reovirus p17 through Its Interaction with Bub3. Viruses 14: 2385. 2022.

183. Tang, K. N., and O. J. Fletcher. Application of the avidin-biotin-peroxidase complex (ABC) technique for detecting avian reovirus in chickens. Avian Dis 31: 591–596. 1987.

184. Tang, K. N., O. J. Fletcher, and P. Villegas. Comparative study of the pathogenicity of avian reoviruses. Avian Dis 31: 577–583. 1987.

185. Teng, L., Z. Xie, L. Xie, J. Liu, Y. Pang, X. Deng, Z. Xie, Q. Fan, and S. Luo. Complete Genome Sequences of an Avian Orthoreovirus Isolated from Guangxi, China. Genome Announc 1: e00495-13. 2013.

186. Tenorio, R., I. Fernández de Castro, J. J. Knowlton, P. F. Zamora, C. H. Lee, B. A. Mainou, T. S. Dermody, and C. Risco. Reovirus σNS and μNS Proteins Remodel the Endoplasmic Reticulum to Build Replication Neo-Organelles. mBio 9: e01253-18. 2018.

187. Tourís-Otero, F., M. Cortez-San Martín, J. Martínez-Costas, and J. Benavente. Avian reovirus morphogenesis occurs within viral factories and begins with the selective recruitment of σNS and λA to μNS inclusions. J Mol Biol 341: 361–374. 2004.

188. Touris-Otero, F., J. Martínez-Costas, V. N. Vakharia, and J. Benavente. Avian reovirus nonstructural protein μNS forms viroplasm-like inclusions and recruits protein σNS to these structures. Virology 319: 94–106. 2004.

189. Tourís-Otero, F., J. Martínez-Costas, V. N. Vakharia, and J. Benavente. Characterization of the nucleic acid-binding activity of the avian reovirus non-structural protein σNS. J Gen Virol 86: 1159–1169. 2005.

190. Troxler, S., P. Rigomier, I. Bilic, D. Liebhart, I. Prokofieva, B. Robineau, and M. Hess. Identification of a new reovirus causing substantial losses in broiler production in France, despite routine vaccination of breeders. Veterinary Record 172: 556. 2013.

191. Varela, R., and J. Benavente. Protein Coding Assignment of Avian Reovirus Strain S1133. J Virol 68: 6775–6777. 1994.

192. Varela, R., J. Martínez-Costas, M. Mallo, and J. Benavente. Intracellular posttranslational modifications of S1133 avian reovirus proteins. J Virol 70: 2974–2981. 1996.

193. Vázquez-Iglesias, L., I. Lostalé-Seijo, J. Martínez-Costas, and J. Benavente. Avian Reovirus SigmaA Localizes to the Nucleolus and Enters the Nucleus by a Nonclassical Energy- and Carrier-Independent Pathway. J Virol 83: 10163–10175. 2009.

194. Walker, E. R., M. H. Friedman, and N. O. Olson. Electron microscopic study of an avian reovirus that causes arthritis. J Ultrastruct Res 41: 67–79. 1972.

195. Wang, Q., W. R. Huang, W. Y. Chih, K. P. Chuang, C. D. Chang, Y. Wu, Y. Huang, and H. J. Liu. Cdc20 and molecular chaperone CCT2 and CCT5 are required for the Muscovy duck reovirus p10.8-induced cell cycle arrest and apoptosis. Vet Microbiol 235: 151–163. 2019.

196. Wang, Q., X. Yuan, C. Li, H. Deng, and C. K. Wang. Distribution of ifitm3 in yellow-feathered broilers and inhibition of avian reovirus multiplication by IFITM3. Rev Bras Cienc Avic 20: 377–386. 2018.

197. Wang, S., L. Wan, H. Ren, Z. Xie, L. Xie, J. Huang, X. Deng, Z. Xie, S. Luo, M. Li, T. Zeng, Y. Zhang, and M. Zhang. Screening of interferon-stimulated genes against avian reovirus infection and mechanistic exploration of the antiviral activity of IFIT5. Front Microbiol 13: 1–15. 2022.

198. Wang, S., L. Xie, Z. Xie, L. Wan, J. Huang, X. Deng, Z. qin Xie, S. Luo, T. Zeng, Y. Zhang, M. Zhang, and L. Zhou. Dynamic Changes in the Expression of Interferon-Stimulated Genes in Joints of SPF Chickens Infected With Avian Reovirus. Front Vet Sci 8. 2021.

199. Wang, Y., Y. Zhang, C. Zhang, M. Hu, Q. Yan, H. Zhao, X. Zhang, and Y. Wu. Cholesterol-Rich Lipid Rafts in the Cellular Membrane Play an Essential Role in Avian Reovirus Replication. Front Microbiol 11. 2020.

200. Wang, Y., Y. Zhang, W. Zuo, Z. Bo, C. Zhang, X. Zhang, and Y. Wu. Avian Reovirus σB Interacts with Caveolin-1 in Lipid Rafts during Dynamin-Dependent Caveolae-Mediated Endocytosis. Viruses 14. 2022.

201. Wickramasinghe, R., J. Meanger, C. E. Enriquez, and G. E. Wilcox. Avian reovirus proteins associated with neutralization of virus infectivity. Virology 194: 688–696. 1993.

202. Williams, L. M., U. Sarma, K. Willets, T. Smallie, F. Brennan, and B. M. J. Foxwell. Expression of constitutively active STAT3 can replicate the cytokine-suppressive activity of interleukin-10 in human primary macrophages. J Biol Chem 282: 6965–6975. 2007.

203. Wood, G. W., J. C. Muskett, and D. H. Thornton. Observations on the ability of avian reovirus vaccination of hens to protect their progeny against the effects of challenge with homologous and heterologous strains. J Comp Pathol 96: 125–129. 1986.

204. Wood, G. W., R. A. J. Nicholas, C. N. Hebert, and D. H. Thornton. Serological comparisons of avian reoviruses. J Comp Pathol 90: 29–38. 1980.

205. Wu, H., Z. He, J. Tang, X. Li, H. Cao, Y. Wang, and S. J. Zheng. A critical role of LAMP-1 in avian reovirus P10 degradation associated with inhibition of apoptosis and virus release. Arch Virol 161: 899–911. 2016.

206. Wu, Y., L. Cui, E. Zhu, W. Zhou, Q. Wang, X. Wu, B. Wu, Y. Huang, and H.-J. Liu. Muscovy duck reovirus σNS protein triggers autophagy enhancing virus replication. Virol J 14: 53. 2017.

207. Wu, Y. F., H. J. Liu, J. H. Shien, S. H. Chiou, and L. H. Lee. Characterization of interleukin-1 b mRNA expression in chicken macrophages in response to avian reovirus. J Gen Virol 89: 1059–1068. 2008.

208. Xiao, R., X. Mi, J. Sun, M. Ding, C. Li, J. Zhu, G. Liu, W. Ma, H. Zhou, and Z. Chen. Interaction between Translocation-associated membrane protein 1 and σC protein of novel duck reovirus controls virus infectivity. Virus Genes 56: 347–353. 2020.

209. Xie, L., S. Wang, Z. Xie, X. Wang, L. Wan, X. Deng, Z. Xie, S. Luo, T. Zeng, M. Zhang, Q. Fan, J. Huang, Y. Zhang, and M. Li. Gallus NME/NM23 nucleoside diphosphate kinase 2 interacts with viral σA and affects the replication of avian reovirus. Vet Microbiol 252: 108926. 2021.

210. Xie, L., Z. Xie, L. Huang, Q. Fan, S. Luo, J. Huang, X. Deng, Z. Xie, T. Zeng, Y. Zhang, and S. Wang. Avian reovirus σA and σNS proteins activate the phosphatidylinositol 3-kinase-dependent Akt signalling pathway. Arch Virol 161: 2243–2248. 2016.

211. Xie, L., Z. Xie, S. Wang, X. Deng, and Z. Xie. Study of the activation of the PI3K/Akt pathway by the motif of σA and σNS proteins of avian reovirus. Innate Immun 26: 312–318. 2020.

212. Xie, L., Z. Xie, S. Wang, J. Huang, X. Deng, Z. Xie, S. Luo, T. Zeng, Y. Zhang, and M. Zhang. Altered gene expression profiles of the MDA5 signaling pathway in peripheral blood lymphocytes of chickens infected with avian reovirus. Arch Virol 164: 2451–2458. 2019.

213. Xie, Z., C. Qin, L. Xie, J. Liu, Y. Pang, X. Deng, Z. Xie, and M. I. Khan. Recombinant protein-based ELISA for detection and differentiation of antibodies against avian reovirus in vaccinated and non-vaccinated chickens. J Virol Methods 165: 108–111. 2010.

214. Xu, W., and K. M. Coombs. Avian reovirus L2 genome segment sequences and predicted structure/function of the encoded RNA-dependent RNA polymerase protein. Virol J 5: 1–11. 2008.

215. Xu, W., and K. M. Coombs. Conserved structure/function of the orthoreovirus major core proteins. Virus Res 144: 44–57. 2009.

216. Xu, W., M. K. Patrick, P. R. Hazelton, and K. M. Coombs. Avian Reovirus Temperature-Sensitive Mutant tsA12 Has a Lesion in Major Core Protein σA and Is Defective in Assembly. J Virol 78: 11142–11151. 2004.

217. Yasuda, K., K. Nakanishi, and H. Tsutsui. Interleukin-18 in Health and Disease. Int J Mol Sci 20: 649. 2019.

218. Yin, C., L. Qin, M. Sun, Y. Gao, X. Qi, H. Gao, Y. Wang, and X. Wang. Antigenic Analysis of Monoclonal Antibodies against Different Epitopes of σB Protein of Avian Reovirus. PLoS One 8: e81533. 2013.

219. Yin, H. S., and L. H. Lee. Identification and characterization of RNA-binding activities of avian reovirus non-structural protein σNS. J Gen Virol 79: 1411–1413. 1998.

220. Yin, H. S., and L. H. Lee. Characterization of avian reovirus non structural protein σNS synthesized in Escherichia coli. Virus Res 67: 1–9. 2000.

221. Yin, H. S., H. K. Shieh, and L. H. Lee. Characterization of the double-stranded RNA genome segment S3 of avian reovirus. J Virol Methods 67: 93–101. 1997.

222. Yin, H. S., J. H. Shien, and L. H. Lee. Synthesis in Escherichia coli of avian reovirus core protein σA and its dsRNA-binding activity. Virology 266: 33–41. 2000.

223. Yin, H. S., Y. P. Su, and L. H. Lee. Evidence of nucleotidyl phosphatase activity associated with core protein σA of avian reovirus S1133. Virology 293: 379–385. 2002.

224. Van de Zande, S., and E. M. Kuhn. Central nervous system signs in chickens caused by a new avian reovirus strain: A pathogenesis study. Vet Microbiol 120: 42–49. 2007.

225. Zhang, C., J. Hu, X. Wang, Y. Wang, M. Guo, X. Zhang, and Y. Wu. Avian reovirus infection activate the cellular unfold protein response and induced apoptosis via ATF6-dependent mechanism. Virus Res 297: 198346. 2021.

226. Zhang, C., X. Liu, F. Zhao, Q. Zhang, W. Zuo, M. Guo, X. Zhang, and Y. Wu. Identification and Functional Analyses of Host Proteins Interacting with the p17 Protein of Avian Reovirus. Viruses 14: 892. 2022.

227. Zhang, K., Z. Xie, L. Huang, L. Xie, X. Deng, Z. Xie, J. Liu, Q. Fan, and SiSi. Luo. The dynamic change of IL-17, IL-18 and IFN-γ mRNA transcription level in chicken embryo fibroblast infected with avian reovirus. Chinese Journal of Veterinary Science 35: 345–349. 2015.

228. Zhang, X., J. Tang, S. B. Walker, D. O'Hara, M. L. Nibert, R. Duncan, and T. S. Baker. Structure of avian orthoreovirus virion by electron cryomicroscopy and image reconstruction. Virology 343: 25–35. 2005.

229. Zhang, Y., X. Hao, H. Geng, and D. Guo. Cloning of σB gene of avian reovirus99G strain and its expression in Escherichia coli. Chinese Veterinary Science 38: 407–411. 2008.

230. Zhang, Z., W. Lin, X. Li, H. Cao, Y. Wang, and S. J. Zheng. Critical role of eukaryotic elongation factor 1 alpha 1 (EEF1A1) in avian reovirus sigma-C-induced apoptosis and inhibition of viral growth. Arch Virol 160: 1449–1461. 2015.

231. Zhou, L., J. Li, A. Haiyilati, X. Li, L. Gao, H. Cao, Y. Wang, and S. J. Zheng. Gga-miR-29a-3p suppresses avian reovirus-induced apoptosis and viral replication via targeting Caspase-3. Vet Microbiol 264: 109294. 2022.

232. Family Reoviridae. In: Virus Taxonomy: Ninth Report of the International Committee on Taxonomy of Viruses. A. M. King, E. Lefkowitz, M. J. Adams, and E. B. Carstens, eds. Elsevier, St. Louis. pp. 541–637. 2011.

REFERENCES: FOWL ADENOVIRAL HEPATITIS IN CHICKENS

1. Abghour, S., M. Mouahid, S. Darkaoui, J. Berrada, K. Zro, and F. Kichou. Pathogenicity of field strain of fowl aviadenovirus serotype 11 isolated from chickens with inclusion body hepatitis in Morocco. PLoS One 16: e0261284. 2021.

2. Ahi, Y. S., and S. K. Mittal. Components of Adenovirus Genome Packaging. Front Microbiol 7: 1503. 2016.

3. Akhtar, S., S. Zahid, and M. Khan. Risk factors associated with hydropericardium syndrome in broiler flocks. Veterinary Record 131: 481–484. 1992.

4. Assen, A. M., A. A. Yegoraw, S. W. Walkden-Brown, and P. F. Gerber. Molecular-based monitoring of live vaccines in dust samples from experimental and commercial chicken flocks and its potential use as a screening test. Res Vet Sci 143: 50–57. 2022.

5. Asthana, M., R. Chandra, and R. Kumar. Hydropericardium syndrome: Current state and future developments. Arch Virol 158: 921–931. 2013.

6. Balamurugan, V., and J. M. Kataria. The Hydropericardium Syndrome in Poultry – A Current Scenario. Vet Res Commun 28: 127–148. 2004.

7. Benkő, M., K. Aoki, N. Arnberg, A. J. Davison, M. Echavarría, M. Hess, M. S. Jones, G. L. Kaján, A. E. Kajon, S. K. Mittal, I. I. Podgorski, C. San Martín, G. Wadell, H. Watanabe, and B. Harrach. ICTV Virus Taxonomy Profile: Adenoviridae 2022. J Gen Virol 103. 2022.

8. Bertran, K., A. Blanco, N. Antilles, M. Nofrarías, R. M. Valle, À. Cobos, A. Ramis, M. Biarnés, and N. Majó. A 10-Year Retrospective Study of Inclusion Body Hepatitis in Meat-Type Chickens in Spain (2011–2021). Viruses 13: 2170. 2021.

9. Bremner, K. H., J. Scherer, J. Yi, M. Vershinin, S. P. Gross, and R. B. Vallee. Adenovirus Transport via Direct Interaction of Cytoplasmic Dynein with the Viral Capsid Hexon Subunit. Cell Host Microbe 6: 523–535. 2009.

10. Cheema, A. E., J. Ahmad, and M. Afzal. An adenovirus infection of poultry in Pakistan. Rev Sci Tech 8: 789–795. 1989.

11. Chen, L., L. Yin, Q. Zhou, P. Peng, Y. Du, L. Liu, Y. Zhang, C. Xue, and Y. Cao. Epidemiological investigation of fowl adenovirus infections in poultry in China during 2015–2018. BMC Vet Res 15: 271. 2019.

12. Chen, Z., S. Shi, B. Qi, S. Lin, C. Chen, C. Zhu, and Y. Huang. Hydropericardium syndrome caused by fowl adenovirus serotype 4 in replacement pullets. J Vet Med Sci 81: 245–251. 2019.

13. Clemmer, D. Age-Associated Changes in Fecal Excretion Patterns of Strain 93 Chick Embryo Lethal Orphan Virus in Chicks. Infect Immun 5: 60–64. 1972.

14. Cook, J. K. A. Pathogenicity of avian adenoviruses for day-old chicks. J Comp Path 84: 505–515. 1974.

15. Cook, J. K. A. Spread of an Avian Adenovirus (CELO Virus) to Uninoculated Fowls. Res Vet Sci 16: 156–161. 1974.

16. El-Shall, N. A., H. S. A. El-Hamid, M. F. Elkady, H. F. Ellakany, A. R. Elbestawy, A. R. Gado, A. M. Geneedy, M. E. Hasan, M. Jaremko, S. Selim, K. A. El-Tarabily, and M. E. A. El-Hack. Epidemiology, pathology, prevention, and control strategies of inclusion body hepatitis and hepatitis-hydropericardium syndrome in poultry: A comprehensive review. Front Vet Sci 9. 2022.

17. Fitzgerald, S. D., S. Rautenschlein, H. M. Mahsoub, F. W. Pierson, W. M. Reed, and S. W. Jack. Adenovirus infections. In: Diseases of Poultry, 14th ed. David E. Swayne, ed. Wiley. pp. 321–363. 2019.

18. Georgi, F., and U. F. Greber. The Adenovirus Death Protein – a small membrane protein controls cell lysis and disease. FEBS Lett 594: 1861–1878. 2020.

19. Grgić, H., C. Philippe, D. Ojkić, and E. Nagy. Study of vertical transmission of fowl adenoviruses. Can J Vet Res 70: 230–3. 2006.

20. Grimes, T. M., D. J. King, S. H. Kleven, and O. J. Fletcher. Involvement of a type-8 avian adenovirus in the etiology of inclusion body hepatitis. Avian Dis 21: 26–38. 1977.

21. Hess, M. Detection and differentiation of avian adenoviruses: A review. Avian Pathol 29: 195–206. 2000.

22. Hess, M., A. Cuzange, R. W. H. Ruigrok, J. Chroboczek, and B. Jacrot. The Avian Adenovirus Penton: Two Fibres and One Base. J. Mol. Biol 252: 379–385. 1995.

23. Hussein, E., N. F. Anwar, H. S. Elsebaey, M. A. Abdelmagid, M. A. Elkhair, and O. Mahana. Isolation and Characterization of Fowl Adenoviruses Associated with Hydro-pericardium Syndrome from Broiler Chickens in Egypt. J Worlds Poult Res 13: 149–160. 2023.

24. Junnu, S., P. Lertwatcharasarakul, S. Jala, S. Phattanakunanan, P. Moonjit, and T. Songserm. Developing an indirect ELISA based on recombinant hexon protein for serological detection of inclusion body hepatitis in chickens. J Vet Med Sci 76: 289–93. 2014.

25. Li, S., R. Zhao, Q. Yang, M. Wu, J. Ma, Y. Wei, Z. Pang, C. Wu, Y. Liu, Y. Gu, M. Liao, and H. Sun. Phylogenetic and pathogenic characterization of current fowl adenoviruses in China. Infect Genet Evol 105. 2022.

26. Matos, M., B. Grafl, D. Liebhart, I. Schwendenwein, and M. Hess. Selected clinical chemistry analytes correlate with the pathogenesis of inclusion body hepatitis experimentally induced by fowl aviadenoviruses. Avian Pathol 45: 520–529. 2016.

27. Mete, A., A. G. Armien, D. Rejmanek, M. Mott, and B. M. Crossley. Emergence of fowl aviadenovirus C-4 in a backyard chicken flock in California. J Vet Diagn Invest 33: 806–809. 2021.

28. Mittal, D., N. Jindal, A. K. Tiwari, and R. S. Khokhar. Characterization of fowl adenoviruses associated with hydropericardium syndrome and inclusion body hepatitis in broiler chickens. Virusdisease 25: 114–119. 2014.

29. Nakamura, K., M. Mase, S. Yamaguchi, and N. Yuasa. Induction of Hydropericardium in One-Day-Old Specific-Pathogen-Free Chicks by Adenoviruses from Inclusion Body Hepatitis. Avian Dis 44: 192. 2000.

30. Niu, Y. J., W. Sun, G. H. Zhang, Y. J. Qu, P. F. Wang, H. L. Sun, Y. H. Xiao, and S. D. Liu. Hydropericardium syndrome outbreak caused by fowl adenovirus serotype 4 in China in 2015. J Gen Virol 97: 2684–2690. 2016.

31. Niu, Y., Q. Sun, X. Liu, and S. Liu. Mechanism of fowl adenovirus serotype 4-induced heart damage and formation of pericardial effusion. Poult Sci 98: 1134–1145. 2019.

32. Ojkić, D., P. J. Krell, T. Tuboly, and E. Nagy. Characterization of fowl adenoviruses isolated in Ontario and Quebec, Canada. Can J Vet Res 72: 236–41. 2008.

33. Pan, Q., J. Wang, Y. Gao, Q. Wang, H. Cui, C. Liu, X. Qi, Y. Zhang, Y. Wang, K. Li, L. Gao, A. Liu, and X. Wang. Identification of chicken CAR homology as a cellular receptor for the emerging highly pathogenic fowl adenovirus 4 via unique binding mechanism. Emerg Microbes Infect 9: 586–596. 2020.

34. Pan, Q., Y. Yang, Y. Gao, X. Qi, C. Liu, Y. Zhang, H. Cui, and X. Wang. An Inactivated Novel Genotype Fowl Adenovirus 4 Protects Chickens against the Hydropericardium Syndrome That Recently Emerged in China. Viruses 9: 216. 2017.

35. Pereira, C. G., S. Y. Marin, B. M. Santos, J. S. Resende, M. Resende, A. M. Gomes, and N. R. S. Martins. Occurrence of Aviadenovirus in chickens from the poultry industry of Minas Gerais. Arq Bras Med Vet Zootec 66: 801–808. 2014.

36. Philippe, C., H. Grgić, D. Ojkić, and E. Nagy. Serologic monitoring of a broiler breeder flock previously affected by inclusion body hepatitis and testing of the progeny for vertical transmission of fowl adenoviruses. Can J Vet Res 71: 98–102. 2007.

37. Schachner, A., M. Matos, B. Grafl, and M. Hess. Fowl adenovirus-induced diseases and strategies for their control – a review on the current global situation. Avian Pathol 47: 111–126. 2018.

38. Schonewille, E., A. Singh, T. W. Göbel, W. Gerner, A. Saalmüller, and M. Hess. Fowl adenovirus (FAdV) serotype 4 causes depletion of B and T cells in lymphoid organs in specific pathogen-free chickens following experimental infection. Vet Immunol Immunopathol 121: 130–139. 2008.

39. Sohaimi, N. M., and U. C. Clifford. Fowl Adenovirus in Chickens: Diseases, Epidemiology, Impact, and Control Strategies to The Malaysian Poultry Industry – A Review. J Worlds Poult Res 11: 387–396. 2021.

40. Sohaimi, N. M., and M. Hair-Bejo. A recent perspective on fiber and hexon genes proteins analyses of fowl adenovirus toward virus infectivity—a review. Open Vet J 11: 569–580. 2021.

41. Tan, P. K., A.-I. Michou, J. M. Bergelson, and M. Cotten. Defining CAR as a cellular receptor for the avian adenovirus CELO using a genetic analysis of the two viral fibre proteins. J Gen Virol 82: 1465–1472. 2001.

42. Toro, H., O. Gonzalez, C. Escobar, L. Cerda, M. A. Morales, and C. Gonzalez. Vertical Induction of the Inclusion Body Hepatitis/Hydropericardium Syndrome with Fowl Adenovirus and Chicken Anemia Virus. Avian Dis 45: 215. 2001.

43. Trotman, L. C., N. Mosberger, M. Fornerod, R. P. Stidwill, and U. F. Greber. Import of adenovirus DNA involves the nuclear pore complex receptor CAN/Nup214 and histone H1. Nat Cell Biol 3. 2001.

44. Vellinga, J., S. Van der Heijdt, and R. C. Hoeben. The adenovirus capsid: Major progress in minor proteins. J Gen Virol 86: 1581–1588. 2005.

45. Wang, X., Q. Tang, L. Qiu, and Z. Yang. Penton-dodecahedron of fowl adenovirus serotype 4 as a vaccine candidate for the control of related diseases. Vaccine 37: 839–847. 2019.

46. Wiethoff, C. M., H. Wodrich, L. Gerace, and G. R. Nemerow. Adenovirus Protein VI Mediates Membrane Disruption following Capsid Disassembly. J Virol 79: 1992–2000. 2005.

47. Wilson, F. D., R. W. Wills, C. G. Senties-Cue, W. R. Maslin, P. A. Stayer, and D. L. Magee. High incidence of glomerulonephritis associated with inclusion body hepatitis in broiler chickens: Routine histopathology and histomorphometric studies. Avian Dis 54: 975–980. 2010.

48. Xu, A. hui, L. Sun, K. hang Tu, Q. yuan Teng, J. Xue, and G. zhong Zhang. Experimental co-infection of variant infectious bursal disease virus and fowl adenovirus serotype 4 increases mortality and reduces immune response in chickens. Vet Res 52. 2021.

49. Yan, T., S. Zhu, H. Wang, C. Li, Y. Diao, and Y. Tang. Synergistic pathogenicity in sequential coinfection with fowl adenovirus type 4 and avian orthoreovirus. Vet Microbiol 251. 2020.

50. Yugo, D. M., R. Hauck, H. L. Shivaprasad, and J. Meng. Hepatitis Virus Infections in Poultry. Avian Dis 60: 576–588. 2016.

Table 1.1 Avian Reoviral genomic segments, protein, and protein locations

| Genome segment | Protein | Location |
|---|---|---|
| L1 | λA | Inner core |
| L2 | λB | Inner core |
| L3 | λC | Turrets |
| M1 | μA | Inner core |
| M2 | μB | Outer capsid |
| M2 (P-T cleavage) | μBC | Outer capsid |
| M2 (P-T cleavage) | μBC δ | Outer capsid, presumed |
| M2 (P-T cleavage) | μBC δ’ | Outer capsid, presumed |
| M2 (P-T cleavage) | μBN | Outer capsid |
| M3 | μNS | Nonstructural |
| M3 (P-T cleavage) | μNSC | Nonstructural |
| M3 (P-T cleavage) | μNSN | Nonstructural |
| S1 (ORF 1) | p10 | Nonstructural |
| S1 (ORF 2) | p17 | Nonstructural |
| S1 (ORF 3) | σC | Outer capsid |
| S2 | σA | Inner core |
| S3 | σB | Outer capsid |
| S4 | σNS | Nonstructural |

# CHAPTER 2

# PATHOGENESIS OF AVIAN REOVIRUS GENOTYPE 2 ISOLATE DISPLAYING ENTERIC AND ARTHRITIC TROPISMS[1]

[1]Kathryn McCullough, Erich Linnemann, Vanessa Gauthiersloan, Holly S. Sellers. 2024. To be submitted to Avian Diseases.

SUMMARY

Avian Reoviruses (ARVs) within genetic cluster (GC) II represent a large, heterologous group of currently circulating ARVs that have been isolated from clinical cases of tenosynovitis and malabsorption. In this study, the pathogenesis of an ARV GC II isolate was investigated via quantitative RT-PCR (RT-qPCR), *in situ* hybridization (ISH), and histopathology, following oral or footpad inoculation. RT-qPCR detected ARV within the digital flexor tendon, heart, lung, liver, spleen, kidney, duodenum, cecum, cloacal bursa, and thymus. The highest viral RNA load was observed within the intestinal tract between 36-72 hours post inoculation (hpi). ISH demonstrated ARV within villous enterocytes throughout the intestines, follicle-associated epithelial (FAE) cells of the bursa, and the synovial membrane of the tendon. Histopathology within the intestine consisted of rare syncytia with negligible inflammation, whereas marked inflammation was present within the synovial tissues. The identity of infected enterocytes as avian "M cells" or infected synovial lining cells as macrophage-like synoviocytes (MLS) could not be histologically determined. However, the susceptibility of these varied cell types to infection an ARV GC II virus demonstrates a simultaneous enteric and arthritic potential plays a role in the pathogenesis of these reoviruses.

INTRODUCTION

Avian Reovirus (ARV) is the causative agent of viral tenosynovitis in chickens and turkeys that results in lameness and welfare-related culling costs in excess of US$120 million annually (1). Additional production losses to ARV-related diseases are due to variable syndromes of enteritis, myocarditis/pericarditis, hepatitis, splenitis, respiratory disease, and immunosuppression (2). ARV is composed of segmented, double stranded RNA (dsRNA) within a non-enveloped, double concentric, turreted, icosahedral capsid, from which protrudes the

highly variable cell attachment protein Sigma C (σC) (3). Genetic characterization of the σC coding region of the S1 gene has grouped currently circulating viruses into seven genetic clusters (4). Historically, extensive research, vaccine development, and widespread disease control was achieved using antigenically similar genotype I ARVs such as the S1133, 1703, and 2177 strains (5–7). However, antigenically and genetically variant Avian Reoviruses (ARV) within genetic clusters (GCs) I – VII have arisen, against which commercial vaccines offer little protection (4), and for which research is more limited. Questions regarding ARV pathogenesis remain, including the identity of cellular attachment receptor and basis for tissue tropism (8,9), as well as any phylogenetic basis predictive of the varying manifestations of disease syndromes (10). ARV GC II's represented the most prevalent reoviruses isolated at the Poultry Diagnostic and Research Center throughout 2020 and 2021, with isolations from both tendons and intestine from field cases of tenosynovitis and malabsorption, respectively (4). In this study, we utilize RT-qPCR, *in situ* hybridization (ISH), and histopathology to characterize the pathogenesis of a genotype II ARV via viral tissue distribution, cellular tropisms, and tissue response to infection.

## MATERIALS AND METHODS

### **Virus**.

ARV GC2 field isolate Ck/USA/147334/AL/Tendon/2022 (ARV 147334), was initially isolated from the tendons of 26-day old broilers exhibiting swollen tendons. The virus was propagated and titrated in a chicken hepatoma cell line (LMH, ATCC CRL-2117). The titer of the stock virus was 106.2 TCID50/mL. MinION nanopore whole genome sequencing of this isolate revealed a single population of reovirus.

**Chickens.**

One hundred and nine, 1-day-old, specific pathogen free chickens (SPF) were divided into the following groups of (n): oral challenge (33), footpad challenge (33), and mock challenge (43). Oral challenge birds received 104.5 TCID50/0.1mL and footpad challenge birds received 104.0 TCID50/0.5mL in the left footpad. Mock challenge birds received sterile phosphate buffered saline (PBS) via oral, intratracheal, or footpad. Birds were housed by group in Horsfall-Bauer isolation units under forced air, negative pressure with access to unmedicated broiler starter feed and water ad libitum and monitored daily for well-being. At 12, 36, and72 hours post inoculation (hpi) and 7 days post inoculation (dpi), 3 birds per challenge group and 3 mock-challenged birds were euthanized. All procedures and processes for the animal work were approved by the University of Georgia Institutional Animal Care and Use committee (AUP# A2023 01-036-A1).

**Footpad measurement.**

At 72 hpi and 7 dpi, digital calipers were used to measure the left footpad thickness of euthanized birds in mock challenge and footpad challenge groups.

**Sample collection and processing**.

Using aseptic technique, the following tissues were collected per bird and split into RNALater solution and 10% neutral buffered formalin: digital flexor tendon, thymus, trachea, heart, lung, liver, spleen, kidney, duodenum, jejunal-ileal junction, cecal tonsil, and cloacal bursa. Tissues in RNALater were held at 4°C overnight, then frozen at -80°C. Formalin-fixed tissues were embedded in paraffin blocks and serially sectioned. Per block, one section was stained with hematoxylin and eosin (H&E), and two sections underwent *in situ* hybridization

(ISH), wherein riboprobe was applied to one section but not applied to the other (negative control).

**RNA extraction and Quantitative RT-PCR.**

Total RNA was extracted from approximately 50 mg of thawed, blotted samples of duodenum, cecum, bursa, thymus, spleen, tendon, heart, liver, lung, and kidney using the RNeasy Plus Universal kit (Qiagen # 73404) and eluted in 50 ul of elution buffer per manufacturer's recommendations. Quantitative RT-PCR primers and a hydrolysis probe were designed based on a 128 base pair region of the 147334 reovirus S3 gene sequence as follows: forward primer, 5'-CAGTGCTGTGGTGTACTCTATT-3', reverse primer, 5'-GTTCTGCCGATCCTCACATATC-3' and probe, 5'-/56-FAM/CCATCACAA/ZEN/ATGCCACCAGCAACA/3IABkFQ/-3' (Integrated DNA Technologies, Coralville, IA, USA). Quantitative RT-PCR was performed using the Applied Biosystems AgPath-ID One-Step RT-PCR Kit (ABI, #4387391) per manufacturer's recommendations. Briefly, 5ul of RNA was added to the quantitative RT-PCR cocktail containing 12.5ul of 2x RT-PCR Buffer, 2ul nuclease free water, 1ul 25X RT enzyme mix, 1ul each of 10µM forward and reverse primers and 1µM of probe in a 25ul reaction The RT-qPCR reaction cycle profile was as follows: reverse transcription at 50C for 30 min, 95C for 15 min, forty cycles at 94C for 10 sec, and 60C for 30 sec.

**Generation of riboprobes.**

An antisense DIG-labeled riboprobe was prepared by *in vitro* transcription of a region of the reovirus 147334 S3 gene (297 base pairs). RNA was extracted from 100ul of infected cell culture supernatant using the Applied Biosystem MagMax Pathogen RNA/DNA Kit

(ThermoFisher Scientific, Waltham, MA, USA) per manufacturer's recommendations. RT-PCR amplification of a 297 basepair region of the 147334 reovirus S3 gene was performed using the Invitrogen SuperScript III RT Kit (#18080044, ThermoFisher Scientific, Waltham, MA, USA) for first strand synthesis per manufacturer's recommendations. Briefly, 2.5ul of RNA, 0.5ul each of 20uM 147334 ARV S3 38 forward primer, 5'-AGACTCCTGCTTGTTGGAATG-3' and 147334 ARV S3 334 reverse primer, 5'-GTTGGCTGATCTCATCGTAGTG-3' (Integrated DNA Technologies, Coralville, IA, USA) were denatured at 98C for 5 min, chilled on ice for 2-3 min followed by the addition of 0.5ul 10mM dNTP mix and 2ul nuclease free water. The reaction was incubated at 70C for 10 min, then on ice for 2-3 min. The reverse transcription cocktail containing 2ul of 5X 1st strand buffer, 1ul 1M DTT, 0.5ul 100mM RnaseOut Ribonuclease Inhibitor, and 0.5ul SuperScriptIII Reverse Transcriptase (ThermoFisher Scientific, Waltham, MA, USA) was added to the RNA/primer/dNTPs then incubated at 42C for 60 min, 70C for 15 min followed by a 10C holding stage. Second strand synthesis was performed using the Platinum Taq Polymerase Kit (#10966026, ThermoFisher Scientific, Waltham, MA, USA) per manufacturer's recommendations. Briefly, 5ul of the first strand cDNA was added to 14.75ul nuclease free water, 2.5ul 10X PCR buffer, 1ul 50mM Magnesium Chloride, 0.5ul 10mM dNTP mix, 0.25ul Platinum Taq Polymerase (ThermoFisher Scientific, Waltham, MA, USA), and 0.5ul each of 20uM 147334 ARV S3 38 forward and 147334 ARV S3 334 reverse primers. The PCR reaction cycles consisted of 95C for 4 min; forty cycles at 95C for 30 sec, 55C for 1 min, 72C for 1 min 10 sec; 72C for 7 min; and a 10C holding stage. The RT-PCR product was electrophoresed on 1% agarose gel with Invitrogen SyBR Safe DNA Gel Stain (#S33102 ThermoFisher Scientific, Waltham, MA, USA) and visualized under UV light. The 297 bp product was excised from the agarose gel and purified using the Qiagen QIAquick Gel

Extraction kit (#28706 Qiagen, Germantown, MD, USA) and eluted in 40ul of elution buffer. Two microliters of the purified product was then cloned into the Invitrogen pCRII TOPO plasmid vector and transformed into E. coli Top10 competent cells using the Invitrogen TOPO TA Cloning Kit with Dual Promoter (#450640 ThermoFisher Scientific, Waltham, MA, USA) per manufacturer's recommendations. Plasmid DNA was purified using the QIAprep Spin Miniprep Kit (#27106 Qiagen, Germantown, MD, USA) per manufacturer's recommendations. The orientation of the plasmid insert was determined by Sanger sequencing using M13 and the 147334 ARV S3 38 forward and 334 reverse gene specific primers. The plasmid DNA was linearized with the restriction enzyme, XbaI (#R0145S New England Biolabs, Ipswich, MA, USA), then purified using the Qiagen QIAquick PCR Purification Kit (Qiagen, Germantown, MD, USA). *In vitro* transcription was performed using SP6 RNA polymerase and the Roche DIG RNA Labeling Kit containing digoxigenin-UTP (DIG) (#11175025910 Roche Diagnostics Corporation, Indianapolis, IN, USA). Concentration of the transcript was determined by Northern dot blot comparison with a standard DIG-labeled RNA (#11175025910 Roche Diagnostics Corporation, Indianapolis, IN, USA).

### ***In situ*** **Hybridization.**

*In situ* hybridization was performed on paraffin sections from formalin fixed, paraffin embedded tissues placed on plus slides (#22230890 ThermoFisher Scientific, Waltham, MA, USA) as previously described (Kang 2012), with the following modifications: 5 ng RNA was applied per slide followed by denaturation at 98°C for 8 min then hybridized overnight at 41°C.

**Microscopic evaluation.**

H&E and ISH slides were evaluated via light microscopy at 40x magnification and scored. On H&E, lesions were scored on a per-tissue basis across categories of necrosis, heterophilic infiltration, mononuclear infiltration, edema, atrophy, hyperplasia, and fibrosis. Each category was scored as 0 (normal), 1 (mild), 2 (moderate), and 3 (marked), and scores were summed to give the final score per tissue. On ISH, the presence of signal expression was scored on the most densely populated field as 0 (absent), 1 (1-10/4x field), 2 (>10/4x), 3 (>10/10x), 4 (>10/20x), and 5 (>10/40x), with a 40x field equal to 0.3 mm2. Signal location was also evaluated.

**Statistical Analysis.**

Two-way ANOVA with Tukey's multiple comparisons test and two-tailed Pearson correlation test with 95% confidence interval were performed using GraphPad Prism version 10.0.0 for Windows (GraphPad Software, Boston, Massachusetts USA, www.graphpad.com).

RESULTS

**Footpad thickness**.

Footpads of footpad challenged birds were significantly thicker than mock challenge birds at 72 hpi ($p=0.015$) but not at 7 dpi.

**Quantitative RT-PCR.**

In orally challenged birds, ARV RNA was detected in all tissues except tendon, with virus present at all timepoints within the intestines, bursa, and thymus and from 36 hpi onwards in remaining viscera (Fig 1A). The highest viral load was detected in the duodenum, cecum, and

bursa, with peaks between 36 hpi and 72 hpi (Fig 1A). In footpad challenged birds, ARV RNA was detected in all tissues, with the highest viral load in the tendon and spleen at 12 hpi and 36 hpi. The viral load in the duodenum, cecum and bursa peaked at the 72 hpi sampling timepoint (Fig 1B). Tissues from mock inoculated birds were negative in all groups at all timepoints.

***In situ* Hybridization**.

In both challenge groups, ARV infected cells were observed in the intestines and cloacal bursa at multiple timepoints, with peak viral staining occurring between 36 to 72 hpi (Fig 2). In both tissues, ISH staining was observed within differentiated enterocytes along the mid to apical villus (Figs 3A,B) of intestinal sections and within the follicle-associated epithelium (FAE) of the bursa (Figs 4A,B). In both challenge groups, rare hepatocytes contained ARV staining at 36 hpi and 72 hpi, and the thymic cortex contained rare ARV staining at 7 dpi. In footpad challenged birds, ARV was detected within few synovial lining cells from 36 hpi to 7 dpi (Fig 5A), and in rare splenocytes from 12 to 72 hpi. Tissues from mock inoculated birds were negative in all groups and at all timepoints.

**Histopathology**.

Total histopathology lesion scores differed amongst treatment groups for the cecum, cloacal bursa, thymus, and tendon at 72 hpi and the tendon and kidney at 7 dpi (Fig 6). Differences were not observed amongst these tissues at 12 hpi or 36 hpi. At 72 hpi, the epithelium of the ceca and cloacal bursa (Fig 4C) of orally inoculated birds contained few aggregates of heterophils and foci of epithelial necrosis with rare syncytia. Bursal follicles contained scattered apoptotic debris (Fig 4C) to a similar degree across all treatment groups. At 7 dpi, the kidneys of orally inoculated birds contained fewer lymphoid centers than those of the

mock or footpad inoculated groups. At 72 hpi, the thymic cortices of footpad-inoculated birds were moderately thinned and contained increased numbers of apoptotic lymphocytes. At both 72 hpi and 7 dpi, the tendons of footpad-inoculated birds contained marked mononuclear and heterophilic expansion of the subsynovial space with rare, multifocal loss and hypertrophy of the synovial membrane (Fig 5B). Total histopathology lesion scores did not differ amongst treatment groups for the duodenum, jejunum, spleen, heart, liver, lung, or trachea at any timepoints; however, rare syncytia, a feature not categorized within the scoring structure, were present within the jejunal epithelium at 36 hpi and within the duodenal epithelium at 72 hpi (Fig 3C), of oral- and footpad-inoculated birds, respectively.

## DISCUSSION

The investigations into the pathogenesis of this ARV GC II isolate are consistent with historic research on GC I viruses from the 1970s-90s, documenting early systemic viral distribution (6,12–14). In this study, our ARV GC II isolate was detectable via PCR within the inoculated regions (tendon or gastrointestinal system, respectively) at 12 hpi, and with infection visualized via ISH within susceptible cells of those systems by 36 hpi. ARV was detected in distant tissues at the earliest timepoint of 12 hpi for parenteral administration, but not until 36-72 hpi for most sites when mimicking natural, oral exposure. The mechanism of ARV translocation from the intestinal tract to systemic circulation remains to be determined. Historic pathogenesis studies posit macromolecular pinocytosis by avian microfold (M) cells or by FAE as a possible route of entry for ARV (6,15). Similar results here demonstrate ARV GC II specifically within the FAE tufts of the cloacal bursa and apically located, differentiated enterocytes throughout the intestine. As varying subsets of chicken M cells, differentiated by CSF1R and SOX8 expression, are located across the bursa, intestinal crypts, and higher along villi, it is possible that the ARV

GC II-infected enterocytes in this study represent apically migrated avian M cells (16,17). Another possibility is that these susceptible enterocytes represent residual, absorptive embryonic epithelium capable of higher macromolecule transport than the digestive epithelium that proliferates post-hatch (18). If so, the changing enterocyte demographics accompanying intestinal development may be a component of the age-related ARV resistance described in many studies(19,20). However, as histopathology alone is inadequate for differentiating these enterocyte subtypes, more work is necessary to fully characterize these susceptible cells.

The question of cellular composition as a determining factor of ARV susceptibility is repeated when observing infected synoviocytes, observed here and historically (21). The synovial membrane is composed of histologically indistinguishable macrophage-like synoviocytes (MLS) and fibroblast-like synoviocytes (FLS) – cells of monocyte or mesenchymal lineage, respectively (22–24). As macrophages have been shown to be susceptible to ARV infection (25–27), it is worth investigating if macrophage-like synoviocytes display similar vulnerability to ARV infection and allow for viral localization within the synovial tissues. Further, ARV has been shown to be reliant on caveolin-1-mediated endocytosis *in vitro* (28,29), and, in mammals, increased caveolin-1 expression plays a role in macrophage differentiation and T-cell activation in some chronic inflammatory conditions (30,31). As T-cell response is a determinant of severity in ARV-induced tenosynovitis, both *in vitro* and *in vivo* investigation is warranted to define the cellular determinants of ARV susceptibility in the joint, and the resultant cell signals initiating the inflammatory response. The simultaneous enteric and arthritic tropisms of the ARVs in this study and in historic studies (6,32), combined with the disparate inflammatory response to infection between tendon and other tissue types, suggest that the

immune response or modulation thereof may play a role in the development of organ-specific ARV-related disease.

## ACKNOWLEDGEMENTS

Authors thank Nicholas Davis-Fields, Amanda Greenway, Brandan Dixon, Jennifer Kempf, Brittany Buckley, and Will Byrum for their assistance in sample processing, Olatunde Oluwayinka and James Stanton for pre-study virus characterization, and Boehringer Ingelheim Animal Health for graduate assistantship funding.

## REFERENCES

1. French D. Incidence and Economic Impact of Reovirus in the Poultry Industries in the United States. Avian Diseases. 2022;66(4):432–434. doi:10.1637/aviandiseases-D-22-99993

2. Pitcovski J, Goyal SM. Avian Reovirus Infections. In: Swayne DF, editor. Diseases of Poultry. Vol. 1. Fourteenth. Wiley; 2020. p. 382–400. https://onlinelibrary.wiley.com/doi/10.1002/9781119371199.ch11. doi:10.1002/9781119371199.ch11

3. Benavente J, Martínez-Costas J. Avian reovirus: Structure and biology. Virus Research. 2007 [accessed 2020 Jan 3];123(2):105–119. doi:10.1016/j.virusres.2006.09.005

4. Sellers HS. Avian Reoviruses from Clinical Cases of Tenosynovitis: An Overview of Diagnostic Approaches and 10-Year Review of Isolations and Genetic Characterization. Avian Diseases. 2023;66(4). https://bioone.org/journals/avian-diseases/volume-66/issue-4/aviandiseases-D-22-99990/Avian-Reoviruses-from-Clinical-Cases-of-Tenosynovitis--An-Overview/10.1637/aviandiseases-D-22-99990.full. doi:10.1637/aviandiseases-D-22-99990

5. Giambrone JJ, Clay RP. Evaluation of broiler breeder pullet vaccination programs for preventing clinical reovirus infections in the progeny. Poultry science. 1986 [accessed 2022 Jan 5];65(3):457–461. doi:10.3382/ps.0650457

6. Jones RC, Islam MR, Kelly DF. Early pathogenesis of experimental reovirus infection in chickens. Avian Pathol. 1989;18(2):239–253. http://www.tandfonline.com/doi/abs/10.1080/03079458908418599. doi:10.1080/03079458908418599

7. Jones RC. Reovirus Infections. In: Swayne DE, editor. Diseases of Poultry. Thirteenth. Ames, Iowa: John Wiley & Sons; 2013. p. 351–373. doi:10.1002/9781119421481.ch11

8. Grande A, Costas C, Benavente J. Subunit composition and conformational stability of the oligomeric form of the avian reovirus cell-attachment protein σC. Journal of General Virology. 2002;83(1):131–139. doi:10.1099/0022-1317-83-1-131

9. Grande A, Rodriguez E, Costas C, Everitt E, Benavente J. Oligomerization and cell-binding properties of the avian reovirus cell-attachment protein σC. Virology. 2000;274(2):367–377. doi:10.1006/viro.2000.0473

10. Ayalew LE, Ahmed KA, Popowich S, Lockerbie B-C, Gupta A, Tikoo SK, Ojkic D, Gomis S. Virulence of Emerging Arthrotropic Avian Reoviruses Correlates With Their Ability to Activate and Traffic Interferon-γ Producing Cytotoxic CD8+ T Cells Into Gastrocnemius Tendon. Frontiers in Microbiology. 2022;13(March):1–14. doi:10.3389/fmicb.2022.869164

11. Mukaka MM. Statistics Corner: A guide to appropriate use of Correlation coefficient in medical research. 2012. www.mmj.medcol.mw

12. Kibenge FSB, Gwaze GE, Jones RC, Chapman AF, Savage CE. Experimental reovirus infection in chickens: Observations on early viraemia and virus distribution in bone marrow, liver and enteric tissues. Avian Pathol. 1985;14(1):87–98. doi:10.1080/03079458508436210

13. Menendez NA, Calnek BW, Cowen BS. Localization of avian reovirus (FDO isolant) in tissues of mature chickens. Avian Diseases. 1975;19(1):112–117. doi:10.2307/1588961

14. Ni Y, Kemp MC. A comparative study of avian reovirus pathogenicity: Virus spread and replication and induction of lesions. Avian Diseases. 1995;39(3):554–566. doi:10.2307/1591809

15. Bockman DE, Cooper MD. Pinocytosis by epithelium associated with lymphoid follicles in the bursa of fabricius, appendix, and Peyer's patches. An electron microscopic study. American Journal of Anatomy. 1973;136(4):455–477. doi:10.1002/aja.1001360406

16. Zeinali S, Sutton K, Zefreh MG, Mabbott N, Vervelde L. Discrimination of distinct chicken M cell subsets based on CSF1R expression. Scientific Reports. 2024;14(1). doi:10.1038/s41598-024-59368-x

17. Jeurissen SHM, Wagenaar F, Janse EM. Further characterization of M cells in gut-associated lymphoid tissues of the chicken. Poultry Science. 1999;78(7):965–972. http://dx.doi.org/10.1093/ps/78.7.965. doi:10.1093/ps/78.7.965

18. Moran ET. Nutrition of the Developing Embryo and Hatchling. Poultry Science. 2007;86(5):1043–1049. https://academic.oup.com/ps/article-abstract/86/5/1043/1620717. doi:https://doi.org/10.1093/ps/86.5.1043

19. Kerr KM, Olson NO. Control of Infectious Synovitis. 14. The Effect of Age of Chickens on the Susceptibility to Three Agents. Avian Diseases. 1964 [accessed 2022 Jan 4];8(2):256. doi:10.2307/1588068

20. Jones RC, Georgiou K. Reovirus-induced tenosynovitis in chickens the influence of age at infection. Avian Pathol. 1984;13(3):441–457. doi:10.1080/03079458408418546

21. Liu HJ, Giambrone JJ. *In situ* detection of reovirus in formalin-fixed, paraffin-embedded chicken tissues using a digoxigenin-labeled cDNA probe. Avian Diseases. 1997 [accessed 2022 Jan 7];41(2):447–451. doi:10.2307/1592203

22. Tu J, Hong W, Zhang P, Wang X, Körner H, Wei W. Ontology and function of Fibroblast-like and macrophage-like synoviocytes: How do they talk to each other and can they be targeted for rheumatoid arthritis therapy? Frontiers in Immunology. 2018;9(JUN). doi:10.3389/fimmu.2018.01467

23. Edwards J. The origin of type A synovial lining cells. Immunology. 1982;161(3–4):227–231.

24. Edwards JCW. The nature and origins of synovium: experimental approaches to the study of synoviocyte differentiation*. 1994.

25. Mills JN, Wilcox GE. Replication of four antigenic types of avian reovirus in subpopulations of chicken leukocytes. Avian Pathol. 1993;22(2):353–361. doi:10.1080/03079459308418926

26. O'Hara D, Patrick M, Cepica D, Coombs KM, Duncan R. Avian Reovirus Major μ-Class Outer Capsid Protein Influences Efficiency of Productive Macrophage Infection in a Virus Strain-Specific Manner. Journal of Virology. 2001;75(11):5027–5035. doi:10.1128/jvi.75.11.5027-5035.2001

27. Chen YS, Shen PC, Su BS, Liu TC, Lin CC, Lee LH. Avian reovirus replication in mononuclear phagocytes in chicken footpad and spleen after footpad inoculation. Can J Vet Res. 2015;79(2):87–94.

28. Huang WR, Wang YC, Chi PI, Wang L, Wang CY, Lin CH, Liu HJ. Cell entry of avian reovirus follows a caveolin-1-mediated and dynamin-2-dependent endocytic pathway that requires activation of p38 Mitogen-activated Protein Kinase (MAPK) and Src signaling pathways as well as microtubules and small GTPase Rab5 protein. J Biol Chem. 2011;286(35):30780–30794. doi:10.1074/jbc.M111.257154

29. Wang Y, Zhang Y, Zuo W, Bo Z, Zhang C, Zhang X, Wu Y. Avian Reovirus σB Interacts with Caveolin-1 in Lipid Rafts during Dynamin-Dependent Caveolae-Mediated Endocytosis. Viruses. 2022;14(10). doi:10.3390/v14102201

30. Fu Y, Moore XL, Lee MK, Fernández-Rojo MA, Parat MO, Parton RG, Meikle PJ, Sviridov D, Chin-Dusting JP. Caveolin-1 Plays a Critical Role in the Differentiation of Monocytes into Macrophages. Arterioscler Thromb Vasc Biol. 2012;(32):e117-125. doi:doi:10.1161/ATVBAHA.112.254151.

31. Ohnuma K, Inoue H, Uchiyama M, Yamochi T, Hosono O, Dang NH, Morimoto C. T-cell activation via CD26 and caveolin-1 in rheumatoid synovium. Modern Rheumatology. 2006;16(1):3–13. doi:10.1007/s10165-005-0452-4

32. Jones RC, Guneratne JRM. The pathogenicity of some avian reoviruses with particular reference to tenosynovitis. Avian Pathol. 1984;13(2):173–189. doi:10.1080/03079458408418522

FIGURES

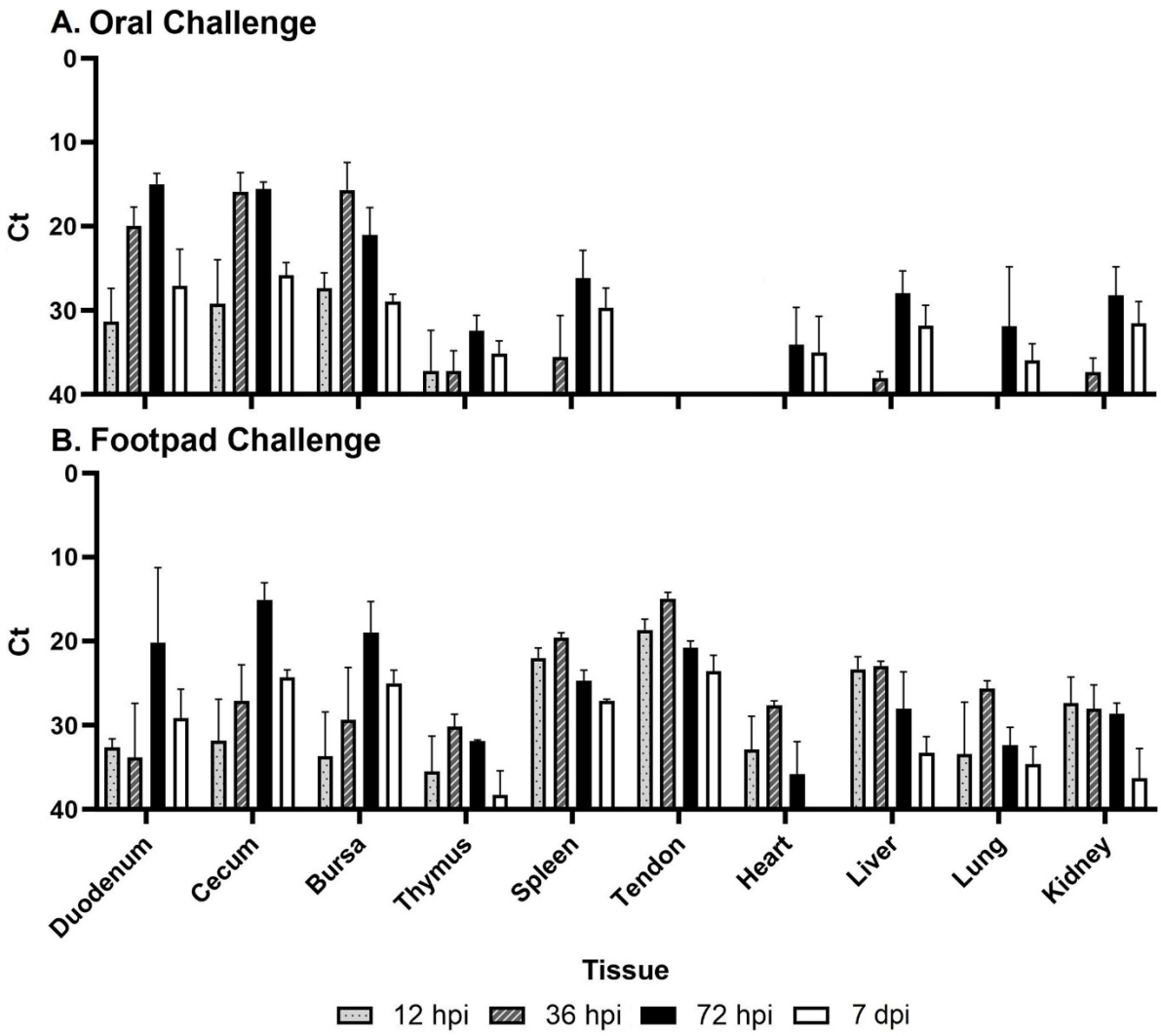


Figure 2.1. Quantitative RT-PCR detection of ARV S3 genomic segment in various tissues following oral (A) or footpad (B) challenge. Timepoints are represented as bars, with 12 hpi (stippled grey), 36 hpi (hatched grey), 72 hpi (black), and 7 dpi (white). Tissue location is represented by the x-axis. Cycle threshold (Ct), inversely related to viral load, is represented by the y-axis, with the standard deviation denoted by capped line.

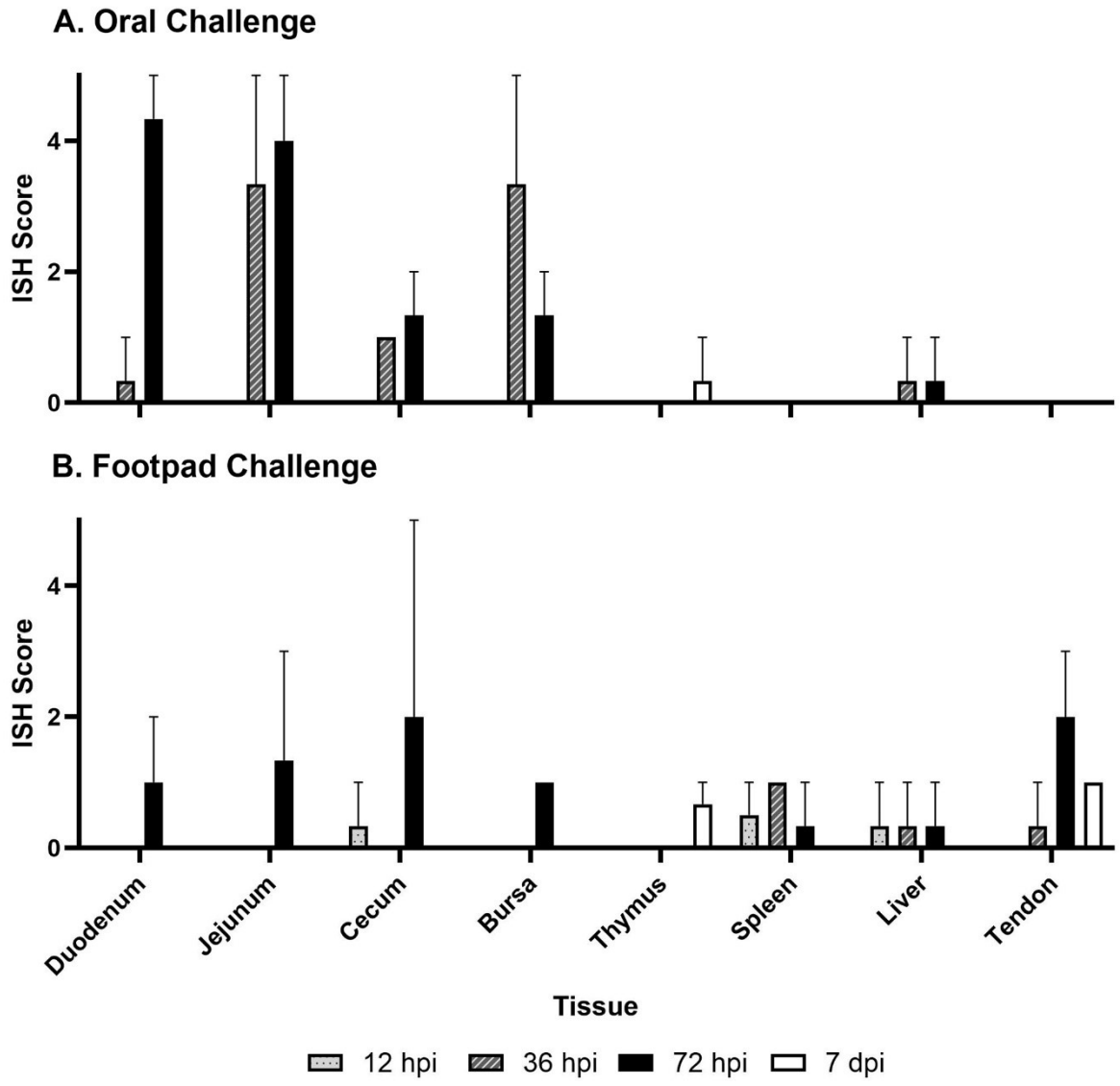


Figure 2.2. In situ hybridization (ISH) detection of ARV in various tissues following oral (A) or footpad (B) challenge. Timepoints are represented as bars, with 12 hpi (stippled grey), 36 hpi (hatched grey), 72 hpi (black), and 7 dpi (white). Tissue location is represented by the x-axis. Mean ISH score is represented by the y-axis, with the range denoted by capped line. ISH scores were assigned by the presence of signal in the most densely populated field as 0 (absent), 1 (1-10/4x field), 2 (>10/4x), 3 (>10/10x), 4 (>10/20x), and 5 (>10/40x), with a 40x field equal to 0.3 mm2.

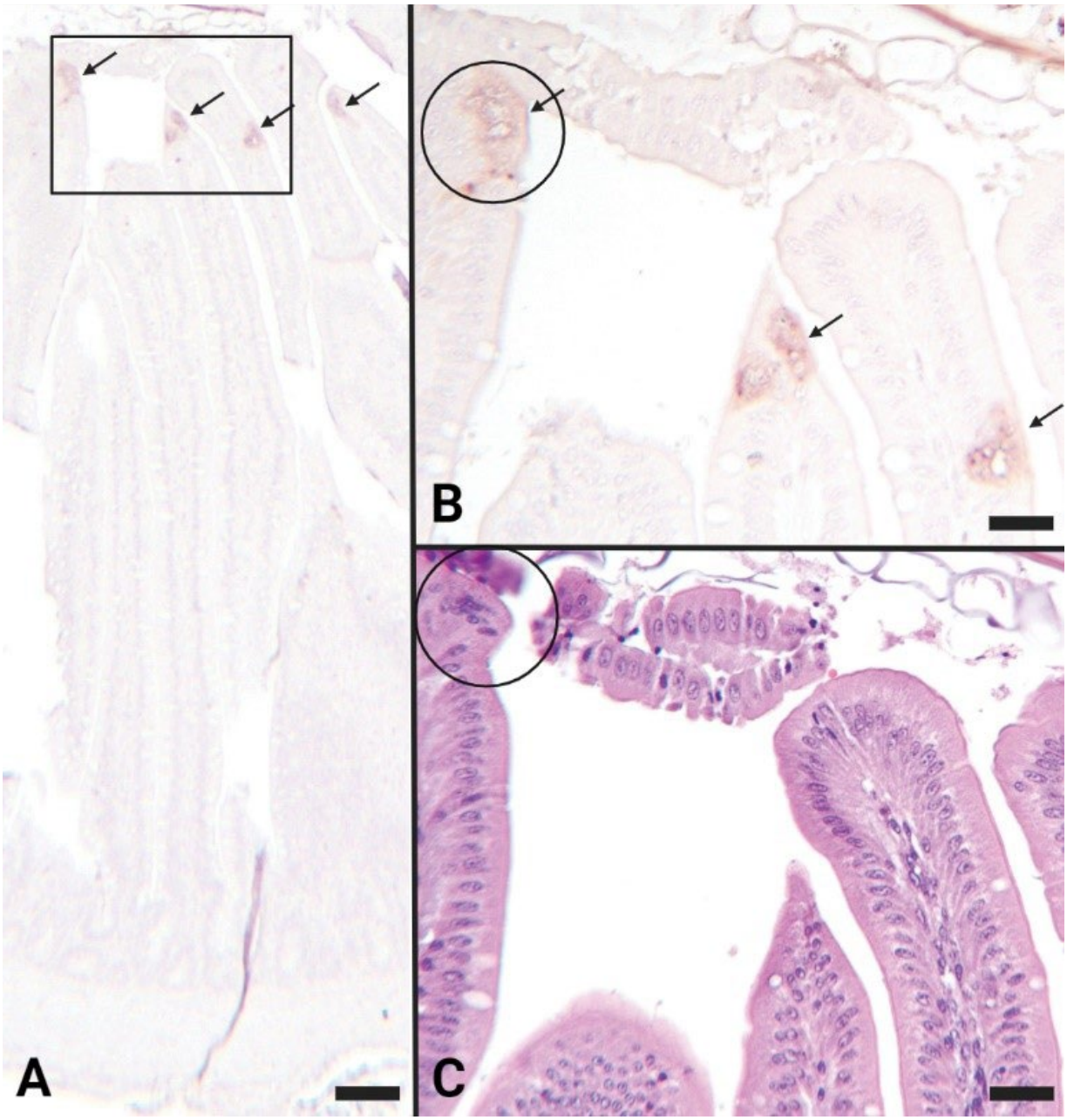


Figure 2.3. Duodenum, ARV footpad challenge 72 hpi. A and its magnified view, B, demonstrate ISH. C represents a serial section of the same location stained with H&E. A: Apical villous enterocytes contain ARV signal (arrows). Boxed area is magnified in (B). ISH, Bar = 50 µm. B: Higher magnification of boxed area of (A). Enterocytes contain ARV signal (arrows). One area of viral staining (circled) corresponds to syncytia formation observed in (C) ISH, Bar = 20 µm.

C: Serial section of (B). Rare ARV-induced syncytia (circled) are present, which share localization with the circled ARV signal observed in (B). Histopathologic changes are otherwise minimal. H&E, Bar = 20 µm.

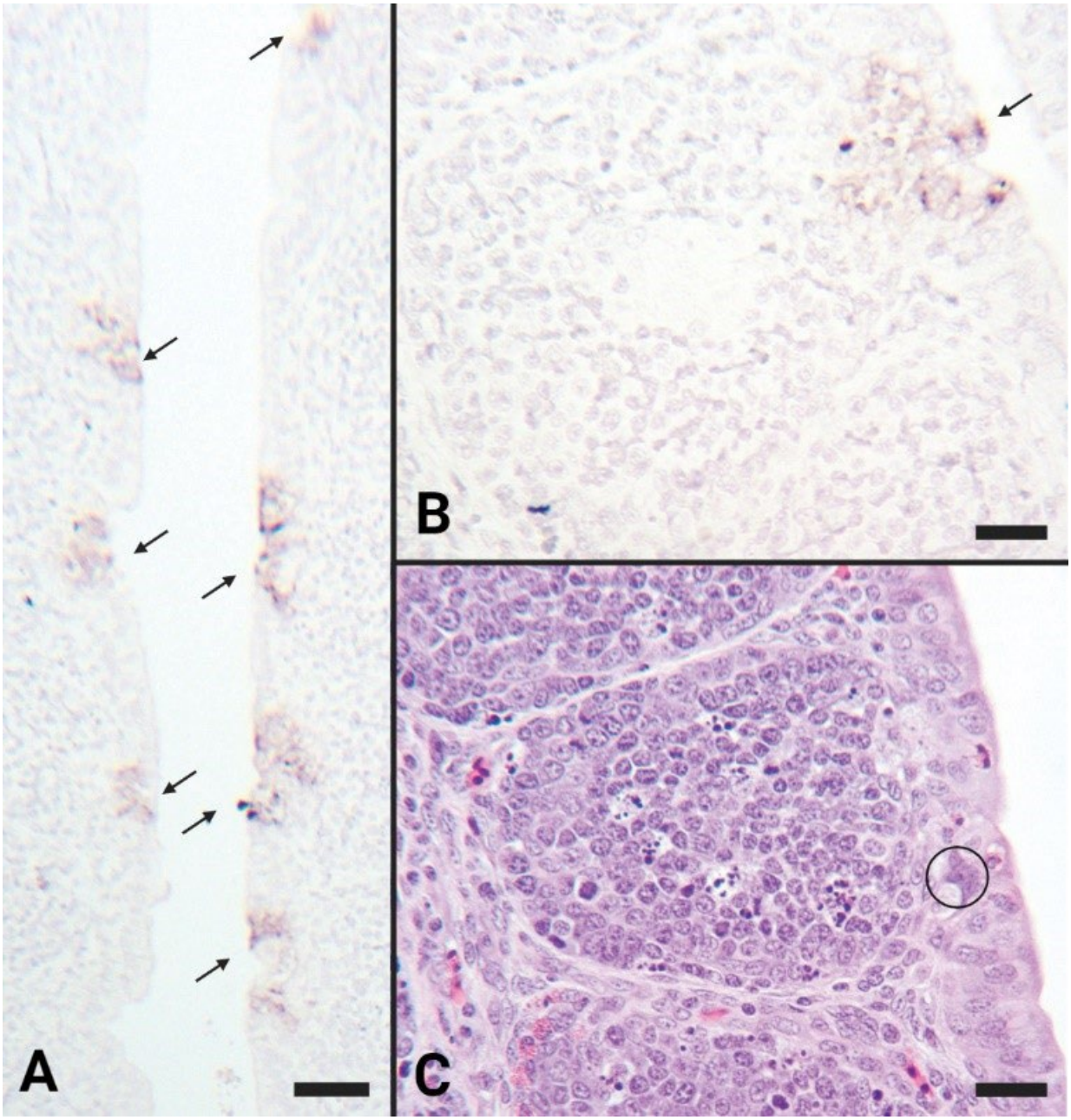


Figure 2.4. Cloacal bursa, ARV oral challenge 36 hpi. A: Follicle-associated epithelial (FAE) cells contain ARV signal (arrows). ISH, Bar = 40 µm. B: Higher magnification of bursal follicle

with overlying, ARV-infected FAE cells (arrow). ISH, Bar = 20 µm. C: The epithelium contains rare ARV-induced syncytia (circle) and infiltrating heterophils. Follicular apoptotic debris and peripheral extramedullary hematopoiesis were features present in both challenge and mock challenge groups. H&E, Bar = 20 µm.

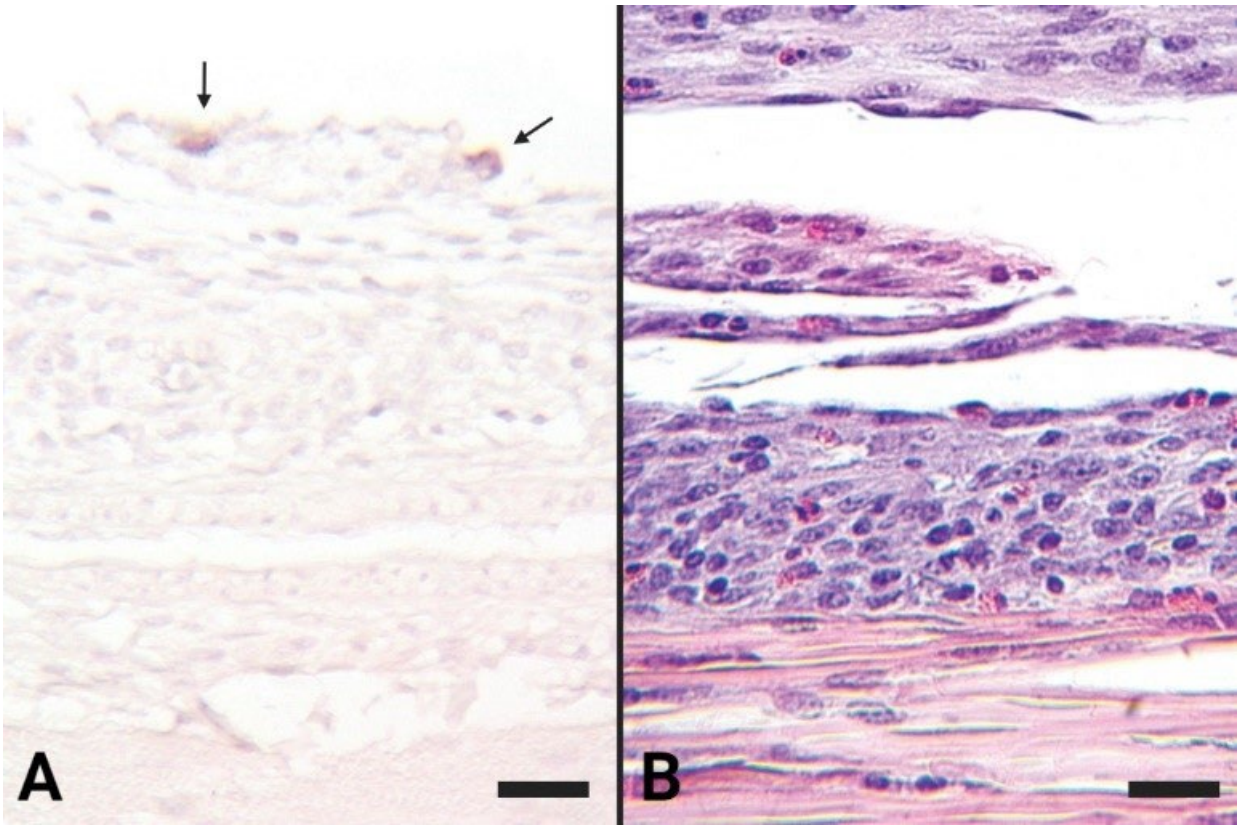


Figure 2.5. Tendon, ARV footpad challenge 72 hpi. A: ISH, Synoviocytes contain ARV signal (arrows). Bar = 20 µm. B: Mononuclear and heterophilic inflammation separates the mildly hyperplastic synovial membrane from the underlying tendon. H&E, Bar = 20 µm.

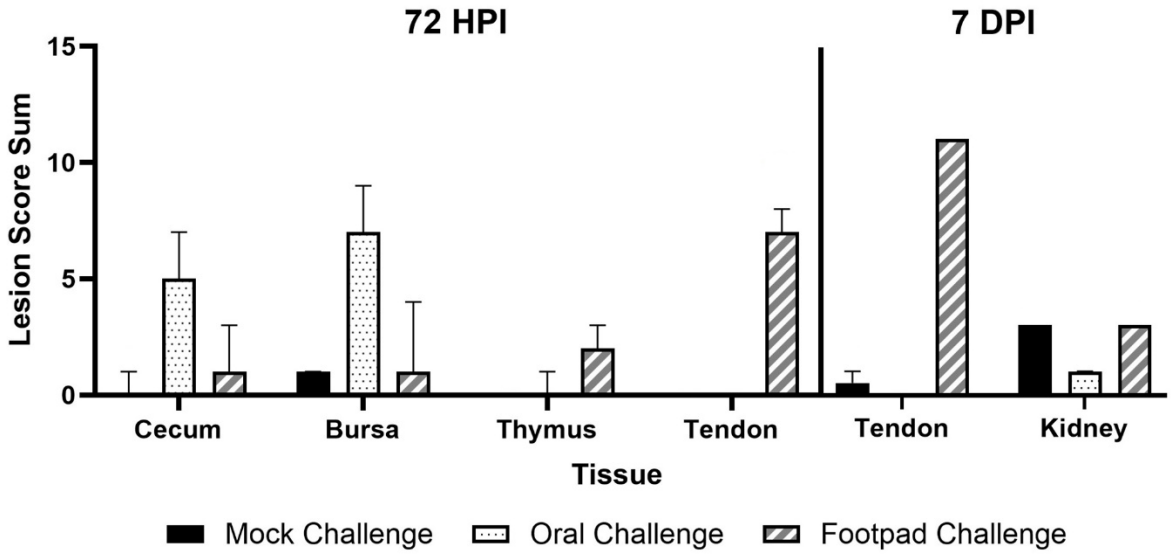


Figure 2.6. Histopathology lesion scores in tissues at 72 hpi and 7 dpi. Treatment groups are denoted by bars, as mock challenge (black), oral challenge (stippled white), and footpad challenge (grey hatched). Tissue location is represented by the x-axis. Lesion scores are represented by the y-axis, with the median score denoted by the bar and range denoted by brackets. Lesion scores represent the sum of scores across categories of necrosis, heterophilic infiltration, mononuclear infiltration, edema, atrophy, hyperplasia, and fibrosis, with each category scored as 0 (normal), 1 (mild), 2 (moderate), and 3 (marked) per tissue.

# CHAPTER 3

# DIAGNOSIS OF INCLUSION BODY HEPATITIS IN CHICKENS BY IMPRESSION SMEAR CYTOPATHOLOGY[2]

[2]Kathryn McCullough, Subhan Ullah, Jenny Nicholds, Maurice Raccoursier, Reece Bowers, Cole Taylor, Jason Sousa, Tiffani Allen, Adrea Mueller Slay, Daniel A. Sebastián Pineda, Silvia Carnaccini, Holly S. Sellers. Submitted to Avian Diseases, 2024.

## SUMMARY

Numerous reports and epidemiologic investigations in recent years identify adenoviral infection as an ongoing to increasing, international disease in commercially raised chickens. Impression smear cytopathology was evaluated as a tool for the diagnosis of adenoviral inclusion body hepatitis (IBH). In this study, 92 paired, Romanowsky-stained cytopathologic preparations and hematoxylin- and eosin-stained histopathologic liver sections were evaluated from 54 chickens with experimentally induced or naturally occurring IBH. Large intranuclear inclusion bodies typical of adenoviruses were visible within hepatocytes on both cytopathology and histopathology. Cytopathologic to histopathologic percent positive agreement and percent negative agreement were 94% and 90%, respectively, with $\kappa = 0.81$ (0.61–1.01, 95% confidence, $p < 0.001$). A subset of 20 cytopathologic samples evaluated by 8 veterinary professionals as consistent or inconsistent with IBH, yielded an average of 66% positive agreement and 98% negative agreement to the histopathologic diagnosis, across all observers, with $\kappa = 0.61$ (0.53–0.68, 95% confidence, $p < 0.001$), resulting in a positive predictive value of 99% and a negative predictive value of 67%. Interobserver agreement was slightly higher (76% positive agreement, 94% negative agreement, $\kappa = 0.68$ (0.65-0.71), 95% confidence, $p < 0.001$) within the 12 of these samples that originated from natural disease, with stable positive and negative predictive values. A rapid, cost-effective, tentative diagnosis of IBH via impression smear cytopathology at the time of necropsy can streamline further confirmatory laboratory testing and facilitate timely communication in the interim to affected parties, especially in locations with delayed access to a diagnostic laboratory.

## INTRODUCTION

Aviadenoviruses are the etiologic agent of inclusion body hepatitis (IBH) and hepatitis-hydropericardium syndrome (HHS) in chickens. Emergence and re-emergence of these diseases internationally and recently within the United States pose an economic and health threat to commercial flocks due to rapid, moderate to high mortality rates; poor growth; and lack of treatment options (1–5). Diagnosis of adenoviral diseases in poultry flocks represents the necessary initial step to quantifying prevalence and economic impact within regions, investigating concurrent predisposing factors, guiding selection and implementation of specific control measures, and preventing further disease spread. Currently, presumptive diagnosis of IBH can be made based on clinical signs and gross lesions; however, histopathology, PCR, or virus isolation is necessary for confirmatory diagnosis (1). These laboratory methods can be costly, laborious, time consuming, and require equipment not available in all laboratories.

Cytopathology is extensively used across veterinary and human medicine to diagnose viral, bacterial, fungal, parasitic, and other infectious and non-infectious diseases (6–13). Impression smear cytopathology utilizing Romanowsky staining techniques is cost-effective, technically simple, and can be performed at any size laboratory or in a field setting with minimal, commercially available reagents, contributing diagnostic data to a case within as little as 5 minutes (14,15). Regarding poultry viral diseases specifically, cytopathology has been used to directly identify fowlpox and herpesvirus inclusions (16–18) as well as to characterize inflammatory patterns within feather pulp predictive of Marek's Disease (19). Despite these broad applications, the use of cytopathology in the diagnosis of aviadenoviral diseases has not yet been described. Here, we evaluate the capability of Romanowsky stains to differentiate

aviadenoviral inclusions and describe the cytopathologic morphology of aviadenoviral inclusions in chicken hepatocytes.

## MATERIALS AND METHODS

### Experimental Infection.

#### *Virus.*

Fowl adenovirus group E/8b field isolate Ck/USA/AL/133805/LiverSpleen/2020 (133805) was propagated and titrated in chicken hepatoma (LMH, ATCC CRL-2117) cells. The titer of the stock virus was 105.5 TCID50/mL.

#### *Chickens.*

Forty-one, 1-day-old, specific pathogen free chickens (SPF) were weighed, tagged, and divided into challenge (20 birds) and control (21 birds) groups of approximately equal average body weight. Birds were orally challenged or mock challenged with 105.2 TCID50/0.5 mL or sterile PBS, respectively. Birds were housed by group in Horsfall-Bauer isolation units with access to unmedicated broiler starter feed and water ad libitum and monitored daily for well-being. Clinical morbidity was not observed during this study. At 4, 6, 10, and 14 days of age, five birds per group were euthanized. All procedures and processes for the animal work were approved by the University of Georgia Institutional Animal Care and Use committee (AUP# A2023 01-036-Y1-A0).

**Natural Infection.**

*Clinical cases.*

Between March and April 2023, 13 commercial broiler chickens from 6 diagnostic necropsy submissions to the University of Georgia Poultry Diagnostic and Research Center were enrolled in the study on the basis of clinical suspicion of IBH. Case histories provided by submitters included acutely increased flock mortality and uneven or reduced flock body weights in broiler flocks ranging from 25 to 36 days of age (Table 1). Birds received were dead-on-arrival or euthanized via cervical dislocation at accessioning.

**Sample collection and processing.**

At necropsy, 2 pieces of ~1 cm3 liver were collected from each bird. Each piece of liver was gently blotted on a paper towel, impressed sequentially along a clean glass slide (Supplemental Figure 1), then placed within a histocassette in 10% neutral-buffered formalin. Glass slides were allowed to air dry for up to 5 minutes then transported in 95% ethanol for approximately 5 minutes. Impression smears were stained with a Romanosky stain (Epredia Shandon Kwik-Diff, Fisher Scientific) by dipping the slides through the three reagents wells of methanol, eosin-y, and methylene blue for approximately 10 seconds per well. Slides were gently rinsed with tap water, allowed to air dry, and sealed using a glass coverslip and nonaqueous mounting media (OpticMount1, Mercedes Scientific). Formalin-fixed tissues were processed routinely for histopathology, and sections were stained with hematoxylin and eosin.

**Pathologic evaluation.**

Per cytopathology slide and per histopathology section, 114, adequate, 400× fields (27 mm2) were evaluated by an anatomic pathologist (KM) via light microscopy and designated as

“IBH-negative” or “IBH-positive" based on the absence or presence, respectively, of 1 or more structures compatible with an aviadenoviral inclusion body. An adequate field consisted of a single layer of at least 15 intact hepatocytes. Of 108 paired samples collected, 16 pairs were excluded due to an insufficient number of observable fields on either the cytopathologic or histopathologic component. Morphologic changes consistent with an aviadenoviral inclusion body consisted of a hepatocyte nucleus containing an 8–15-um-diameter, basophilic to amphophilic, globular material that disrupted to peripheralized the native chromatin and variably enlarged the nucleus by 10–100%. Experimentally produced samples from inoculated and mock-inoculated groups were comingled, then evaluated in a blinded and randomized fashion. Clinically received samples were evaluated on a rolling basis with no blinding. Percent positive agreement and percent negative agreement between cytopathology and histopathology for all paired sample observations were determined via sensitivity and specificity calculations, respectively, with the measure of agreement determined by Fleiss Kappa analysis.

**Observers.**

Eight, non-pathologist, veterinary professionals were provided self-study images of histopathologic IBH inclusion bodies, cytopathologic putative IBH inclusions, and cytologic normal and artifactual structures (Supplemental Figure 2). Individuals then evaluated pre-determined, randomized order, subset of 20 unknown impression smears and designated each as consistent with, or inconsistent with, IBH (Table 2). Veterinary expertise varied amongst individuals but included a familiarity with routine, point-of-care microscopic parasitology, with observers A, B, and C having > 10 years clinical DVM experience, observers D, E, F, and G having < 2 years clinical DVM experience, and observer H being a current DVM student. Two IBH-positive and two normal (as determined by paired histopathology) impression smear

reference slides were provided alongside unknown slides. Cytopathologic designations made by observers were compared to the previously determined, paired histopathologic diagnosis per sample. Percent positive agreement and percent negative agreement were determined via sensitivity and specificity calculations, respectively, for all cytopathologic designations relative to the final histopathologic diagnosis, with the measure of agreement determined by Fleiss Kappa analysis. Positive and negative predictive values of cytologic designations were similarly calculated relative to histopathology.

## RESULTS

### Gross pathology.

The livers of experimentally infected birds rarely contained solitary to few 1–2-mm-diameter, tan to dark red foci. The livers of clinically submitted birds were variably swollen and mottled pale yellow to dark red, with disseminated, pinpoint, tan or dark red foci of necrosis and hemorrhage (Figure 1).

### Histopathology and Cytopathology.

Intranuclear inclusion bodies typical of aviadenoviruses (Figure 2) were present in 14 of 35 liver histopathology sections from inoculated birds, and 0 of 34 sections from mock-inoculated birds, and 19 of 23 sections from clinical birds. Putative inclusion bodies (Figure 3A-D), based on morphologic similarity to histopathology, were observed in hepatocyte nuclei of 18 of 35 liver impression smears from inoculated birds, and 0 of 34 impression smears from mock-inoculated birds, and 19 of 23 impression smears from clinical birds. Cytopathologic to histopathologic percent positive agreement and percent negative agreement for all samples were 94% and 90%, respectively, with $\kappa = 0.81$ (0.61–1.01, 95% confidence, $p < 0.001$) interpreted as

"almost perfect agreement" (20). The positive predictive value of cytopathology to histopathology across all samples was 84% and the negative predictive value was 96%. Within experimentally-derived samples, percent positive agreement and percent negative agreement for all samples were 86% and 89%, respectively, with $\kappa = 0.60$ (0.36–0.84, 95% confidence, $p< 0.001$), with a positive predictive value of 67% and a negative predictive value of 96%. Within clinically-derived samples, percent positive and negative agreement and positive and negative predictive values were all 100%, and $\kappa = 1$ (0.59–1.41, 95% confidence, $p< 0.001$). When present, the total inclusion body count ranged from 2 to 50 (median = 8) histologically and 1 to 46 (median = 4) cytologically per experimentally derived sample and from 58 to 6402 (median = 201) histologically and 11 to 504 (median = 44) cytologically per clinically derived sample. Bacterial hepatitis was diagnosed histopathologically in 4/23 clinical liver sections that lacked inclusion bodies.

**Observer agreement.**

Observers collectively averaged 66% positive agreement and 98% negative agreement to the histopathologic diagnosis (Table 2), with $\kappa = 0.61$ (0.53–0.68, 95% confidence, $p< 0.001$) interpreted as "substantial agreement" (20) , yielding a positive predictive value of 99% and a negative predictive value of 67%. Interobserver agreement was higher (76% positive agreement, 94% negative agreement, $\kappa = 0.68$ (0.65–0.71), 95% confidence, $p< 0.001$) within the 12 of these samples that originated from natural disease (Table 2).

## DISCUSSION

Romanowsky-stained impression smear cytopathology of the liver is a useful technique for the diagnosis of inclusion body hepatitis in chickens. IBH is a prevalent disease within

commercial broilers that can cause moderate to high mortality within flocks. Using impression smear cytopathology, a tentative diagnosis of IBH can be made at the site of necropsy. This rapid and cost-effective diagnostic option increases the opportunity to identify and track positive cases, communicate to affected parties in a timely manner, and focus valuable time and monetary resources on specific confirmatory laboratory tests or response measures. In particular, impression smear cytopathology represents a highly accessible and portable means of tentative diagnosis of IBH for veterinarians in locations without immediate access to a diagnostic laboratory. High agreement was present in the diagnosis of IBH- positive or -negative cytopathologic specimens as compared to the paired histopathologic diagnosis for both pathologist and non-pathologist veterinary professionals. Notably, the high positive predictive value highlights the rarity of false positive calls made within the veterinary observations group, regardless of personal experience level. As such, a degree of diagnostic confidence can reasonably be held by a practicing veterinarian encountering a suspected cytopathologic IBH inclusion body in clinical cases. Further, the higher degree of positive agreement amongst observers for clinically derived samples is suspected to be due to the higher density of inclusion bodies present in these clinical samples, offering more opportunities to recognize the pathologic feature. However, in these clinical samples, disparity of inclusion body density was noted between cytopathology and histopathology, often observed as extensive areas of cellular and nuclear rupture on impression smear. This cell rupture was attributed to the increased fragility of diseased hepatocytes compared to their normal counterparts, emphasizing the importance of obtaining samples of high diagnostic quality using gentle impression technique during specimen preparation. In contrast, the rarity of inclusion bodies within experimentally derived samples, both cytologically and histologically, likely contributed to the lower agreement and predictive

values associated with pathologist evaluation. In several of these sample sets, IBH presence was determined by 1-2 inclusions total on either the cytopathology or histopathology component, resulting in discrepant diagnoses if no inclusions were also located within the paired sample. These results highlight a limitation of both cytopathology and histopathology in the definitive diagnosis of IBH, as both modalities are dependent on sample collection coinciding with a window of high viral replication with inclusion body formation. As these mismatched diagnoses occurred only within the experimentally inoculated group, and no incongruous designations occurred within the mock inoculated group or clinically submitted cases, these results support pathologist-evaluated cytopathology as comparable method to histopathology in cases of natural IBH infection exhibiting clinical morbidity. Further sensitivity and specificity characterizations of IBH-targeted cytopathology could be investigated using a larger sample set, sampling of inoculated birds exhibiting morbidity, blinded evaluation of clinically derived samples, and comparison of cytopathology to other laboratory tests, such as PCR or virus isolation.

ACKNOWLEDGEMENTS

Authors thank Susan M. Williams, Karen Grogan, Harlee Ingram, Llewelyn Sellers, Brittany Buckley, Will Byrum, Erich Linnemann, and Angel Olvera for their assistance in case management and sample processing.

REFERENCES

1. Nahed A El-Shall, Hatem S Abd El-Hamid, Magdy F Elkady, Hany F Ellakany, Ahmed R Elbestawy, Ahmed R Gado, Amr M Geneedy, Mohamed E Hasan, Mariusz Jaremko, Samy Selim, et al. Epidemiology, pathology, prevention, and control strategies of inclusion body hepatitis and hepatitis-hydropericardium syndrome in poultry: A comprehensive review. Frontiers in Veterinary Science. 2022;9. doi:10.3389/fvets.2022.963199

2. Chen L, Yin L, Zhou Q, Peng P, Du Y, Liu L, Zhang Y, Xue C, Cao Y. Epidemiological investigation of fowl adenovirus infections in poultry in China during 2015-2018. BMC Veterinary Research. 2019;15(1). doi:10.1186/s12917-019-1969-7

3. Shah MS, Ashraf A, Khan MI, Rahman M, Habib M, Chughtai MI, Qureshi JA. Fowl adenovirus: history, emergence, biology and development of a vaccine against hydropericardium syndrome. Archives of Virology. 2017;162(7):1833–1843. doi:10.1007/s00705-017-3313-5

4. Zhang J, Xie Z, Pan Y, Chen Z, Huang Y, Li L, Dong J, Xiang Y, Zhai Q, Li X, et al. Prevalence, genomic characteristics, and pathogenicity of fowl adenovirus 2 in Southern China. Poultry Science. 2024;103(1). doi:10.1016/j.psj.2023.103177

5. Schachner A, Matos M, Grafl B, Hess M. Fowl adenovirus-induced diseases and strategies for their control–a review on the current global situation. Avian Pathol. 2018;47(2):111–126. doi:10.1080/03079457.2017.1385724

6. El-Shewy T, El-Morsi B, El-Bolkeiny N. Diagnostic cytology in some conjunctival diseases. Bulletin of the Ophthalmological Society of Egypt. 1976;69(73):27–37.

7. Thiel MA, Bossart W, Bernauer W, Thiel M. Improved impression cytology techniques for the immunopathological diagnosis of superficial viral infections. British Journal of Ophthalmology. 1997;81:984–988. doi:10.1136/bjo.81.11.984

8. Thiel MA, Bossart W, Bernauer W. Clinical evaluation of impression cytology in diagnosis of superficial viral infections. Klinische Monatsblätter für Augenheilkunde. 1998;212(5):388–391. doi:10.1055/s-2008-1034914

9. Latimer KS, Goodwin MA, Davis MK. Rapid Cytologic Diagnosis of Respiratory Cryptosporidiosis in Chickens. Avian Diseases. 1988;32(4):826–830. doi:https://doi.org/10.2307/1591006

10. Al-Noaimy ZAÂ, Al-Alhially AA. A cytopathological study of the role of liver impression as a diagnostic tool in pigeons. Iraqi Journal of Veterinary Sciences. 2021;35(3):555–560. doi:10.33899/ijvs.2020.127170.1477

11. Sousa J, Edwards E, Piccione J. What is your diagnosis: Liver nodules in a Turkey Poult. Veterinary Clinical Pathology. 2023;52(S2):146–148. doi:10.1111/vcp.13128

12. Khatun A, Begum JA, Naznin F, Parvin R, Rahman MM, Sayem SM, Chowdhury EH. Cytological evaluation of necropsy guided impression smears of chronic respiratory disease of chickens. SAARC Journal of Agriculture. 2012;10(2):95–105. doi:10.3329/sja.v10i2.18331

13. Babu Prasath N, Selvaraj J, Ponnusamy P, Sasikala AM. An outbreak of pasteurellosis in Japanese quail chicks (Coturnix coturnix Japonica). Indian J. Anim. Hlth. 2018;57(2):189–194. doi:10.36062/ijah.57.2.2018.189-194

14. Kalinin V, Padnya P, Stoikov I. Romanowsky staining: history, recent advances and future prospects from a chemistry perspective. Biotechnic and Histochemistry. 2024;99(1):1–20. doi:10.1080/10520295.2023.2273860

15. Chantziantoniou N, Donnelly AD, Mukherjee M, Boon ME, Austin RM. Inception and development of the papanicolaou stain method. Acta Cytologica. 2017;61(4–5):266–280. doi:10.1159/000457827

16. Stilz CR, Fry MM, Craig LE. What is your diagnosis? Postmortem tracheal swab from a chicken. Veterinary Clinical Pathology. 2023;52(S2):149–151. doi:10.1111/vcp.13187

17. Sivaseelan S. Evaluation of efficacy of cytology for the prompt diagnosis of infectious Laryngotracheitis in commercial chicken. Indian Journal of Veterinary Pathology. 2016;40(4):372. doi:10.5958/0973-970x.2016.00088.2

18. Tripathy DN, Hanson LE. A Smear Technique for Staining Elementary Bodies of Fowlpox. Avian Diseases. 1976;20(3):609–610. doi:https://doi.org/10.2307/1589398

19. Cho K-O, Park N-Y, Endoh D, Ohashi K, Sugimoto C, Itakura C, Onuma M. Cytology of Feather Pulp Lesions from Marek's Disease (MD) Virus-Infected Chickens and Its Application for Diagnosis and Prediction of MD. J. Vet. Med. Sci. 1998;60(7):843–847. doi:10.1292/jvms.60.843

20. Viera AJ, Garrett JM. Understanding Interobserver Agreement: The Kappa Statistic. Family Medicine. 2005;37(5):360–363.

TABLES

Table 3.1. Summarized clinical history and necropsy findings of chickens enrolled from diagnostic cases suspected of inclusion body hepatitis.

| Bird ID | Age (d) | Status | Provided History | Gross Pathology |
|---|---|---|---|---|
| DX 01 | 27 | Dead on Arrival | Suspect IBH | Hepatomegaly with pallor, petechia, and multifocal necrosis |
| DX 02 | 27 | Dead on Arrival | Suspect IBH | Hepatic pallor and mottled hemorrhage |
| DX 03 | 27 | Euthanized | Suspect IBH | Hepatomegaly with pallor, petechia, and multifocal necrosis |
| DX 04 | 28 | Dead on Arrival | High mortality, loose droppings | Hepatomegaly with pallor and petechia |
| DX 05 | 28 | Dead on Arrival | High mortality, loose droppings | Hepatomegaly with pallor, petechia, and multifocal necrosis |
| DX 06 | 28 | Dead on Arrival | High mortality, loose droppings | Hepatomegaly with pallor and mottled hemorrhage |
| DX 07 | 28 | Euthanized | High mortality, loose droppings | Hepatic pallor and petechia |
| DX 08 | 29 | Dead on Arrival | High mortality, low growth rate | Hepatomegaly with pallor and mottled hemorrhage |
| DX 09 | 29 | Dead on Arrival | High mortality, low growth rate | Multifocal hepatic necrosis, pallor, and mottled hemorrhage |
| DX 10 | 33 | Euthanized | High mortality | Multifocal, pinpoint hepatic necrosis |
| DX 11 | 33 | Euthanized | High mortality | Focal, pinpoint hepatic necrosis |
| DX 12 | 36 | Dead on Arrival | High mortality, culls, and leg problems | Hepatomegaly with pallor, petechia, and multifocal necrosis |
| DX 13 | 36 | Euthanized | High mortality, culls, and leg problems | Hepatic pallor and mottled hemorrhage |

Table 3.2. Non-pathologist veterinary designations of twenty IBH-unknown liver impression smears. Each sample set (rows) origin is listed in the first column. Observers are identified as A-H, each with independent designations of unknown cytopathologic samples as consistent ("Yes") or not consistent ("No") with inclusion body hepatitis (IBH). A cytopathologic designation is highlighted if in agreement with the final histopathologic diagnosis (last column) per sample set.

| Sample | Observer Cytopathology IBH designation (agreement to histopathology) | | | | | | | | Paired |
|---|---|---|---|---|---|---|---|---|---|
| Source | A | B | C | D | E | F | G | H | Histopathology |
| Diagnostic | Yes | No | No | No | No | No | No | No | No |
| Diagnostic | No | No | No | No | No | No | No | No | No |
| Experimental | No | No | No | No | No | No | No | No | No |
| Experimental | No | No | No | No | No | No | No | No | No |
| Experimental | No | No | No | No | No | No | No | No | No |
| Experimental | No | No | No | No | No | No | No | No | No |
| Experimental | No | No | No | No | No | No | No | No | No |
| Experimental | No | No | No | No | No | No | No | No | No |
| Diagnostic | Yes | Yes | Yes | Yes | Yes | Yes | Yes | Yes | Yes |
| Diagnostic | Yes | Yes | Yes | Yes | Yes | Yes | Yes | Yes | Yes |
| Diagnostic | Yes | Yes | Yes | Yes | Yes | Yes | Yes | Yes | Yes |
| Diagnostic | Yes | Yes | Yes | Yes | Yes | Yes | No | Yes | Yes |
| Diagnostic | No | Yes | Yes | Yes | Yes | Yes | Yes | Yes | Yes |
| Diagnostic | Yes | Yes | Yes | No | No | Yes | Yes | Yes | Yes |
| Diagnostic | No | No | Yes | No | Yes | Yes | Yes | Yes | Yes |
| Diagnostic | Yes | No | No | No | Yes | Yes | Yes | Yes | Yes |
| Diagnostic | Yes | Yes | No | No | Yes | No | Yes | Yes | Yes |
| Diagnostic | Yes | No | No | No | No | No | No | Yes | Yes |
| Experimental | No | No | No | No | No | Yes | No | No | Yes |
| Experimental | No | No | No | No | No | No | Yes | No | Yes |

FIGURES

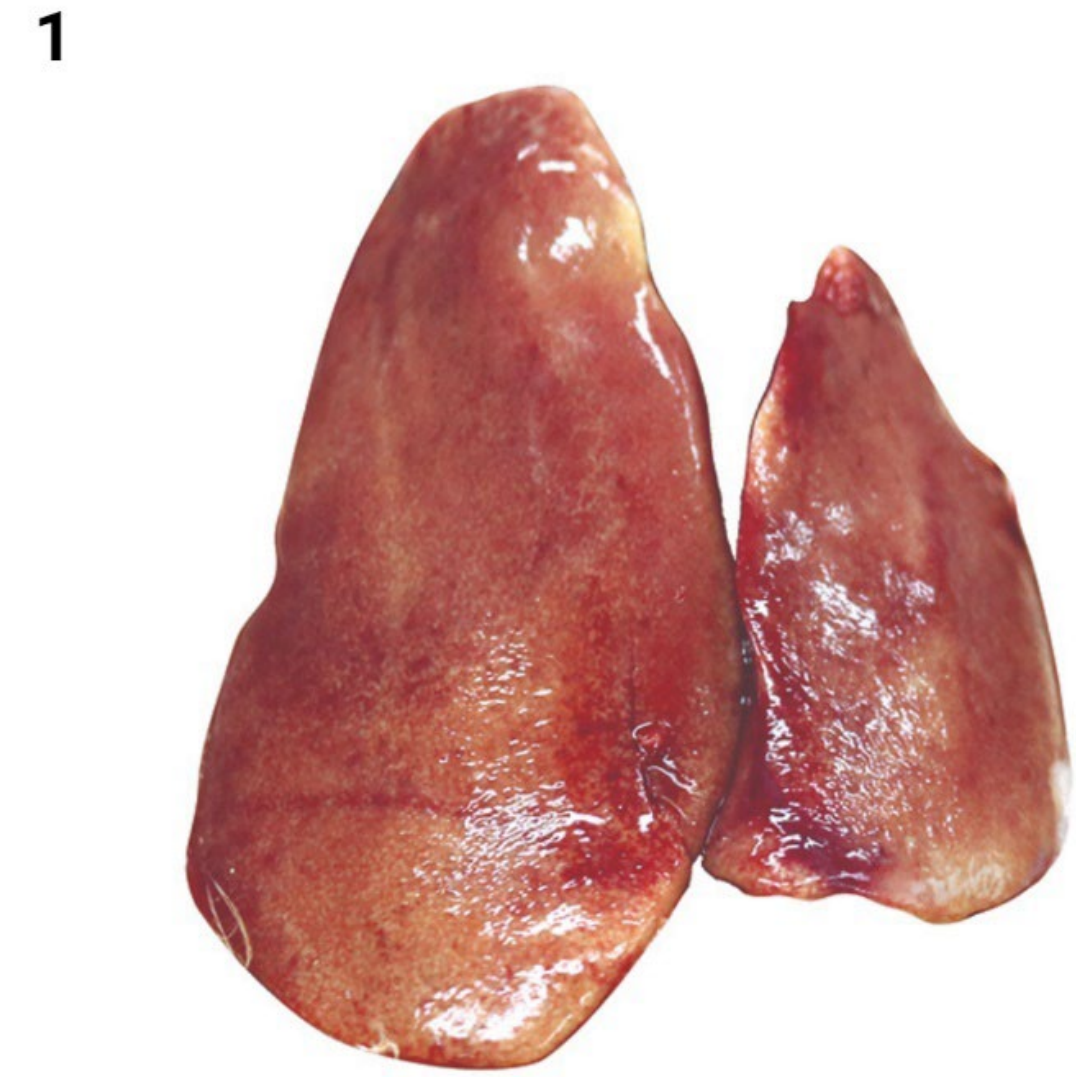


Figure 3.1. Gross liver pathology of a naturally infected, clinically submitted chicken enrolled into the study at necropsy as bird “DX 05” for gross features typical of IBH infection. The liver is enlarged and has rounded margins, diffuse pallor, disseminated hemorrhage, and multifocal necrosis.

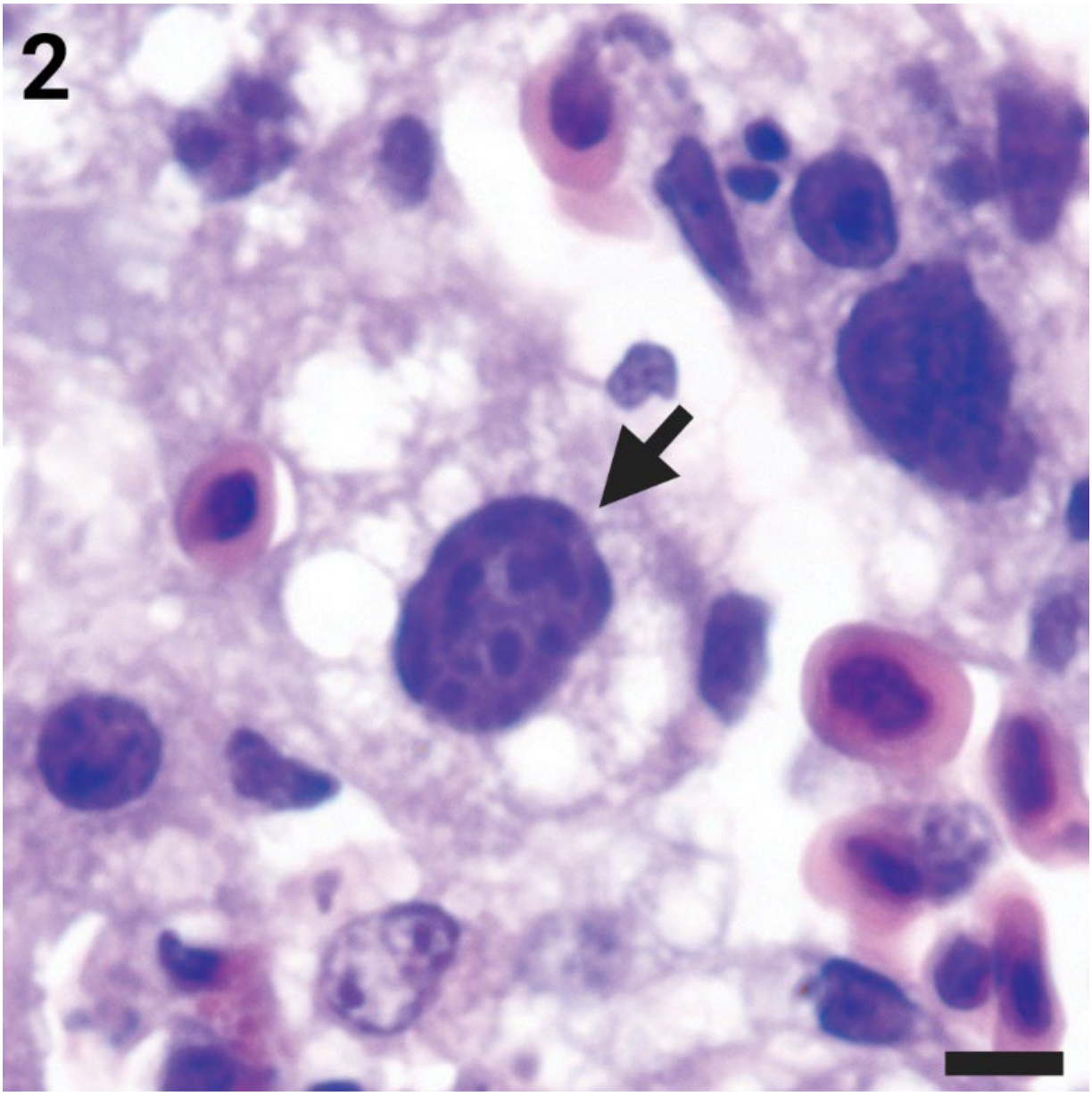


Figure 3.2. Histopathology of the liver, bird “DX 01”. An intranuclear inclusion body (arrow), typical of aviadenovirus infection, enlarges a hepatocyte nucleus. Hematoxylin and eosin. Scale bar = 5 μm.

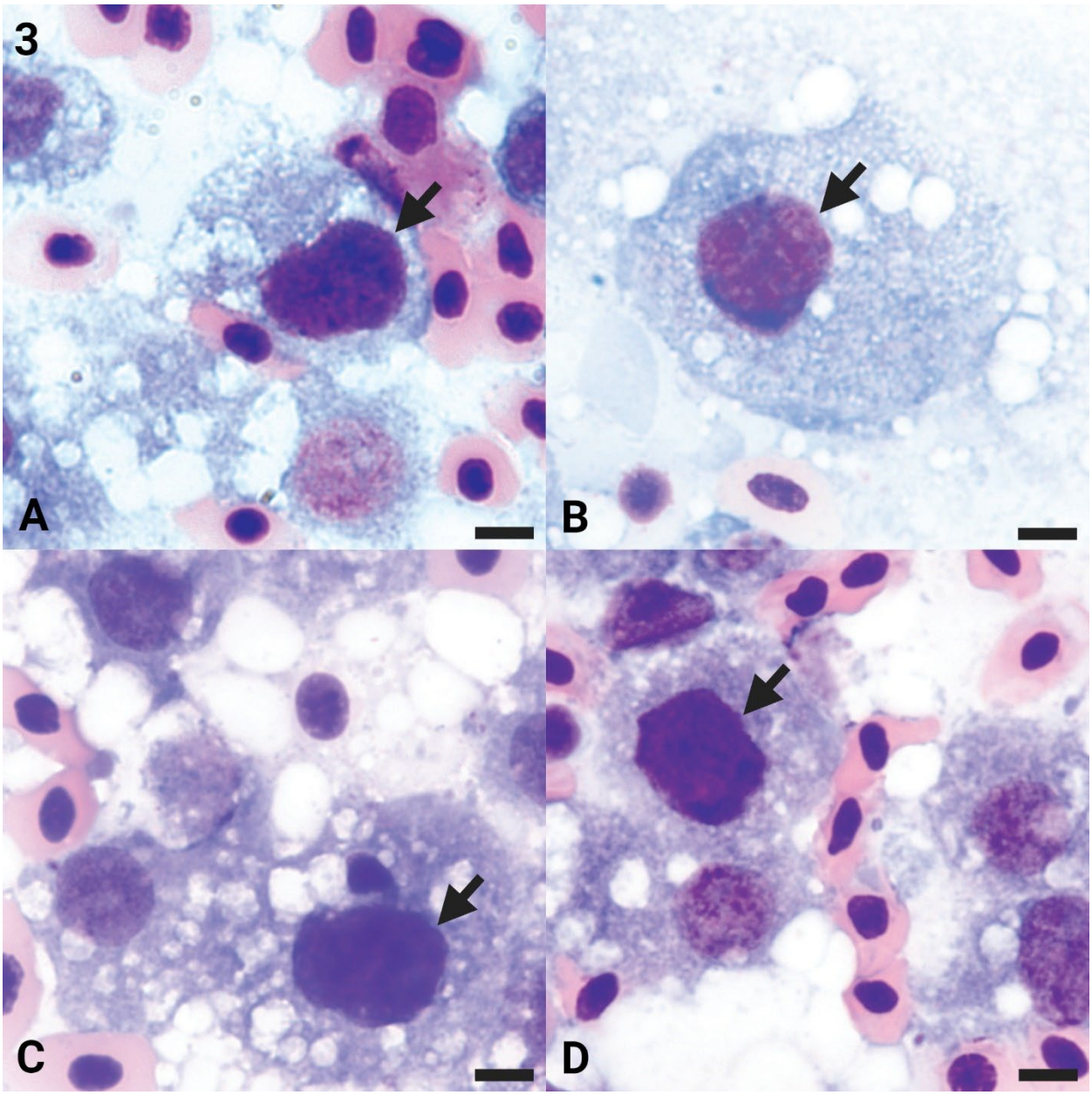


Figure 3.3. Cytopathology of the liver, A–D. Birds DX 04 (A, C, D) and DX 01 (B). Intranuclear material (arrows), morphologically compatible with aviadenoviral inclusion bodies, enlarges hepatocyte nuclei. Romanowsky stain. Scale bar = 5 μm.

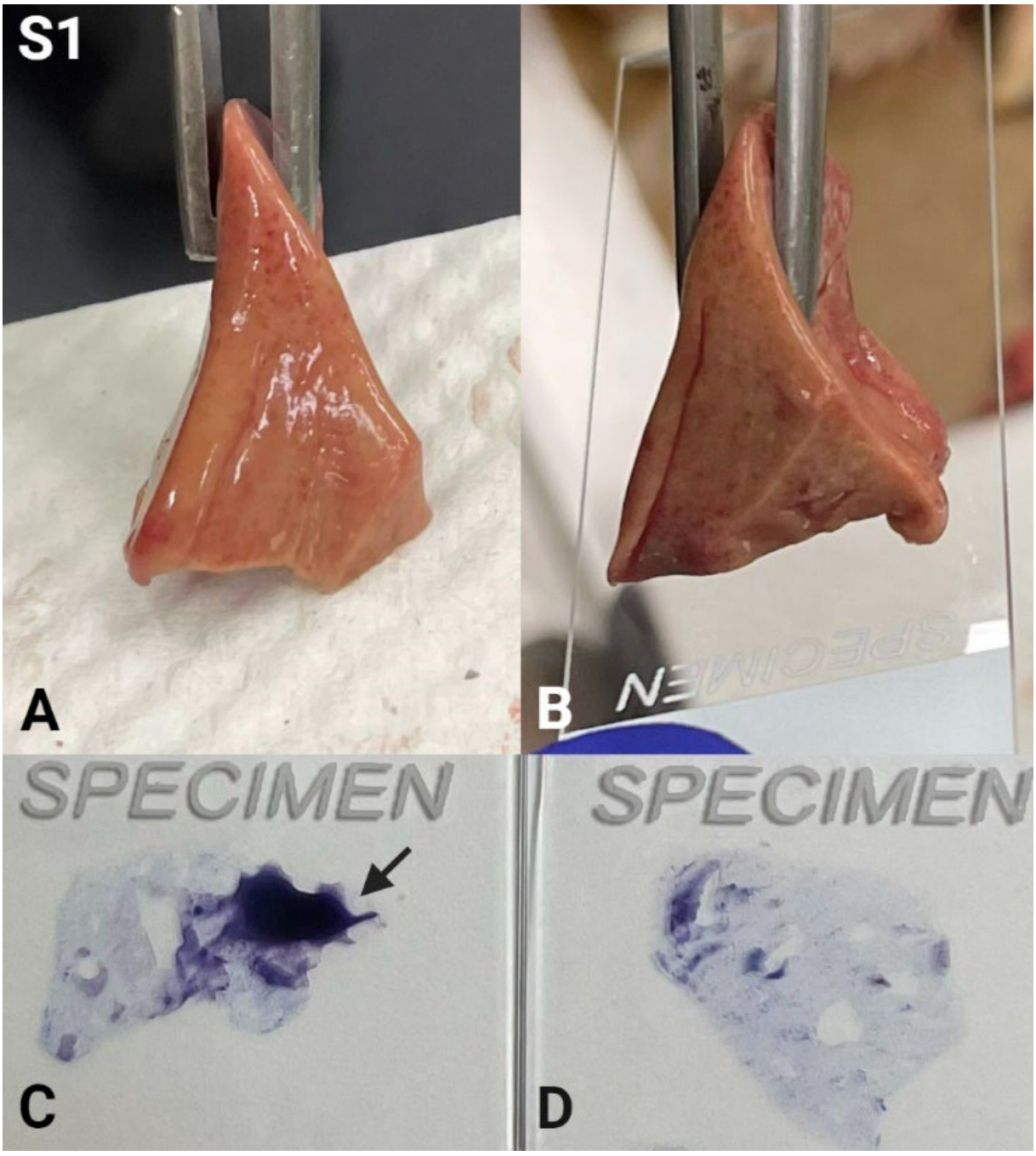


Supplemental Figure 3.1. Impression smear technique. A. Fresh liver is gently blotted until slightly tacky. B. Liver is gently impressed along a clean glass slide. C. Insufficient blotting results in areas that are too thick (arrow) to evaluate. D. Proper blotting allows a single layer of cells across the majority of the impression smear.

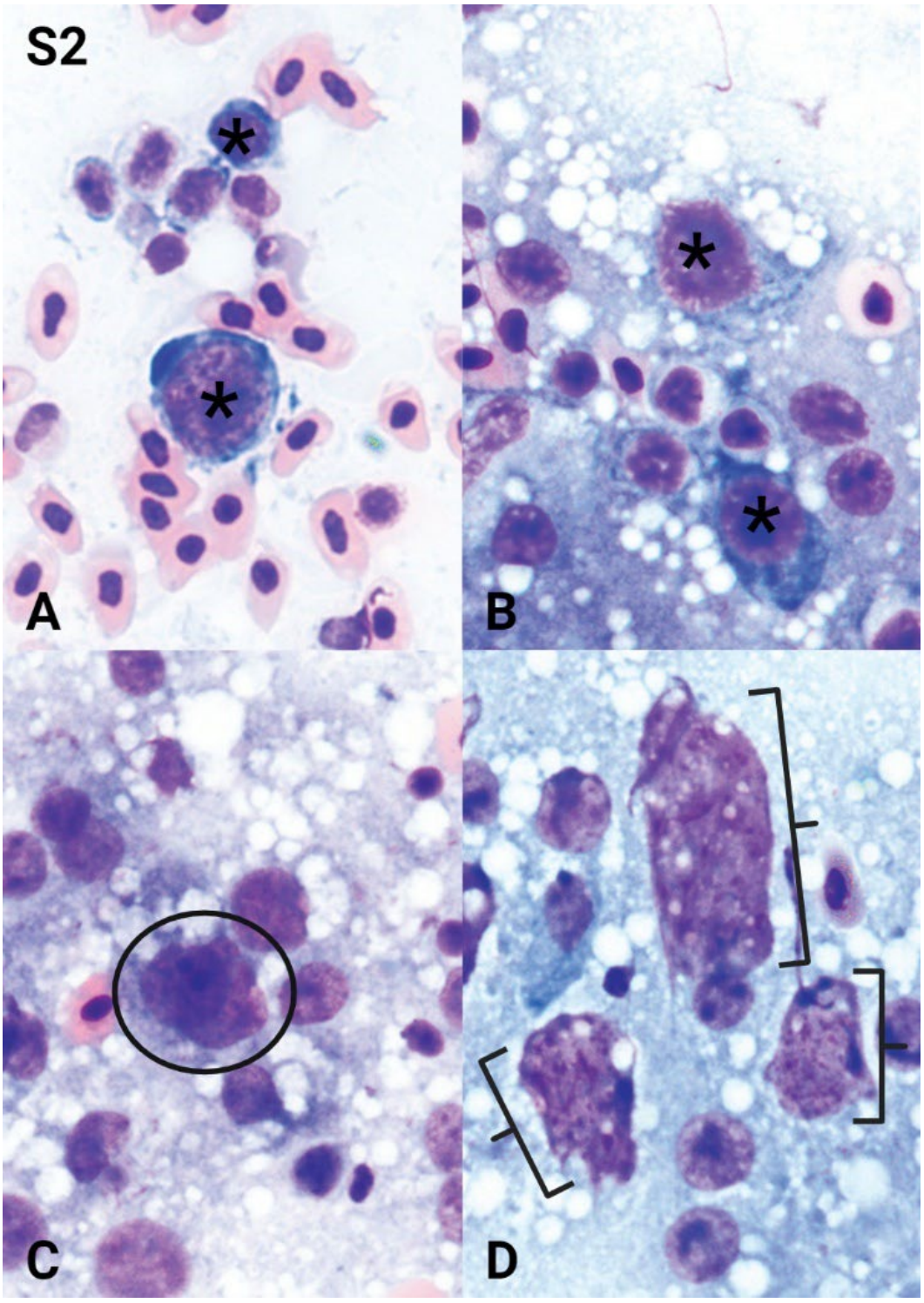


Supplemental Figure 3.2. Nondiagnostic structures that should not be interpreted as inclusion bodies. A. Large and small lymphocytes (asterisks) B. Monocytes (arrowheads). C. Overlapped nuclei (circled). D. Ruptured nuclei (brackets).

# CHAPTER 4

# DISCUSSION AND CONCLUSION

Avian reoviruses and fowl adenoviruses are responsible for diseases of economic importance in commercial broiler production, due to high morbidity or mortality, respectively. An understanding of disease pathogenesis can aid disease prevention measures, and rapid diagnosis at the time of an outbreak can facilitate disease containment.

## Localization of ARV GC2 in tissues by ISH.

ARVs in chickens have been demonstrated as etiologic agents of tenosynovitis and have been associated with enteric disease, hepatitis, immunosuppression, myocarditis, and respiratory disease. Currently, the clinicopathologic manifestation of an ARV isolate cannot by predicted by genetic or antigenic features. The dual enteric and arthritic tropism demonstrated by the ARV GC 2 isolate studied here supports innate potential of the virus to infect multiple organ systems. As the inflammatory response to ARV infection differs greatly between tendon and other tissue types, the host immune response, or modulation thereof, may partially determine the development of organ-specific ARV-related disease. As such, investigation into early cell response following infection, via cytokines or other markers of cell distress, may further characterize the differing inflammatory responses and disease progressions between tissues. Further, ARV presence within differentiated cells in specific locations of the intestinal tract and

within the synovial membrane suggests a shared susceptibility of these cells to infection. As such, investigation into the identity and shared features of these cells may yield valuable information regarding unknown ARV cell receptors.

**Diagnosis of IBH by cytopathology.**

Adenoviral hepatitis in chickens is a concern globally, with IBH endemic to most poultry-producing countries, and HHS endemic to epidemic in many others. As these diseases can present with sudden-onset, high mortality in field settings, rapid differentiation of these diseases from others of concern is imperative. Currently, IBH and HHS diagnoses depend on laborious and time-consuming laboratory techniques, which may add several days to a diagnostic investigation. This study demonstrates the utility of impression smear cytopathology for the rapid diagnosis of IBH. While results here are encouraging, future studies expanding the size and scope of work are needed. Comparison of cytopathology to other laboratory techniques such as PCR or virus isolation may allow for better establishment of sensitivity and specificity values, and investigations internationally may allow for study of, and applicability to, cases of HHS.

In conclusion, despite decades of research dedicated to the characterization of viral diseases of poultry, a wealth of information may still be gleaned from classic methods of pathologic evaluation. However, the studies performed here point to additional avenues of investigation that warrant exploration. For avian reoviruses, determinants of cell susceptibility and the role of the host inflammatory response by tissue must be considered as key components of further pathogenesis studies. For fowl adenoviruses, as well as other viruses of economic importance, rapid, cost-effective, accurate testing modalities must continue to be developed for use in the field as front-line options for disease diagnosis and containment.